Development of biomarkers and their application to the study of chromatin epistate effect on DNA damage and repair

TECHNISCHE
UNIVERSITÄT
DARMSTADT

Vom Fachbereich Biologie der Technischen Universitaet Darmstadt
zur
Erlangung des akademischen Grades
eines Doctor rerum naturalium
genehmigte Dissertation von

Malini Rajan M. Tech
aus Madurai, Indien

Berichterstatter (1. Referent): Prof. M. Cristina Cardoso
Mitberichterstatter (2. Referent): Prof. Dr. Heribert Warzecha

Tag der Einreichung: 09.12.2014
Tag der muendlichen Pruefung: 13.02.2015
Darmstadt 2015
D17

Dem Fachbereich Biologie der Technischen Universität Darmstadt zur Erlangung des akademischen Grades eines Doctor rerum naturalium vorgelegte Dissertation von Malini Rajan aus Madurai, Indien

1. Referentin: Prof. Dr. M. Cristina Cardoso
2. Referent: Prof. Dr. Heribert Warzecha

Tag der Einreichung: 09.12.2014
Tag der mündlichen Prüfung: 13.02.2015
Darmstadt- D17

TABLE OF CONTENTS

LIST OF FIGURES

LIST OF TABLES

Summary

Direct live cell analysis markers are very important for the better understanding of cellular processes and pathways. In this thesis we describe the development and characterization of live cell markers and their application to the study of interplay between chromatin epistate and DNA damage and repair.

Initially, we did an *in vivo* characterization of γ-H2AX nanobody (heavy chain antibodies from alpacas) based live cell DNA double strand break marker. As so far the analysis of the post-translational modifications of histone H2AX (γ-H2AX) involved in DNA double strands breaks, was not studied in living cells, we used nanobodies as a tool. These single chain nanobodies can be genetically encoded and fused to a fluorescent tag, which can then be used to detect and trace proteins and other cellular components *in vivo*. After *in vivo* characterization, we found that epitope recognition was competed by endogenous proteins recognzing the same modification (e.g., MDC1) and suffered also from alternative binding to mimicking SQ motifs present in proteins such as XRCC1 repair factor.

In parallel, a novel live cell marker for DNA replication and repair was developed by targeting the PCNA factor using cell penetrating peptide technology. PCNA is a key protein involved in DNA replication and repair pathways. Cells transfected with the fluorescent fusions of PCNA are widely used. To prevent the need for prior transfection and circumvent the problem of difficult to transfect and/or short lived cells, we developed and validated a cell permeable PCNA interacting peptide. This is the first ever attempt in developing an instantaneous biomarker, which needs only seconds to label the target.

To further extend the applicability of the cell penetrating peptide system for site specific labeling of any recombinant histidine tagged as well as naturally existing histidine rich proteins in living cells, tris-nitrilotriacetic acid (NTA) probes was used. Here, we also optimized a labeling protocol so that histidine tagged proteins overexpressed in cells can be labeled with fluorescently tagged trisNTA in fixed and living cells.

Finally, we explored DNA damage and repair in the context of open and closed chromatin states achieved by incorporation of different histone H2A variants (canonical H2A versus H2A.Bbd). Our established replication/repair marker was used here to test its co-localization with replication factors like PCNA. On a first set of experiments we analyzed DNA replication. Our data suggested that H2A.Bbd is enriched in the sites of active DNA replication leading to shortened S phase duration. On a second set of experiments, H2A.Bbd-GFP expressing cells were found to be more sensitive than H2A-GFP when exposed to UVC, The sensitivity was quantified by the level of cyclobutane pyrimidine dimer (CPD). Based on these results we hypothesized the reason for this increased damage could be due to more open chromatin comprising the H2A.Bbd and, on the other hand, the decreased damage due to more condensed chromatin comprising H2A. Hence, for the validation of our hypothesis we reversed the chromatin condensation states in both stable cell lines, i.e., we induced condensation of the chromatin of H2A.Bbd overexpressing cell lines and decondensation of the chromatin of H2A. overexpressing cell lines. Subsequent CPD damage analysis supported our hypothesis. The open chromatin nature leading to increased DNA damage susceptibility and shortened S-phase corelated with phenotypic characteristics of Hodgkin lymphoma cells known to overexpress H2A.Bbd.

Zusamenfassung

Zum besseren Verständnis zellulärer Prozesse ist es wichtig für Lebendzell-Experimente auf gute und verlässliche Marker für zelluläre Strukturen und Prozesse zurückgreifen zu können. In Rahmen dieser Thesis beschreiben wir die Entwicklung und Charakterisierung solcher Marker, die zur Untersuchung der DNA-Replikation sowie von DNA-Reparatur-Prozessen in lebenden Zellen verwendet werden können. Der Fokus liegt hierbei auf der Untersuchung von Chromatinveränderungen während der DNA-Reparatur.
Hierfür wurde zuerst ein Nanobody (Einzeldomänen-Antikörper aus *Camelidae*) gegen die posttranslational phosphorylierte Form der Histonvariante H2AX, γ-H2AX, die als Indikator für DNA-Doppelstrangbrüche dient, *in vivo* charakterisiert. Bisher wurde der Phosphorylierungstatus der Histonvariante H2AX lediglich in fixierten Zellen mittels Immunofluoreszensfärbung untersucht. Nanobodies können rekombinant an fluoreszente Proteine gekoppelt werden und entsprechend genutzt werden, um Proteine oder andere zelluläre Bestandteile zu visualisieren. Im Zuge der *in vivo* Charakterisierung des γ-H2AX Nanobodys taten sich zwei große Probleme bei der Epitop-Erkennung auf. So wird das Epitop des Nanobodys kompetitiv von anderen Proteinen wie MDC1 gebunden. Außerdem bindet der Nanobody das von ihm erkannte SQ-Motiv auch in anderen Reparaturproteine, wie beispielsweise XRCC1.
Parallel zur Nanobody-Charakterisierung wurde ein, auf zellpenetrierenden Peptiden basierender, Marker für Lebendzell-Studien zu DNA-Replikation und DNA-Reparatur entwickelt. Hierfür fokussierten wir uns auf PCNA, ein Schlüsselprotein der DNA-Replikation und der DNA-Reparatur welches häufig als fluoreszentes Fusions-Protein überexprimiert eingesetzt wird. Um die Transfektion von Zellen und die damit verbunden Probleme, wie schlechte Transfektionsraten und Auswirkungen auf das Zellüberleben zu umgehen, entwickelten wir ein zellpermeables, mit PCNA interagierendes Peptid das in Studien zu DNA-Replikation und DNA-Reparatur benutzt werden kann. Dabei handelte es sich um das erste Experiment überhaupt in dem erfolgreich ein Biomarker entwickelt wurde, der innerhalb von Sekunden gewünschte Zielstrukturen sichtbar macht.
Um diese Anwendungsmöglichkeiten zellpenetrierender Peptide noch zu erweitern und rekombinat mit einem Histidin-Tag versehene Proteine oder natürlich Histidin-reiche Proteine zu markieren, wurden Nitriloessigsäure (NTA) basierte Sonden in lebenden Zellen getestet. Außerdem wurde ein Färbeprotokoll optimiert, um sowohl in lebenden als auch in fixierten Zellen überexprimierte Proteine mit Histidin-Tag und auch endogen, Histidin-reiche Proteinen mit Hilfe eines, an die NTA gekoppelten, fluoreszierenden Moleküls sichtbar zu machen.
Letztlich untersuchten wir noch DNA Reparaturmechanismen im Kontext offener und geschlossener Chromatinregionen in denen die erst kürzlich entdeckte Isoform von Histon H2A, H2A.Bbd, vorkommt. Hierfür wurde der von uns etablierte Replikations- und Reparatur-Marker benutzt um Lokalisationsstudien von endogenem PCNA durchzuführen. In einem ersten Experiment untersuchten wir die DNA Replikation. Hier legen unsere Daten eine Anreicherung von H2A.Bbd in Regionen mit aktiver DNA Replikation nahe, was in einer verkürzten S-Phase resultiert. In weiteren Experimenten zeigte sich, dass eine Zelllinie, die stabil H2A.Bbd-GFP überexprimierte, sensitiver auf UVC-Bestrahlung reagierte, als stabil H2A-GFP überexprimierenden Zellen, was an Hand der Level von Cyclobutan-Pyrimidn-Dimeren (CPD) quantifiziert wurde. Dies wurde dem weniger stark kondensierten Chromatin in den H2A.Bbd-Zellen zugeschrieben. Um diese Hypothese zu überprüfen, wurden die Chromatin-Kondensationslevel der beiden Zelltypen invertiert, also eine Kondensation des Chromatins in H2A.Bbd-Zellen und eine Auflockerung der Chromatinstruktur in den H2A-Zellen herbeigeführt. Die anschließende Analyse der Cyclobutan-Pyrimidin-Dimer Level stütze diese Hypothese. Die offene Chromatin-Struktur, die H2A.Bbd überexprimierende Zelle anfälliger für DNA Schäden macht sowie die verkürzte S-Phase Dauer spiegelt die phänotypischen Charakteristika von Hodgkin Lymphomen wieder, in denen ebenfalls eine H2A.Bbd-Überexpression beobachtet wird.

1. General Introduction

1.1. Understanding of DNA damage and repair processes in mammalian systems

Genome integrity is under constant threat and undergoes tremendous damage every day (Lindahl, 1993; Lindahl & Barnes, 2000), contributing significantly to carcinogenesis and mutagenesis. DNA damage may occur in several different ways, such as DNA base alteration, single- and double-strand breaks, and cross links, leading to genomic instability. All these types of damage occur as consequences of cellular physiological process (Sancar et al., 2004) and are perturbed by endogenous and exogenous factors (De Bont & van Larebeke, 2004). Such damage can occur either directly or indirectly to the DNA.

Endogenous DNA damage is caused by several cellular processes. Oxidative DNA damage may be induced by reactive oxygen species (ROS) (Fang et al., 1996) which may lead to 8-oxo-7,8-dihydroguanine (8-oxoG; Fortini et al., 2003). Lipid peroxidation processes can cause DNA adducts of malonaldehyde, propeno, and etheno adducts (Fang et al., 1996; Hecht et al., 2001; Nair et al., 1999). S-adenosyl methionine can donate methyl groups, leading to the formation of methyl guanine (Rydberg & Lindahl, 1982). Apurinic and apyrimidic sites are formed as a result of an endogenous labile condition (Nakamura & Swenberg, 1999). DNA damage by carbonyl stress causes reactive carbonyl species (RCS) due to endogenous lipid peroxidation and glycation processes (Roberts et al., 2003; Vaca et al., 1998). Through redox cycling processes oestrogen metabolites can generate reactive radical species (Yager & Liehr, 1996).

Some exogenous damage is induced by environmental factors like UV irradiation from the sun. UV-induced DNA damage results in covalent cross-links that occur in cytosine and thymidine residues. Cyclobutane pyrimidine dimers (CPD) and pyrimidine (6-4) pyrimidone photoproducts (6-4PP) are the most commonly occurring types of damage. Chemicals like polycyclic aromatic hydrocarbons (PAHs) are atmospheric pollutants, which generates damage via ROS (Toyooka & Ibuki, 2007). A short list of different DNA damage are illustrated in Figure 1.1.

What these damages have in common is that they can affect cellular physiologies in a wide variety of ways, potentially leading to mutagenesis and cancer. Our improved understanding and critical detection of DNA damage can help us to understand cancer development and prevention.

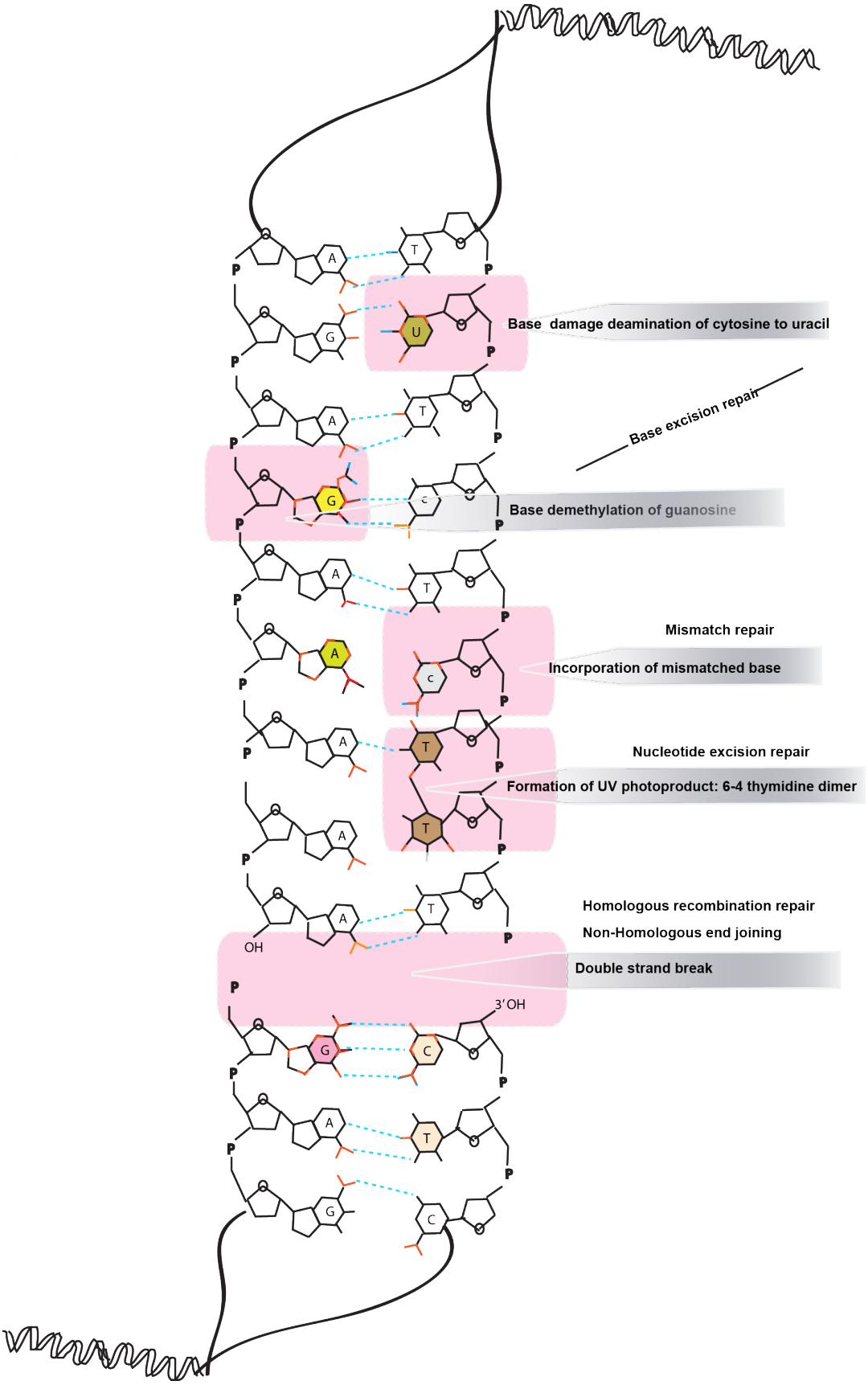

Figure 1.1. Types of DNA damage. Molecular illustration of multiple types of DNA damage and their respective repair pathways are shown in this figure.

Over the past few decades, several types of methods have been developed to understand different types of DNA damage and their corresponding repair processes. In the following table we present a short list of detection methods for DNA damage.

Table 1.1. List of DNA damage detection methodologies

Type of damage	Detection methods	Reference
DNA damage on a single cell level	Comet assay (single-cell gel electrophoresis)	(Olive et al., 1990)
	Fast Halo assay	(Sestili et al., 2006)
Relative number of 3'OH end breaks	Random Oligonucleotide Primed Synthesis (ROPS) assay	(Basnakian & James, 1996)
DNA fragmentation	Terminal deoxyribonucleotidyl transferase mediated deoxyuridine triphosphate nick end labeling (TUNEL assay)	(Labat-Moleur et al., 1998)
	Dielectric relaxation spectroscopy	(Sheu & Sheu, 2006)
In vivo footprinting and DNA adducts	Ligation mediated PCR (LMPCR)	(Tagoh et al., 2006)
	Terminal transferase-dependent PCR (TDPCR)	(Komura & Riggs, 1998)
	Random amplified polymorphic DNA (RAPD)	(Atienzar et al., 2002)
	Immuno-coupled PCR (ICPCR)	(Denissenko et al., 1994)
Region specific DNA damage	Comet-Fluorescent in situ hybridization (FISH)	(Spivak, 2010)
Oxidative damage	HPLC-electrospray tandem mass spectrometry	(Yue et al., 2007)
	Gas chromatography-mass spectrometry (GC-MS)	(Halliwell & Dizdaroglu, 1992)
Base modifications DNA cross links DNA double strand breaks, and single strand breaks	Immunological Methods Immuno slot blot assay Immunohistochemistry Western blot	(Karbaschi et al., 2012) (Santella, 1999)

Direct and efficient identification of DNA lesions is crucial for cellular survival. Once the DNA damage is successfully detected, it is efficiently handed over to repair machinery system. The DNA damage response system requires multiple steps, which involves the lesions' uncovering, treating the repair intermediates with repair factors, checkpoint activation, and the recovery of genetic and epigenetic information.

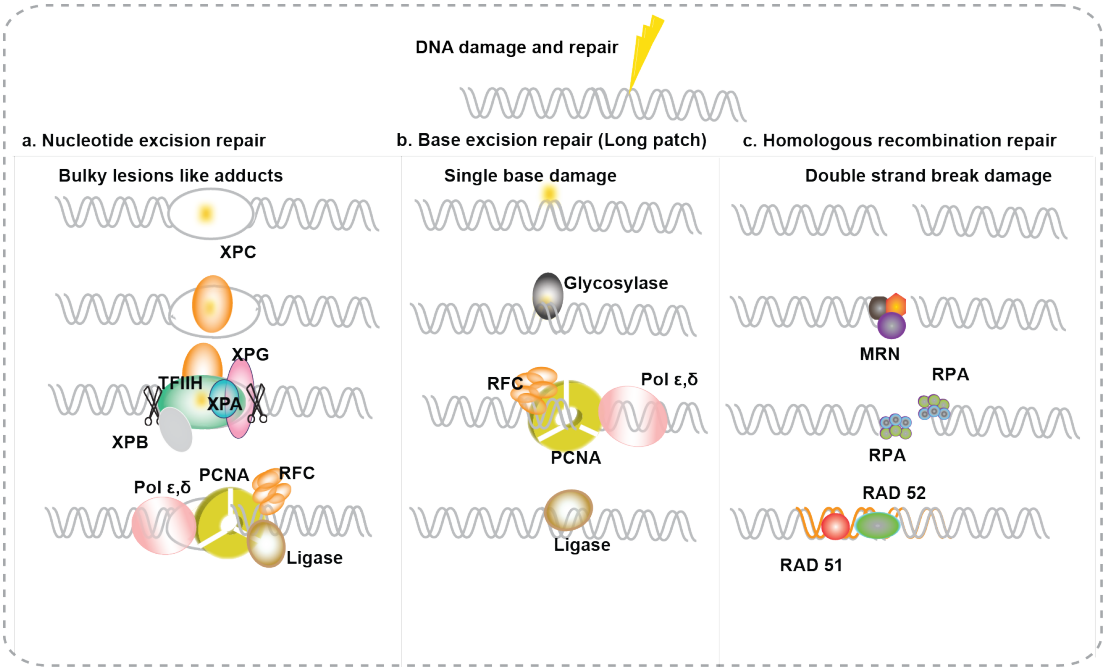

Figure 1.2. DNA repair pathways.(A) Nucleotide excision repair (NER;) (Marteijn et al., 2014), (B) Base excision repair (BER), (long patch repair; (Robertson et al., 2009), and (C) homologous recombination (HR) repair (Li & Heyer, 2008) for double strand break repair, are shown.

The repair pathways shown in Figure 1.2 require sequential steps and specific repair proteins associated with them. Primarily, detection of the DNA damage is performed by proteins like XPC (Xeroderma pigmentosum, complementation group C) in NER, Glycosylases in BER, or the MRN complex (Mre11, Rad50, and Nbs1) in DNA DSB (Double strand break) repair pathways. Following the detection step, repair factors are recruited. Xeroderma pigmentosum, complementation group G, A, B (XPG, XPA, XPB), and transcription factor II human (TFIIH) are involved in the NER, while replication protein A (RPA) plays a role in in DSB repair during the excision of the damaged DNA. Resynthesis of the excised DNA strand is performed by polymerases δ (delta) and ε (epsilon), RFC (replication factor C), and PCNA (proliferating cell nuclear antigen) in both NER and BER. In the final stages of the repair pathways, ligase is involved in ligation of the resynthesized strand in NER, BER and in DSB repair. Rad 52 catalyzes the function of the Rad 51 protein that binds to the DNA and thereby anneals complementary single stranded DNA.

We need to utilize a tool that helps us to understand the DNA damage and repair process with a high spatial/temporal resolution. Activation of different types of DNA damage, their corresponding pathways, and the study of repair proteins involved in them with spatio-temporal dynamics are extensively reviewed, particularly with a focus on the use of laser microirradiation tools (Mortusewicz, 2007; Muster, 2014). In table 1.2 we present a chronological development of laser microirradiation as a tool to induce DNA damage and the study of repair processes. In the present work we primarily used microirradiation as a tool to create localized DNA damage in living cells.

Table 1.2. Microirradiation as a key tool for understanding repair in the context of chromatin

Type of damage/repair	Type of microirradiation	Reference
DNA photo lesions	UV-laser microirradiation was used to induce DNA damage and then antibodies for the relevant damage was used for detection	(Cremer et al., 1980)
DNA Double Strand breaks (DSBs)	Pre-sensitized cells with BrdU followed by UV-A light	(Limoli & Ward, 1993)
	Pulsed UV-laser	(Rogakou et al., 1999)
DNA repair proteins recruitment to the microirradiated sites where the DNA is damaged	Live cell imaging of UV-laser induced DSBs	(Bekker-Jensen et al., 2005)
	Solid state diode laser 405 nm	(Mortusewicz et al., 2005)
		(Muster, 2014)
Discrimination of short patch and long patch Base excision repair	488 nm and 561 nm laser for discriminating short patch repair from long patch repair in living cells	

1.2. Understanding DNA replication process in mammalian system

During the S-phase of the cell cycle, the entire genome of a replicating cell needs to be duplicated. Continual synthesis of DNA takes place in a 5′ to 3′ direction on the leading strand and discontinued synthesis takes place in the lagging strand as shown in Figure 1.3

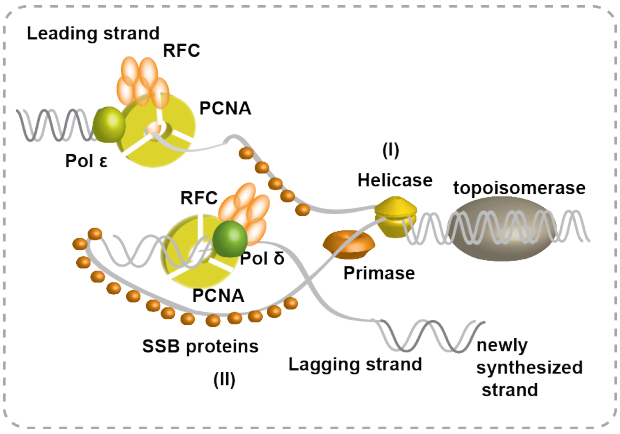

Figure 1.3. Illustration of major factors involved in DNA replication. Replication takes place in three important steps: (i) DNA double helix is opened up and unwound, (ii) the template strand is prepared, and (newly synthesized DNA segments are finally assembled.

The replication machinery involves various proteins that perform specialized functions as illustrated in Figure 1.3. DNA helicases (Cdc45-MCM2) confirm that each replication origin is initiated only once (Tognetti et al., 2014). DNA topoisomerases perfect the steady-state level of DNA supercoiling in order to facilitate the protein interaction (Champoux, 2001). DNA primase promotes the synthesis of small RNA molecules that act as primers for DNA polymerases (Frick & Richardson, 2001).

Single stranded DNA binding proteins (replication protein A) safeguard the DNA to remain unfolded and ensures the organization of assembly and disassembly of multiprotein complexes (Prakash & Borgstahl, 2012). DNA polymerase (Pol) δ/ε and replication factor C (RFC) are the accessory factors needed for the replication fork to load the essential processivity factor PCNA onto the 3′-ends of newly formed DNA strands (Majka & Burgers, 2004). Proliferating cell nuclear antigens (PCNA) are components necessary to the DNA replication process. The major functions of PCNA are well described in Chapter 3.2 of this thesis. As a consequence of DNA replications there is high probability of the formation of DSBs that should be accurately repaired.

Replication forks may sometimes get stalled or broken down leading to some base lesions (Helleday et al., 2007). Thus DNA replication pose a potential risk; a damaged base may change nucleotides and single strand breaks (SSBs) may degenerate into severe DSBs, which require complex processing steps for precise repair. Understanding replication with the right method is very important for the diagnosis and treatment of several diseases that are associated with defective repair of replication-induced stress. (Zeman & Cimprich, 2014). Varieties of methods listed in Table 1. 3 are used to study this process.

Table 1.3. Methods to study DNA replication

Replication study	Type of detection	Reference
In vitro analysis	Photo affinity labeling technique (to study structural and functional aspects of protein-DNA interactions)	(Khodyreva & Lavrik, 2005)
	2D gel analysis (purification of restriction fragments containing replication intermediates)	(Mesner et al., 2009)
	DNA combing analysis (fork velocity, origin initiation rate, fork density, numbers of potential and utilized origins)	(Lebofsky & Bensimon, 2003)
In situ analysis	Double label analysis (to study initiation and elongation rates).	(Aten et al., 1992)
*In v*ivo analysis	Fluorescent fusion proteins (to study the dynamics of DNA replication factories)	(Leonhardt et al., 2000)
	PCNA Chromobody (to study endogenous DNA replication)	(Burgess et al., 2012)

1.3. Challenges with present methodologies to monitor DNA replication, damage, and repair processes

Monitoring DNA damage and repair processes in living cells is more beneficial than other methods because of the importance of monitoring the repair of individual DNA lesions on a single cell basis. All the above-described methods in tables 1.1, 1.2, and 1.3 were used to understand DNA associated cellular processes. However, the methodologies mentioned in

Tables 1.1, 1.2, and 1.3 have potential drawbacks that have remained unaddressed so far. (1) Most of methodologies are *in vitro*, hence cannot provide real time kinetic measurements. (2) In live cell methods, fluorescent fusions are used, which does not allow us to investigate post translational modifications and is limited by spectral range. (3) Transfection efficiency is a big obstacle in hard to transfect cells. (4) Endogenous protein dynamics are not measured in living cells. Hence it has become very important to try novel methodologies with which one can overcome the above mentioned problems and successfully understand the cellular processes. An attempt to solve all of the above mentioned problems with different technologies is described in Chapter 3.1–3.3.

1.4. Role of chromatin organization in DNA metabolism

The categorization of primary, secondary, tertiary, and quaternary structures used for proteins is also applied to chromatin structural orders. The primary structure of chromatin is comprised of a beads-on-a-string structure of nucleosomes and linker DNA. Figure 1.4 shows the primary structure of the nucleosome with the core histones. Unlike proteins that are made of amino acids, chromatin is comprised of repeating units of identical nucleosomes, and thus is expected to form highly “ordered” secondary structures (Woodcock & Ghosh, 2010).

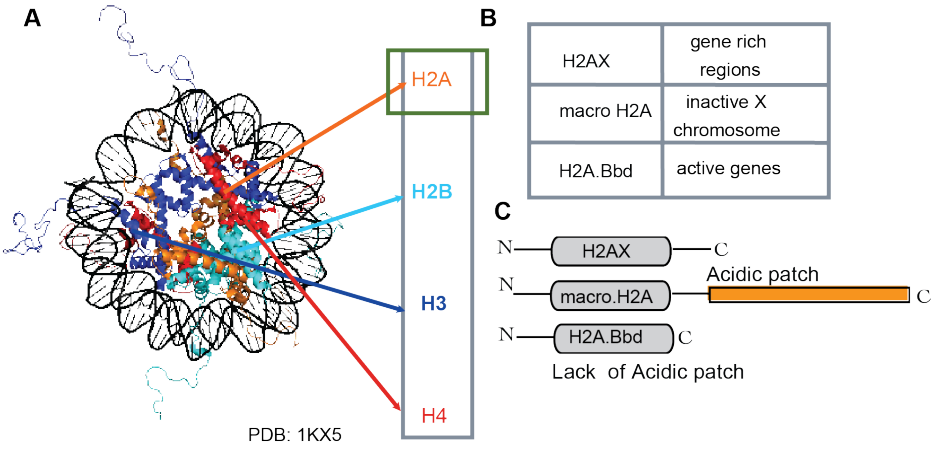

Figure 1.4. Core histones and variants of histone H2A. (A) DNA wrapped around the histones H2A, H2B, H3, H4 are shown. (B) Variants of H2A (i.e., H2AX, macro H2A, and H2A. Bbd) and their enrichment regions in the genome and functional significance is shown here and in Table 1.4 (C) The coding region of histone macro H2A possesses a long C terminus acidic patch, whereas H2A.Bbd completely lacks them.

Table 1.4. H2A variants and their functions in context of DNA damage and repair

H2A variants of interest	Functions	Reference
H2AX	Evolutionarily conserved at C terminus of H2AX have been phosphorylated specifically at serine 139 on DNA double strand breaks	(Huang et al., 2004)
macroH2A	Macro H2A represses transcription, regulates cell cycle and inhibits PARP-1 activity in recognizing DNA damage	(Nusinow et al., 2007)
H2A.Bbd	H2A. Bbd overexpressing cells are sensitive to DNA damage and the H2A.Bbd comprising histone are not affected by remodeling complex SWI/SNF during repair	(Sansoni et al., 2014) (Menoni et al., 2007)

The higher-order organization of the genome that leads to the formation of chromatin fibers and chromosomes is known to play a major role in gene regulation and global genome stability maintenance (Fraser & Bickmore, 2007). It is therefore expected that flaws in higher-order chromatin and its organization can cause disease. There is a collective list of diseases in which alterations in histone modifications were observed, although it is not precisely known whether these histone alterations are just a side-effect or the major cause of the disease (Misteli, 2010).

Histone H2A family is the largest among histone classes with the most variants (total 19 in number), coded by 26 genes. Out of these 26 genes, 9 are not part of any cluster and code for atypical histones like macro-H2A, H2A-Bbd (described in Chapter 3.4). They are diverse in sequence homology and have a functional role in DNA damage repair, transcriptional, cell cycle, and chromatin compaction. A few variants of histone H2A that seem to play a crucial role in biological processes are shown in Figure 1.4B and C and summarized in Table 1.4. The exact mechanistic aspects of histone H2A variant are not yet fully understood. In general, the carboxyl-terminus of the H2A variants interacts with the "linker" region of the nucleosomal DNA and histone H1, and hence variants of H2A can potentially affect the chromatin compaction and its stability. The chromatin compaction generally helps to protect the DNA from being damaged (Cann & Dellaire, 2011) and delays the repair process. In response to DNA damage, chromatin relaxes and increases its chromatin accessibility for repair factors (Rubbi & Milner, 2003). Hence it is quite reasonable to assume that H2A variants may have an effect on the DNA damage response. Due to its biologically significant role we have examined H2A and H2A.Bbd in Chapter 3.4 in the context of DNA damage sensitivity.

References

Aten, J. A., Bakker, P. J., Stap, J., Boschman, G. A., & Veenhof, C. H. (1992). DNA double labelling with IdUrd and CldUrd for spatial and temporal analysis of cell proliferation and DNA replication. *Histochem J, 24*(5), 251-259.

Atienzar, F. A., Venier, P., Jha, A. N., & Depledge, M. H. (2002). Evaluation of the random amplified polymorphic DNA (RAPD) assay for the detection of DNA damage and mutations. *Mutat Res, 521*(1-2), 151-163.

Basnakian, A. G., & James, S. J. (1996). Quantification of 3'OH DNA breaks by random oligonucleotide-primed synthesis (ROPS) assay. *DNA Cell Biol, 15*(3), 255-262.

Bekker-Jensen, S., Lukas, C., Melander, F., Bartek, J., & Lukas, J. (2005). Dynamic assembly and sustained retention of 53BP1 at the sites of DNA damage are controlled by Mdc1/NFBD1. *Journal of Cell Biology, 170*(2), 201-211.

Burgess, A., Lorca, T., & Castro, A. (2012). Quantitative live imaging of endogenous DNA replication in mammalian cells. *PLoS One, 7*(9), e45726.

Cann, K. L., & Dellaire, G. (2011). Heterochromatin and the DNA damage response: the need to relax. *Biochem Cell Biol, 89*(1), 45-60.

Champoux, J. J. (2001). DNA topoisomerases: structure, function, and mechanism. *Annu Rev Biochem, 70*, 369-413.

Cremer, C., Cremer, T., Fukuda, M., & Nakanishi, K. (1980). Detection of laser--UV microirradiation-induced DNA photolesions by immunofluorescent staining. *Hum Genet, 54*(1), 107-110.

De Bont, R., & van Larebeke, N. (2004). Endogenous DNA damage in humans: a review of quantitative data. *Mutagenesis, 19*(3), 169-185.

Denissenko, M. F., Venkatachalam, S., Yamasaki, E. F., & Wani, A. A. (1994). Assessment of DNA damage and repair in specific genomic regions by quantitative immuno-coupled PCR. *Nucleic Acids Res, 22*(12), 2351-2359.

Fang, J. L., Vaca, C. E., Valsta, L. M., & Mutanen, M. (1996). Determination of DNA adducts of malonaldehyde in humans: effects of dietary fatty acid composition. *Carcinogenesis, 17*(5), 1035-1040.

Fortini, P., Pascucci, B., Parlanti, E., D'Errico, M., Simonelli, V., & Dogliotti, E. (2003). 8-Oxoguanine DNA damage: at the crossroad of alternative repair pathways. *Mutat Res, 531*(1-2), 127-139.

Fraser, P., & Bickmore, W. (2007). Nuclear organization of the genome and the potential for gene regulation. *Nature, 447*(7143), 413-417.

Frick, D. N., & Richardson, C. C. (2001). DNA primases. *Annu Rev Biochem, 70*, 39-80.

Halliwell, B., & Dizdaroglu, M. (1992). The measurement of oxidative damage to DNA by HPLC and GC/MS techniques. *Free Radic Res Commun, 16*(2), 75-87.

Hecht, S. S., McIntee, E. J., & Wang, M. (2001). New DNA adducts of crotonaldehyde and acetaldehyde. *Toxicology, 166*(1-2), 31-36.

Helleday, T., Lo, J., van Gent, D. C., & Engelward, B. P. (2007). DNA double-strand break repair: from mechanistic understanding to cancer treatment. *DNA Repair (Amst), 6*(7), 923-935.

Huang, X., Halicka, H. D., & Darzynkiewicz, Z. (2004). Detection of histone H2AX phosphorylation on Ser-139 as an indicator of DNA damage (DNA double-strand breaks). *Curr Protoc Cytom, Chapter 7*, Unit 7 27.

Karbaschi, M., Brady, N. J., Evans, M. D., & Cooke, M. S. (2012). Immuno-slot blot assay for detection of UVR-mediated DNA damage. *Methods Mol Biol, 920*, 163-175.

Khodyreva, S. N., & Lavrik, O. I. (2005). Photoaffinity labeling technique for studying DNA replication and DNA repair. *Curr Med Chem, 12*(6), 641-655.

Komura, J., & Riggs, A. D. (1998). Terminal transferase-dependent PCR: a versatile and sensitive method for in vivo footprinting and detection of DNA adducts. *Nucleic Acids Res, 26*(7), 1807-1811.

Labat-Moleur, F., Guillermet, C., Lorimier, P., Robert, C., Lantuejoul, S., Brambilla, E., & Negoescu, A. (1998). TUNEL apoptotic cell detection in tissue sections: critical evaluation and improvement. *J Histochem Cytochem, 46*(3), 327-334.

Lebofsky, R., & Bensimon, A. (2003). Single DNA molecule analysis: applications of molecular combing. *Brief Funct Genomic Proteomic, 1*(4), 385-396.

Leonhardt, H., Rahn, H. P., Weinzierl, P., Sporbert, A., Cremer, T., Zink, D., & Cardoso, M. C. (2000). Dynamics of DNA replication factories in living cells. *Journal of Cell Biology, 149*(2), 271-280.

Li, X., & Heyer, W. D. (2008). Homologous recombination in DNA repair and DNA damage tolerance. *Cell Res, 18*(1), 99-113.

Limoli, C. L., & Ward, J. F. (1993). A new method for introducing double-strand breaks into cellular DNA. *Radiation Research, 134*(2), 160-169.

Lindahl, T. (1993). Instability and decay of the primary structure of DNA. *Nature, 362*(6422), 709-715.

Lindahl, T., & Barnes, D. E. (2000). Repair of endogenous DNA damage. *Cold Spring Harb Symp Quant Biol, 65*, 127-133.

Majka, J., & Burgers, P. M. (2004). The PCNA-RFC families of DNA clamps and clamp loaders. *Prog Nucleic Acid Res Mol Biol, 78*, 227-260.

Marteijn, J. A., Lans, H., Vermeulen, W., & Hoeijmakers, J. H. (2014). Understanding nucleotide excision repair and its roles in cancer and ageing. *Nat Rev Mol Cell Biol, 15*(7), 465-481.

Menoni, H., Gasparutto, D., Hamiche, A., Cadet, J., Dimitrov, S., Bouvet, P., & Angelov, D. (2007). ATP-dependent chromatin remodeling is required for base excision repair in conventional but not in variant H2A.Bbd nucleosomes. *Mol Cell Biol, 27*(17), 5949-5956.

Mesner, L. D., Dijkwel, P. A., & Hamlin, J. L. (2009). Purification of restriction fragments containing replication intermediates from complex genomes for 2-D gel analysis. *Methods Mol Biol, 521*, 121-137.

Misteli, T. (2010). Higher-order genome organization in human disease. *Cold Spring Harb Perspect Biol, 2*(8), a000794.

Mortusewicz, O. (2007). Analysis of the DNA damage response in living cells . *[Online Edition:* http://edoc.ub.uni-muenchen.de/8555/*] LMU-Muenchen*.

Mortusewicz, O., Schermelleh, L., Walter, J., Cardoso, M. C., & Leonhardt, H. (2005). Recruitment of DNA methyltransferase I to DNA repair sites. *Proc Natl Acad Sci U S A, 102*(25), 8905-8909.

Muster, B. (2014). DNA repair and Chromatin. *[Online-Edition:* http://tuprints.ulb.tu-darmstadt.de/id/eprint/3989*] TU Darmstadt*

Nair, J., Barbin, A., Velic, I., & Bartsch, H. (1999). Etheno DNA-base adducts from endogenous reactive species. *Mutat Res, 424*(1-2), 59-69.

Nakamura, J., & Swenberg, J. A. (1999). Endogenous apurinic/apyrimidinic sites in genomic DNA of mammalian tissues. *Cancer Res, 59*(11), 2522-2526.

Nusinow, D. A., Hernandez-Munoz, I., Fazzio, T. G., Shah, G. M., Kraus, W. L., & Panning, B. (2007). Poly(ADP-ribose) polymerase 1 is inhibited by a histone H2A variant, MacroH2A, and contributes to silencing of the inactive X chromosome. *J Biol Chem, 282*(17), 12851-12859.

Olive, P. L., Banath, J. P., & Durand, R. E. (1990). Heterogeneity in Radiation-Induced DNA Damage and Repair in Tumor and Normal-Cells Measured Using the Comet Assay. *Radiation Research, 122*(1), 86-94.

Prakash, A., & Borgstahl, G. E. (2012). The structure and function of replication protein A in DNA replication. *Subcell Biochem, 62*, 171-196.

Roberts, M. J., Wondrak, G. T., Laurean, D. C., Jacobson, M. K., & Jacobson, E. L. (2003). DNA damage by carbonyl stress in human skin cells. *Mutat Res, 522*(1-2), 45-56.

Robertson, A. B., Klungland, A., Rognes, T., & Leiros, I. (2009). DNA repair in mammalian cells: Base excision repair: the long and short of it. *Cell Mol Life Sci, 66*(6), 981-993.

Rogakou, E. P., Boon, C., Redon, C., & Bonner, W. M. (1999). Megabase chromatin domains involved in DNA double-strand breaks in vivo. *Journal of Cell Biology, 146*(5), 905-916.

Rubbi, C. P., & Milner, J. (2003). p53 is a chromatin accessibility factor for nucleotide excision repair of DNA damage. *EMBO J, 22*(4), 975-986.

Rydberg, B., & Lindahl, T. (1982). Nonenzymatic methylation of DNA by the intracellular methyl group donor S-adenosyl-L-methionine is a potentially mutagenic reaction. *EMBO J, 1*(2), 211-216.

Sancar, A., Lindsey-Boltz, L. A., Unsal-Kacmaz, K., & Linn, S. (2004). Molecular mechanisms of mammalian DNA repair and the DNA damage checkpoints. *Annu Rev Biochem, 73*, 39-85.

Sansoni, V., Casas-Delucchi, C. S., Rajan, M., Schmidt, A., Bonisch, C., Thomae, A. W., Staege, M. S., Hake, S. B., Cardoso, M. C., & Imhof, A. (2014). The histone variant H2A.Bbd is enriched at sites of DNA synthesis. *Nucleic Acids Res, 42*(10), 6405-6420.

Santella, R. M. (1999). Immunological methods for detection of carcinogen-DNA damage in humans. *Cancer Epidemiol Biomarkers Prev, 8*(9), 733-739.

Sestili, P., Martinelli, C., & Stocchi, V. (2006). The fast halo assay: An improved method to quantify genomic DNA strand breakage at the single-cell level. *Mutation Research-Genetic Toxicology and Environmental Mutagenesis, 607*(2), 205-214.

Sheu, J. I., & Sheu, E. Y. (2006). Characterization of DNA degradation using direct current conductivity and dynamic dielectric relaxation techniques. *AAPS PharmSciTech, 7*(2), E36.

Spivak, G. (2010). The Comet-FISH assay for the analysis of DNA damage and repair. *Methods Mol Biol, 659*, 129-145.

Tagoh, H., Cockerill, P. N., & Bonifer, C. (2006). In vivo genomic footprinting using LM-PCR methods. *Methods Mol Biol, 325*, 285-314.

Tognetti, S., Riera, A., & Speck, C. (2014). Switch on the engine: how the eukaryotic replicative helicase MCM2-7 becomes activated. *Chromosoma*.

Toyooka, T., & Ibuki, Y. (2007). DNA damage induced by coexposure to PAHs and light. *Environ Toxicol Pharmacol, 23*(2), 256-263.

Vaca, C. E., Nilsson, J. A., Fang, J. L., & Grafstrom, R. C. (1998). Formation of DNA adducts in human buccal epithelial cells exposed to acetaldehyde and methylglyoxal in vitro. *Chem Biol Interact, 108*(3), 197-208.

Woodcock, C. L., & Ghosh, R. P. (2010). Chromatin higher-order structure and dynamics. *Cold Spring Harb Perspect Biol, 2*(5), a000596.

Yager, J. D., & Liehr, J. G. (1996). Molecular mechanisms of estrogen carcinogenesis. *Annu Rev Pharmacol Toxicol, 36*, 203-232.

Yue, J., Wang, P., Liu, Y. H., Wu, J. Y., Chen, J., & Peng, R. X. (2007). Fast evaluation of oxidative DNA damage by liquid chromatography-electrospray tandem mass spectrometry coupled with precision-cut rat liver slices. *Biomed Environ Sci, 20*(5), 386-391.

Zeman, M. K., & Cimprich, K. A. (2014). Causes and consequences of replication stress. *Nat Cell Biol, 16*(1), 2-9.

2. AIMS OF THE STUDY

The aims of the present work can be divided into two categories (1) to develop live cell biomarkers to study DNA damage, repair and replication; (2) to investigate the impact of chromatin epistate on these processes.

1. The first goal was to develop a γ-H2AX based live cell marker using chromobody technology to be used in combination with laser microirradiation technique and monitor phosphorylation of H2AX in living cells.

2. The second goal was to exploit cell penetrating peptides for delivering high affinity PCNA binding peptides and, thus, label endogenous PCNA at sites of replication and repair.

3. The third goal was to further broaden the applicability of cell penetrating peptides by delivering small molecular probe i.e., trisNTA and label oligohistidine containing proteins.

4. The final goal was to study the effect of chromatin condensation state, dependent on histone H2A variants, on replication, damage and repair and its relevance to disease.

3. CHAPTERS

3.1. *In vivo* epitope recognition pitfalls affect γ-H2AX chromobody function in living cells

This chapter has the following major contributors

Malini Rajan[1], Oliver Mortusewicz [2], Ulrich Rothbauer [3], Koroush Zolghadr [3], Katrin Schmidthals[3], Alexander Rapp [1],Heindrich Leonhardt [2], M. Cristina Cardoso[1].

1- Technische Universitaet Darmstadt, Germany

2- Ludwigs Maxmillian Universitaet- Munich, Germany

3- Chromotek GmbH, Munich, Germany

This chapter is under preparation for submission.

Abstract

As live cell analysis of post-translational modifications of histone H2AX (γ-H2AX) involved in DNA double strands breaks has been impossible so far, the idea of using labeled nanobodies (chromobodies) was conceived. Animals like llamas and camels produce single-chain antibodies. These single-chain antibodies can be genetically encoded and fused to a fluorescent fusion tag. These fluorescent antigen-binding proteins called “chromobodies” can then be used to detect and trace proteins and other cellular components *in vivo*. Chromobodies against γ-H2AX were generated. Relevant fluorescent fusion constructs were transfected into living cells and DNA double strand breaks were induced in these cells by microirradiation with a 405 nm laser microbeam. However, some potential epitope recognition problems were encountered when using γ-H2AX chromobodies in living cells. The present study sheds light on major pitfalls like epitope masking by endogenous MDC1 and alternative epitope recognition by overexpressed XRCC1, which must be considered in the future development and screening of live cell markers.

Highlights

- γ-H2AX chromobody/binder was able to get bound to phosphorylated H2AX peptide *in vitro*.
- *In vivo* conditions were not suitable for the optimal performance of the γ-H2AX binder.
- Accessibility of γ-H2AX binder was hindered by MDC1 *in vivo*.
- Unspecificity of γ-H2AX binder was triggered in the presence of XRCC1 overexpression.

Introduction

Damage to the DNA in a cell is a common event generally occurring in the life of a cell due to exogenous factors like carcinogens, ionizing radiation, viruses, environmental factors and endogenous factors like age and defects in the immune system. These factors may lead to mutations in DNA, causing cancer and other harmful effects in the cell. Hence, the study of cellular DNA damage is very important and requires extensive data on the modification, localization and interaction of cellular components. Phosphorylation of the serine at the 139th residue of histone H2AX (γ-H2AX) is associated with DNA double strand breaks (Rogakou et al., 1998; Sharma et al., 2012). Because of its function, γ-H2AX is the most sensitive biomarker used to study DNA double-strand breaks (DSBs) and its subsequent repair processess occurring in the cell. There are already a wide variety of methods that have been developed to observe the molecular changes that take place during the repair of DNA DSBs, but their application is not suitable for live cells (Rothbauer et al., 2006). Though microinjection of antibodies is possible for a live cell analysis, it is not preferred due to antibody accessibility and potential stress induced to the cell (Adams et al., 1989). Fluorescent fusions allow live cell kinetic measurements but cannot be used to detect post-translational modification. Here we introduce a novel technology, towards the aim of understanding DNA double strand breaks and post-translational modification (i.e., phosphorylation associated with H2AX in living cells). Sera of llamas and camels were found to have both conventional heterotetrameric and also heavy chain antibodies that lack light chains. These heavy chain antibodies possess a single variable domain (VHH) and two constant domains CH2 and CH3 (Hamers-Casterman et al., 1993). These antigen binding domains of heavy chain antibodies (VHH), known as nanobodies, are of small size (ca. 12-15 kDa) and retain fully functional antigen-binding capacity. These domains of VHHs can be fused with fluorescent tags and subsequently expressed in living cells. These fluorescent antigen binding nanobodies or binders, which are called chromobodies, can be used to detect, trace proteins and other cellular components *in vivo* (Zolghadr et al., 2012). The convex-shaped paratope of the nanobody makes its accessibility easier in comparison with the flat paratope of monoclonal antibodies. Nanobodies are very stable and their highly soluble nature makes them easily purified on a large scale in heterologous expression systems (Conrath et al., 2001; Frenken et al., 2000; Salema & Fernandez, 2013). Their antigen binding affinities are within nanomolar range (Muyldermans & Lauwereys, 1999), possessing high stability in a wide spectrum of temperatures and showing very good resistance to chemical and thermal denaturation compared to their monoclonal counterparts (Arbabi Ghahroudi et al., 1997; Dumoulin et al., 2002; van der Linden et al., 1999). Based on the choice of the epitope, chromobodies can be used to detect endogenous factors and

dynamic events occurring in the living cell. In principle, any antigenic property including post-translational modifications or non-protein structures can be detected.

Only a single domain is involved in antigen binding, and this fragmemt (15 KDa) is fully functional. The small size, monomeric property, and versatile antigen binding properties of VHHs have made them very promising molecules for various biological applications (Chakravarty et al., 2014; De Meyer et al., 2014; Kirchhofer et al., 2010; Rothbauer et al., 2008; Tang et al., 2013). To expand our present understanding of DNA DSBs, we developed a chromobody based γ-H2AX-binder that can specifically detect histone H2AX phosphorylated in the serine at residue 139. Though the γ-H2AX binder was able to bind to the histone γ-H2AX *in vitro*, its binding specificity was uncertain *in vivo* (i.e., in the double strand break environment).

Our present study focuses on *in vitro*, *in vivo* characterization of the γ-H2AX binder and the potential pitfalls caused by endogenous and exogenous factors for detection of histones in live cells.

Materials and Methods

Quick outline for the production of chromobodies

1. An alpaca named “Anna” was immunized with γH2AX-KLH for 49 days, and the alpaca “Ferdl” was immunized with non-infective HIV-capsid protein. Sera were generated by centrifugation of blood (2000 rpm, 10 min and 4°C). The supernatant containing sera was reserved in 5 ml aliquots.
2. For the serum ELISA, 1 µg of the appropriate antigen was coated in a 96 well plate (Maxisorp, Thermo Scientific) and the serum was added in serial dilutions. Bound alpaca antibodies were further detected with HRP-conjugated anti-alpaca IgG antibody (Bethyl Laboratories).
3. The isolation of B cells was performed by with a Ficoll gradient using UNI-SEPMAXI (NOVAmed).
4. From B cells, RNA was extracted with TRIzol reagent (Life Technologies) according to the manufacturer´s protocol.
5. From this RNA, complementary DNA (cDNA) was generated using the First-Strand cDNA Synthesis Kit from GE Healthcare according to the manufacturer´s protocol.
6. VHHs were amplified by three subsequent nested PCR reactions. cDNA was used as the DNA template for the first PCR.
7. The amplified product and the plasmid vector pHEN4 was restricted with specific restriction endonucleases producing compatible overhangs to ligate.

8. Electro-competent TG1 cells (Agilent) were used to generate VHH libraries. They were transformed by electroporation with the ligation preparations performed according to the manufacturer´s protocol.

9. The transformed TG1 cells were incubated with hyperphage (Progen GmbH, Germany). The phage particles presenting the VHH library on their tips were collected.

10. Solid phase panning is a conventional method to select antibody fragments. Initially 10 µg of the antigen was coated in the immunotubes at 4°C. Phage particles were added to them and incubated for 1.5 hours at room temperature.

11. The bound phages were eluted and used for reinfection of TG1 cells, which were then used for the subsequent panning round.

A more detailed description of the above mentioned are extensively as described (Schmidthals, 2013).

Phage ELISA

Phage ELISA is a method used to select phage clones presenting antigen specific VHHs on their tips. Phage particles were prepared. Initially 1 µg of antigen was coated onto 96 well plates. After blocking the plates with 3% milk in PBS, phage particles were added to the plates coated with antigen and incubated at room temperature for 2 hours. After washing multiple times with PBST (0.05% Tween20), bound phages were detected with an anti M13-HRP antibody (GE Healthcare). This procedure as described (Schmidthals 2013)

Dot blot assay

Dot blot analysis was performed to map the epitope of an antigen specific to VHH. Firstly 2 µg of peptide or recombinant protein was spotted on nitrocellulose membrane and incubated with FITC labeled VHHs. The binding signals were obtained by scanning with a Typhoon Scanner and normalized against the background. Quantification of the signals was performed with the Image Quant software. Peptides were dissolved either in 1X PBS or DMSO. Protocol details were as described (Schmidthals, 2013).

Immunoprecipitation

For one immunoprecipitation reaction, HEK293T cells transfected with γ-H2AX binder-GFP were resuspended in lysis buffer (20 mM Tris/Cl pH7,5, 150 mM NaCl, 0.5 mM EDTA, 0.5% NP-40) plus 1 mM PMSF, 1X protease inhibitor mix (Serva), 0.5 µg/µl Dnase, and 2.5 mM $MgCl_2$. The lysed solution was centrifuged and the supernatant was diluted with dilution buffer (20 mM Tris/Cl pH 7.5, 150 mM NaCl, 0.5 mM EDTA). Then 50 µl slurry of NHS-activated sepharose beads covalently coupled with a VHH, as detailed by (Rothbauer et al., 2008), were equilibrated by washing three times with dilution buffer. HEK293T cell lysate was added to the equilibrated beads and incubated for 4 hours at 4°C. The samples were loaded in an SDS-PAGE. Details were as described (Schmidthals, 2013).

Western Blot

Proteins from SDS gels were transferred to a nitrocellulose membrane by semi-dry blotting at 240 mA. The membrane was incubated for 1 hour with 3% milk powder in Tris buffered saline with 0.075% Tween-20 (TBST) at room temperature (RT). Primary antibody anti-GFP (1:1000) and anti γ-H2AX (1:1000) were incubated in 3% milk-TBST at 4°C overnight. Secondary antibodies (1:1000) were diluted in 3% milk-TBST and incubated for 1 hour at RT. The membrane was washed with TBST and treated with ECL solution and bound protein were detected with the Typhoon scanner. Protocol were again as described (Schmidthals 2013)

Cell culture and Transfection

HeLa, HEK293, H2AX knock out, and wild-type mouse embryonic fibroblasts (MEFs) cells were obtained from A. Nussenzweig via Heindrich Leonhardt's lab-LMU as explained in Mortusewicz et al. (2008) were used. Cells were cultured at 37°C, 5% CO_2 in DMEM containing 50 µg/ml gentamicin supplemented with 10% FCS. For optimal growth cells were washed with 2 ml PBS, and 1 ml Trypsin/EDTA was added and distributed to the cell layer. After 3 min, once the cells were detached, 9 ml of DMEM was added to stop the enzymatic action of trypsin.

For live cell analysis, cells were seeded 24 hours before transfection in a µ-8 well ibidi. For fixed cell analysis, cells were grown on glass cover slips. Polyethylenimine (PEI) from Sigma, St. Louis, MO, USA with pH 7 was used to transfect the MEFs and HEK 293 cells and PEI with pH 10 was used for HeLas. Hiperfect (Qiagen GmbH, Germany) was used for the transfection of siRNAs according to the manual instructions.

Plasmids

Mammalian expression constructs of γ-H2AX binder-GFP were obtained from (Chromotek GmbH, Munich, Germany), mRFP tagged to XRCC1 (developed by Dr. Alexander Rapp), were mainly used for the studies. For cloning convenience, a small region in the C-terminus of the XRCC1 coding region was deleted by Xho enzyme and self ligated, which was used as the full length mRFP-XRCC1. The N-terminal domain of mRFP-XRCC1, which is devoid of phosphorylation sites, was obtained by removing the sequence that starts before the phosphorylation site by cutting with XmaI and then self ligated further. The phospho-mutant of the XRCC1 (CKM) was obtained from Keith Caldecott as described in (Loizou et al. 2004). The CKM mutant region of the XRCC1 was restricted with XmaI and Xho and placed into the mRFP-XRCC1 wild type version oft he construct. MDC1-GFP plasmid was obtained from Anna Friedl, LMU Munich.

Microscopy

Live cell experiments were performed using a confocal microscope. Confocal images were collected using an UltraVIEW VoX spinning disc system (Perkin Elmer) on a Nikon Ti microscope equipped with an oil immersion Plan-Apochromat x60/1.45 numerical aperture (NA) objective lens (pixel size in XY 120.45 nm/pixel) in a live-cell microscopy chamber (ACU control, Olympus) with a temperature of 37°C, 5% CO_2, and 60% humidity. For fixed cell analysis, fluorescent images were obtained from a Zeiss Axiovert 200 microscope equipped with Plan-Apochromat x63/1.4 NA oil immersion objective lens and a CCD camera Sensicam (PCO).

Irradiation experiments

In living cells, microirradiation was carried out with a 405 nm diode laser set to maximum power at 100% transmission available in the Nikon Ti spinning disc microscope. Preselected spots of ~1 μm in diameter within the nucleus were microirradiated for 1200 ms resulting in 1 mJ energy. Before and after microirradiation confocal image series were recorded. For fixed cell experiments the living cells were irradiated with an X-Ray tube (GE isovolt titan) set to 90 kV and 19 mA filtered by a 2 mm aluminium sheet prior to fixation. The dose rate was controlled by DIADOS T11003 Diagnostikdosimeter and a dose of 2 Gy was achieved by varying the distance and duration of the irradiation.

Knockdown experiments

For knockdown experiments, siRNA with the sequence of sense strand 5′-CCAGAAATCTTTATGAATAAA-3′ (Invitrogen) targeting MDC1 was used, and universal siRNA (Invitrogen) was used as a negative control. Hiperfect was used as a cationic lipid cell transfection reagent. Cells like HeLa and HEK 293 were seeded at a density of 4×10^4 cells/well in an Ibidis 100 μm eight well slide. Transfection was carried out with 20 nM MDC1 siRNA with γ-H2AX binder-GFP incubated up to 40–80 hours for knockdown.

Immunofluorescence

Cells were grown on glass coverslips, fixed in 3.7% formaldehyde for 10 minutes at room temperature (RT), and permeabilized for 20 minutes at RT in 0.5% triton/PBS. Immunofluorescence staining was performed in 4% BSA/PBS for 1 hour at RT (primary antibodies) and for 45 minutes at RT (secondary antibodies). The following primary antibodies were used: mouse anti-γ-H2AX (Clone JBW301, 1:500, Upstate), anti-MDC1 (1:100) (Sigma Aldrich Inc, St. Louis, MO, USA). For detection, the cells were stained with donkey anti-mouse Alexa 488 (Jackson Immuno Research) and goat anti-mouse Cy3 (Jackson Immuno Research). Nuclear DNA was visualized with 4,6-diamidino-2-phenylindole (DAPI) (Sigma-Aldrich) for 10 minutes. Cells were mounted in vectashield antifade (Vector Laboratories Inc).

Image analysis and quantification

For evaluation of the kinetics of the accumulation of γ-H2AX binder from microirradiation data, a minimum of 8–10 cells were analyzed. To visualize data, normalization of the raw recovery curves, and fitting curves was done by easyFRAP a matlab standalone application (Rapsomaniki et al., 2012). Raw intensities of bleached area (ROI1), the whole cell (ROI2), and a background area (ROI3) as well as the corresponding time-points are calculated using a custom made ImageJ macro made by Dr. Alexander Rapp (Kind et al., 2014). Results were saved in .csv, .txt, and .xls file formats and analyzed with easyFRAP software, which computes the recovery curves, according to the formula of double normalization and maximal accumulation representing the highest ratio from each experiment. Stepwise descriptions are explained in the manual (http://ccl.med.upatras.gr/data/uploads/easyfrap_manual.pdf). Foci of γ-H2AX/MDC1 were counted manually and confirmed with foci picker 3D, an Image J plug-in (Du et al., 2011).

Results

Outline on the development of γ-H2AX specific VHH

The outline in Figure 3.1 summarizes the main steps of the nanobody generation process. Alpacas were immunized with specific peptides following a 7 week period, RNA from lymphocytes was extracted and retrotranscribed to DNA, and the sequences corresponding to the VHH domains were amplified with specific primers for cloning into a phage display vector. This library was then separately subjected to several rounds of panning on plates coated with the antigens (peptides). VHH clones that showed strong binding activity were detected with a phage-ELISA assay, and the high affinity clones were used for further analysis. The binding ability of VHH to γ-H2AX was tested by *in vitro* methods like dot blot, immunoprecipitation and *in vivo* methods like live cell assays (Figure 3.1).

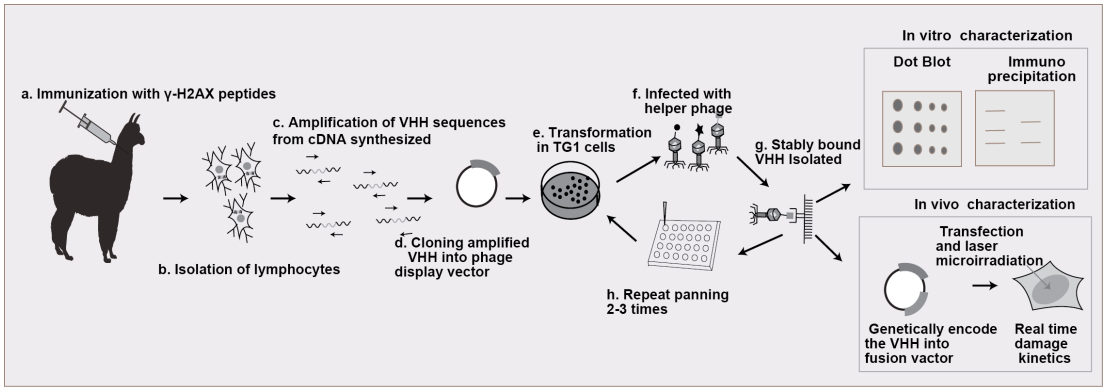

Figure 3.1. Schematic representation of alpaca derived γ-H2AX chromobody generation and application. γ-H2AX specific VHH generation, which starts from immunization of the alpacas. Production is illustrated with the intermediate steps, and further details are available in the text. The *in vitro* and *in vivo* characterization results of the γ-H2AX binder are discussed in this chapter.

Biochemical characterization of γ-H2AX binder/chrombody

The γ-H2AX binder obtained by the screening methods as described above was checked for its binding ability *in vitro* (Figure 3.2). The different VHH clones were tested *in vitro* using phage ELISA, where the titre plates were coated with γ-H2AX peptides and the phage displaying the VHH were allowed to bind to the peptides, and the stably bound phages were eluted. Clones 3, 4, and 19 were selected; the experimental results with clone 3 are shown in this chapter (Figure 3.2B). Clone 3 was picked for immunoprecipitation experiments. The cells transfected with the γ-H2AX binder-GFP were treated with 50 µg neocarcinostatin (NCS) to generate DSBs and γ-H2AX. The cell lysate containing γ-H2AX and γ-H2AX binder 3-GFP were expected to bind to each other, and they were allowed to bind to the GBP beads (Rothbauer et al., 2008). The results showed substantial binding of γ-H2AX binder 3-GFP to γ-H2AX.

For the dot blot assay (Figure 3.2C) the peptides were spotted at different concentrations on the membrane, and the purified γ-H2AX binder 3-GFP was chemically coupled to FITC, allowed to bind to the peptides, and tested for its binding affinity. The γ-H2AX peptide was coupled to a different carrier (i.e., BSA), which was used in order to check for the affinity of the binder to the carrier. The γ-H2AX binder 3-FITC showed better binding to γ-H2AX peptide-KLH than with γ-H2AX peptide-BSA. For this reason, the immunization was performed with γ-H2AX peptide-KLH which has some degree of specificity generated to KLH.

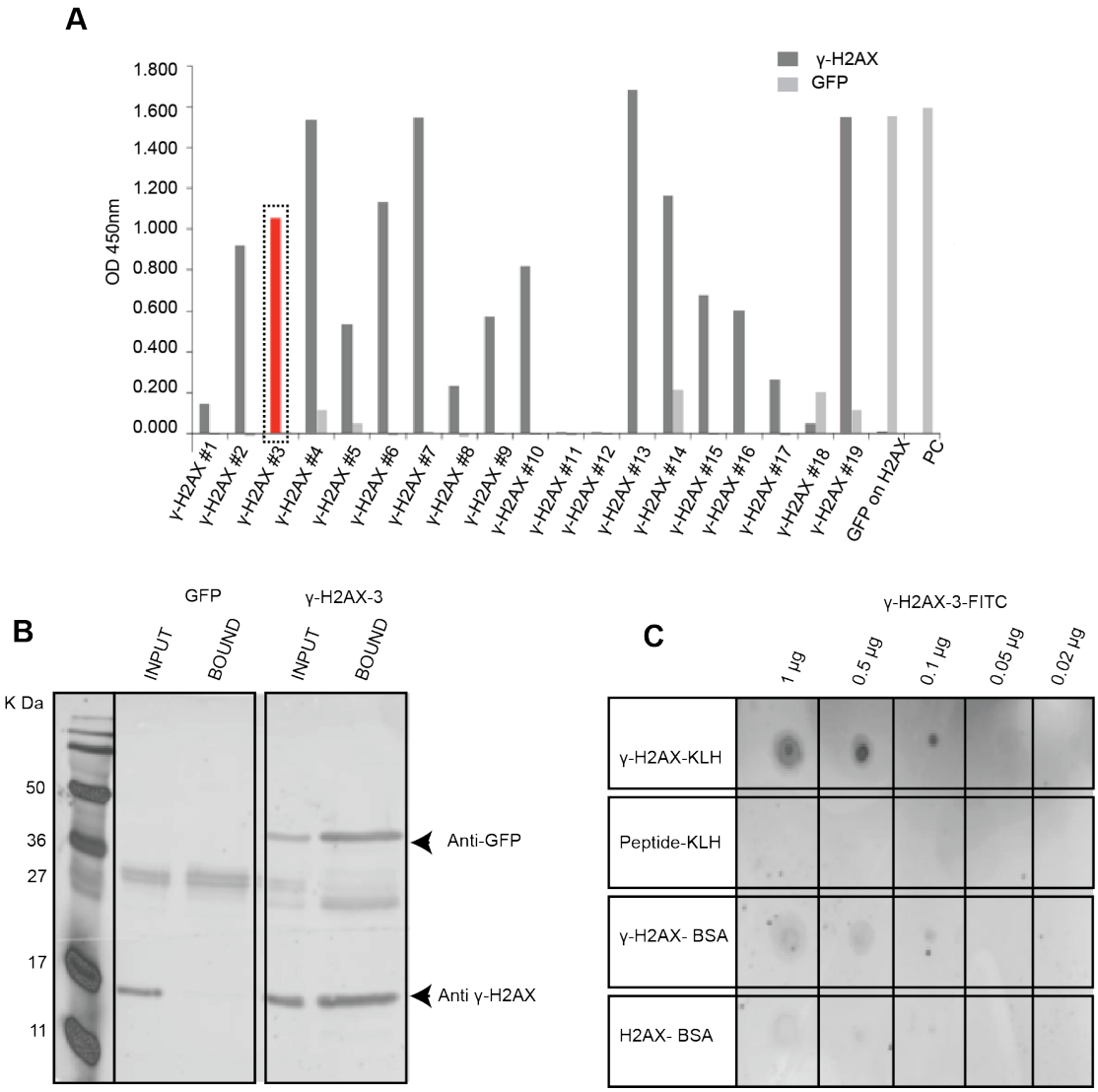

Figure 3.2 *In vitro* characterization of γ-H2AX binder. (A) Phage ELISA after three rounds of panning are shown. In the experiment, wells were coated with γ-H2AX peptide and γ-H2AX binder displaying phage was used. As a positive control (PC) the HIV protein was coated, and HIV binder displaying phage were used. GFP on H2AX represents GFP protein coated and γ-H2AX binder, and GFP binder displaying phage were allowed to bind. The amount of specifically bound phage particles are found by measuring the absorbance at a wavelength of 450 nm. γ-H2AX binder 3 highlighted in red was used for subsequent analysis steps. (B) For immunoprecipitation experiments, cells expressing γ-H2AX binder 3-GFP and GFP alone were treated with NCS. After cell lysis, the extract was incubated with the GBP bound beads (Rothbauer et al., 2008). The bound fraction was loaded seperately, and protein amounts used for this interaction determination assay were loaded as input control and visualized by western blotting with anti-GFP and anti-γ-H2AX. (C) In the dot blot assay, γ-H2AX binder 3-FITC was allowed to get bound to the multiple concentration of γ-H2AX peptide-KLH, γ-H2AX peptide-BSA, control peptide, and H2AX was spotted on the membrane. γ-H2AX binder 3-FITC bound better to γ-H2AX peptide-KLH than to γ-H2AX peptide-BSA (data obtained from Chromotek GmbH).

In vivo characterization of γ-H2AX binder

The γ-H2AX binder was tested for its ability to mark DNA double strand breaks in living cells (Figure 3.3). Here we wanted to mark the phosphorylation event that occurs on the histone H2AX after the DNA double strand breaks.

Initially, the cells were transfected with γ-H2AX binder and irradiated with the 405 nm laser, which has been shown to create different types of DNA damage as explained by Muster (2014). As there was no recruitment pattern of γ-H2AX binder observed at the sites of DNA damage, XRCC1, (X-Ray cross complementing protein 1) was co-transfected along with the γ-H2AX binder and then microirradiated. XRCC1, (X-Ray cross complementing protein 1) a loading protein (Mortusewicz & Leonhardt, 2007) involved in base excision and single strand break repair in mammalian cells was used with the aim to aid its recruitment. Recruitment of γ-H2AX binder was observed in the presence of the XRCC1 at the microirradiated sites.

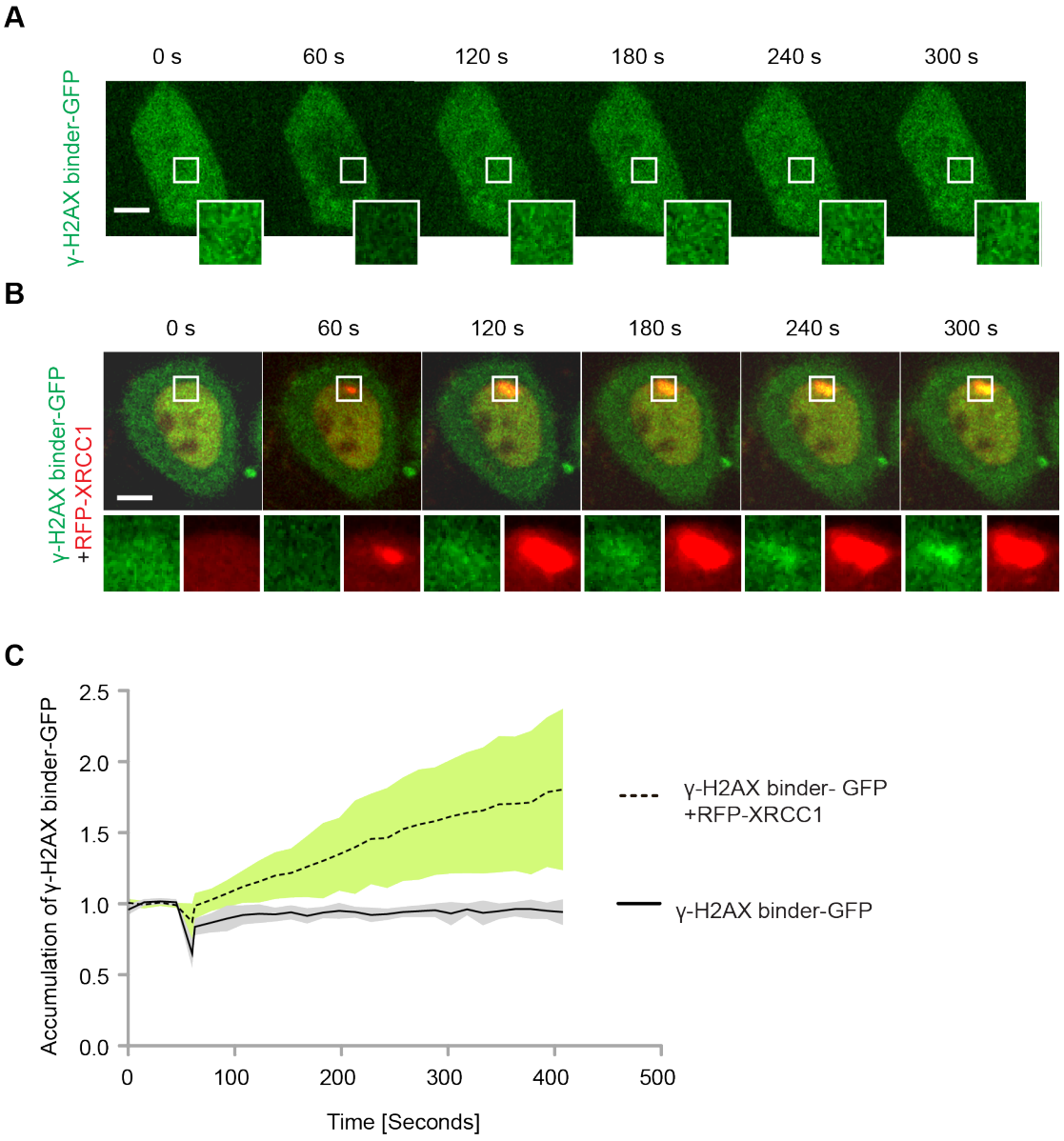

Figure 3.3. γ-H2AX binder's specificity in living cells. (A) Cells were transfected with γ-H2AX binder and were microirradiated with a 405 nm laser, and no recruitment was observed. (B) Cells co-transfected with XRCC1 showed the recruitment of the γ-H2AX binder 3. (C) Kinetics of the recruitment of the γ-H2AX binder in the presence and absence of XRCC1 is shown. Experiments were performed with HeLa and HEK 293 cell lines and both showed similar effects. Mean values were plotted and the error bar (shaded) denotes standard deviation. The scale bar represents 5 µm.

To check if XRCC1 overexpression only aids the binding of γ-H2AX binder to the target or has a role in altering its specificity, similar experiments were performed in the H2AX knockout MEF cell lines (Figure S1), where XRCC1 unexpectedly triggered the unspecific recruitment of γ-H2AX binder at the sites of irradiation. Based on these findings two potential questions arise in the *in vivo* characterization. Why is the γ-H2AX chromobody/binder recruited when co-expressed with the XRCC1? Why the γ-H2AX chromobody/binder cannot get recruited at the sites of double strand breaks in the living cell on its own?

Alternative epitope recognition of γ-H2AX binder

In order to determine why the binder is recruited in the presence of the over expressed XRCC1, mutants of XRCC1 were developed. XRCC1 has been found to have multiple phospho sites (Figure S2A) whose serine residues are phosphorylated by CK2 (Casein Kinase II), a highly conserved protein serine/threonine kinase. The mutants of XRCC1 were obtained by first mutating the linker region between BRCT1 and BRCT2 domains, and then the N-terminal domain deletion mutant was obtained by deleting the linker region containing the phospho sites and the BRCT2 domain in the C-terminus.

All these mutants were compared with the full length XRCC1 as shown in Figure 3.4. The mutants were thus developed with the aim of providing a contingency if XRCC1's multiple phospho sites were misrecognized by γ-H2AX binder instead of recognising the unique phospho site in S(p)Q motif available in the γ-H2AX histone at the sites of DNA DSBs. From the results, the mutants showed mild difference in the recruitment of the γ-H2AX binder, the recruitment of the γ-H2AX binder was reduced slightly in the presence to XRCC1-CKM mutant when compared to XRCC1 full length. The γ-H2AX binder recruitment was abolished completely with respect to XRCC1-NTD mutant.

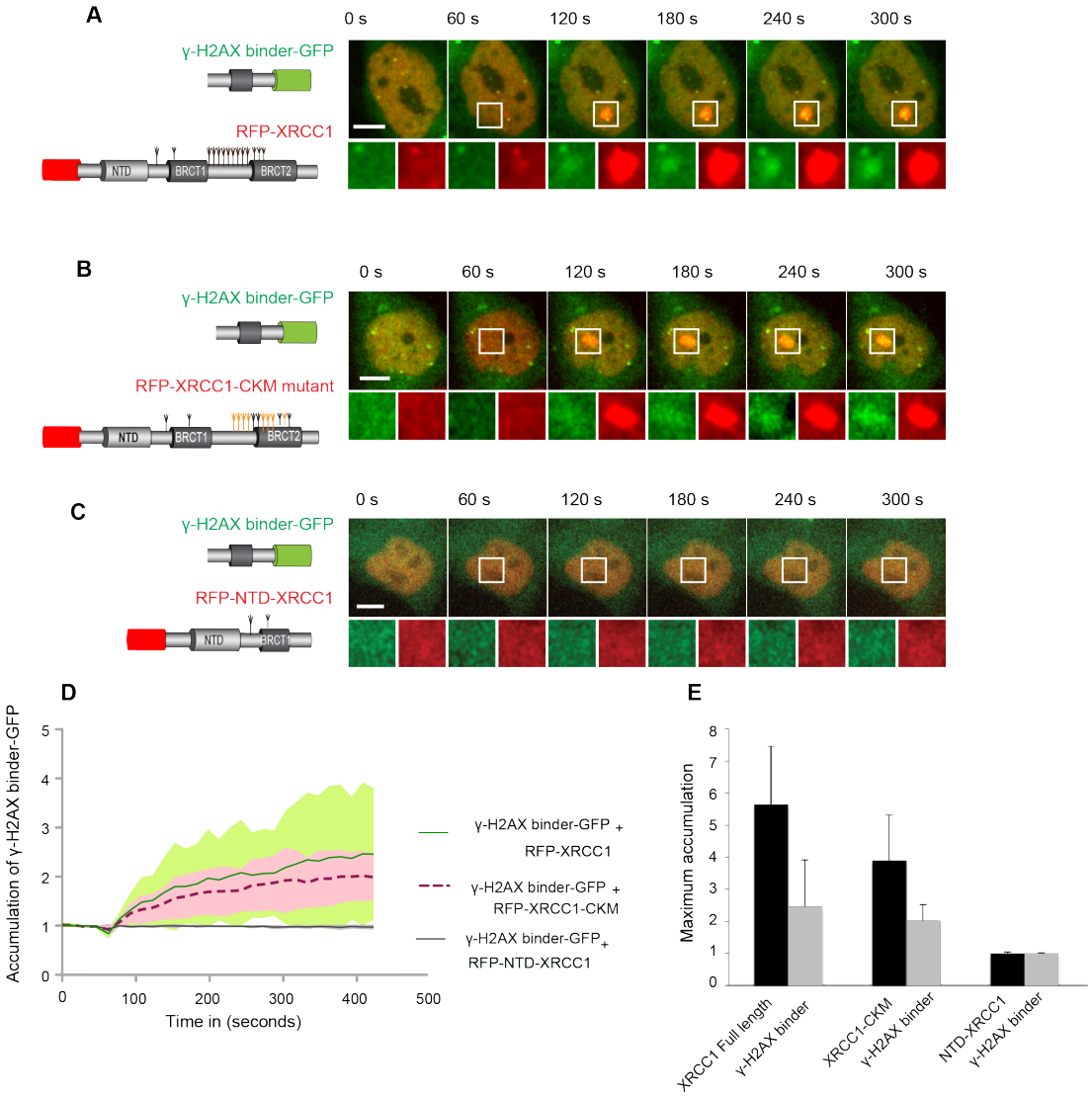

Figure 3.4. Efficiency of alternative epitope recognition (A) Cells co-transfected with XRCC1-full length showed strong recruitment of the γ-H2AX binder 3. (B) Cells co-transfected with XRCC1-CKM mutant showed less recruitment of the γ-H2AX binder. (C) Cells co-transfected with XRCC1-NTD showed no recruitment of the γ-H2AX binder 3. (D) Kinetics of the recruitment of the γ-H2AX binder in the presence of multiple versions of XRCC1 are shown. Shaded error bar represents standard deviation. (E) Maximum accumulation of the γ-H2AX binder is provided along with the maximum accumulation of multiple XRCC1 mutants. The error bar represents standard deviation, and the scale bar represents 5 μm.

Epitope (γ-H2AX) unmasking studies for better epitope recognition

When the γ-H2AX binder did not recognize the phosphorylated histone H2AX, we hypothesized that the epitope to be recognized may have been masked by other cellular proteins. Hence MDC1 (Mediator of DNA damage checkpoint protein 1), a protein that binds to H2AX (Figure 3.5A, S3), was knocked down to determine if this improves epitope recognition for the γ-H2AX binder. HEK 293 cells were knocked down with MDC1 siRNA, the knockdown of MDC1 was checked by immunostaining the cells at different time intervals, specifically at the 40 and 80 hours (Figure S4). Around 72 hours, the siRNA treated cells

were microirradiated with a 405 nm laser. Mild recruitment of the γ-H2AX binder was achieved at the irradiated sites in MDC1 siRNA treated cells but not in the control siRNA cells (Figure 3.5B, C).

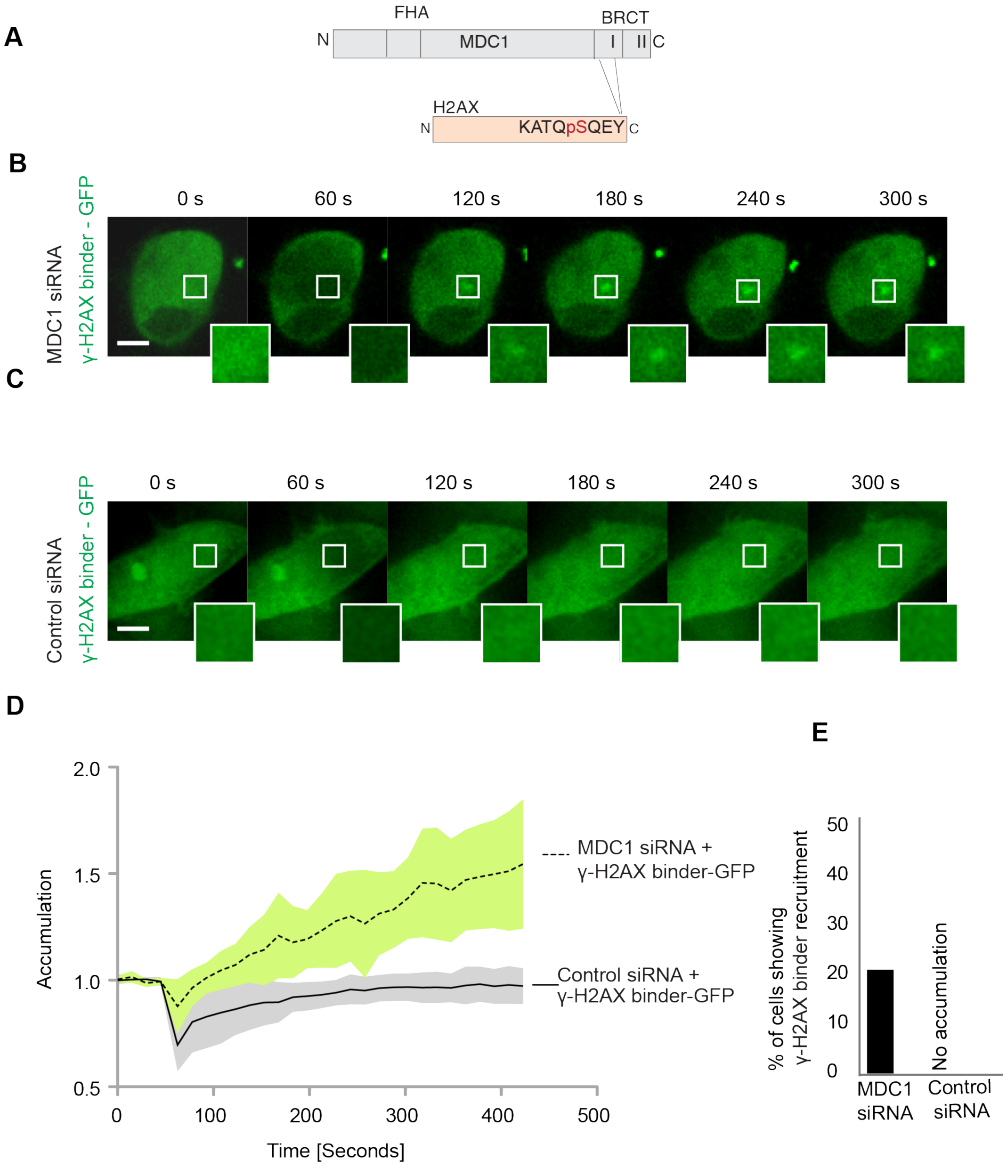

Figure 3.5. Epitope unmasking by knocking down MDC1. (A) MDC1 binds to the tyrosine at the 142nd residue of phosphorylated H2AX. (B) Cells knocked down for MDC1 with its respective siRNA showed the recruitment of γ-H2AX binder upon microirradiation. (C) Cells mock transfected with control siRNA showed no recruitment. (D) Kinetics of the recruitment of the γ-H2AX binder in the presence of MDC1 siRNA and control siRNA is shown. Shaded error bar represents standard deviation. Experiments were performed in HEK 293 cell lines. (E) The percentage of cells that showed γ-H2AX binder recruitment with MDC1 siRNA and control siRNA is shown. The scale bar represents 5 μm.

Discussion

It has been shown that γ-H2AX binder can bind efficiently to the phosphorylated histone H2AX *in vitro*; however, the *in vivo* binding ability was challenged by some factors such as alternative epitope recognition (i.e., XRCC1) and endogenous epitope masking factor (i.e., MDC1). In order to determine if the binder recruitment to the desired epitope is enhanced by XRCC1 or if it is misleading the protein to some other site, the binder was cotransfected with XRCC1 in H2AX knock out and wildtype MEFs cells, where we observed the recruitment of the binder, which strictly should not recruit the γ-H2AX binder (Figure S1). This shows the unspecificity or alternative epitope recognition problem of the chromobody. However, from the mutation experiment results maximal accumulation of the γ-H2AX binder depends on the increased XRCC1 accumulation. Hence it could be concluded that the binder's recruitment is propotional to the XRCC1 accumulation and XRCC1 recruitment is slightly affected by the phospho site mutation and completely affected by the deletion mutation. This explains how the binder could possibly recognize XRCC1 alternatively. The phospho sites in XRCC1 may possibly not be solely responsible for misrecruitment of the binder but that the *in vivo* structural conformation of XRCC1 have several sites for repair proteins to be bound thus triggering such recruitment (Cuneo et al., 2011).

It has been shown that MDC1 binds to the tyrosine at the 142nd residue of the phosphorylated histone H2AX, (Stucki et al., 2005). It is well known that the molecular weight of MDC1 is ~250 kDa. MDC1 facilitates the binding of repair proteins and initiates the cascade of the DNA repair process (Stewart et al., 2003; Xu & Stern, 2003). Its ability to bind to the histone H2AX is described in the Figure S3. This leads us to the hypothesis that the size of MDC1 is huge and could potentially mask the site needed for free accessibility of the the γ-H2AX binder. Hence knocking down of MDC1 was proposed, and this lead to the successful recruitment of the binder at the irradiated sites. However, when MDC1 was knocked down there was a mild decrease in the γ-H2AX foci numbers (Figure S4B), which shows that MDC1 is critical for γ-H2AX formation at high densities near DSB (Savic et al., 2009) and also indicates why γ-H2AX binder recruitment is so low at the irradiated sites in the MDC1 knockdown cells.

References

Adams, A. E. M., Botstein, D., & Drubin, D. G. (1989). A Yeast Actin-Binding Protein Is Encoded by Sac6, a Gene Found by Suppression of an Actin Mutation. *Science, 243*(4888), 231-233.

Arbabi Ghahroudi, M., Desmyter, A., Wyns, L., Hamers, R., & Muyldermans, S. (1997). Selection and identification of single domain antibody fragments from camel heavy-chain antibodies. *FEBS Lett, 414*(3), 521-526.

Chakravarty, R., Goel, S., & Cai, W. (2014). Nanobody: the "magic bullet" for molecular imaging? *Theranostics, 4*(4), 386-398.

Conrath, K. E., Lauwereys, M., Galleni, M., Matagne, A., Frere, J. M., Kinne, J., Wyns, L., & Muyldermans, S. (2001). Beta-lactamase inhibitors derived from single-domain antibody fragments elicited in the camelidae. *Antimicrob Agents Chemother, 45*(10), 2807-2812.

Cuneo, M. J., Gabel, S. A., Krahn, J. M., Ricker, M. A., & London, R. E. (2011). The structural basis for partitioning of the XRCC1/DNA ligase III-alpha BRCT-mediated dimer complexes. *Nucleic Acids Res, 39*(17), 7816-7827.

De Meyer, T., Muyldermans, S., & Depicker, A. (2014). Nanobody-based products as research and diagnostic tools. *Trends Biotechnol, 32*(5), 263-270.

Du, G., Drexler, G. A., Friedland, W., Greubel, C., Hable, V., Krucken, R., Kugler, A., Tonelli, L., Friedl, A. A., & Dollinger, G. (2011). Spatial dynamics of DNA damage response protein foci along the ion trajectory of high-LET particles. *Radiat Res, 176*(6), 706-715.

Dumoulin, M., Conrath, K., Van Meirhaeghe, A., Meersman, F., Heremans, K., Frenken, L. G., Muyldermans, S., Wyns, L., & Matagne, A. (2002). Single-domain antibody fragments with high conformational stability. *Protein Sci, 11*(3), 500-515.

Frenken, L. G., van der Linden, R. H., Hermans, P. W., Bos, J. W., Ruuls, R. C., de Geus, B., & Verrips, C. T. (2000). Isolation of antigen specific llama VHH antibody fragments and their high level secretion by Saccharomyces cerevisiae. *J Biotechnol, 78*(1), 11-21.

Hamers-Casterman, C., Atarhouch, T., Muyldermans, S., Robinson, G., Hamers, C., Songa, E. B., Bendahman, N., & Hamers, R. (1993). Naturally occurring antibodies devoid of light chains. *Nature, 363*(6428), 446-448.

Kind, B., Muster, B., Staroske, W., Herce, H. D., Sachse, R., Rapp, A., Schmidt, F., Koss, S., Cardoso, M. C., & Lee-Kirsch, M. A. (2014). Altered spatio-temporal dynamics of RNase H2 complex assembly at replication and repair sites in Aicardi-Goutieres syndrome. *Hum Mol Genet, 23*(22), 5950-5960.

Kirchhofer, A., Helma, J., Schmidthals, K., Frauer, C., Cui, S., Karcher, A., Pellis, M., Muyldermans, S., Casas-Delucchi, C. S., Cardoso, M. C., Leonhardt, H., Hopfner, K. P., & Rothbauer, U. (2010). Modulation of protein properties in living cells using nanobodies. *Nature Structural & Molecular Biology, 17*(1), 133-U162.

Loizou, J. I., El-Khamisy, S. F., Zlatanou, A., Moore, D. J., Chan, D. W., Qin, J., Sarno, S., Meggio, F., Pinna, L. A., & Caldecott, K. W. (2004). The protein kinase CK2 facilitates repair of chromosomal DNA single-strand breaks. *Cell, 117*(1), 17-28.

Mortusewicz, O., & Leonhardt, H. (2007). XRCC1 and PCNA are loading platforms with distinct kinetic properties and different capacities to respond to multiple DNA lesions. *BMC Mol Biol, 8*, 81.

Mortusewicz, O., Roth, W., Li, N., Cardoso, M. C., Meisterernst, M., & Leonhardt, H. (2008). Recruitment of RNA polymerase II cofactor PC4 to DNA damage sites. *J Cell Biol, 183*(5), 769-776.

Muster, B. (2014). DNA repair and chromatin. *[Online-Edition:* http://tuprints.ulb.tu-darmstadt.de/id/eprint/3989*] TU Darmstadt*.

Muyldermans, S., & Lauwereys, M. (1999). Unique single-domain antigen binding fragments derived from naturally occurring camel heavy-chain antibodies. *J Mol Recognit, 12*(2), 131-140.

Rapsomaniki, M. A., Kotsantis, P., Symeonidou, I. E., Giakoumakis, N. N., Taraviras, S., & Lygerou, Z. (2012). easyFRAP: an interactive, easy-to-use tool for qualitative and quantitative analysis of FRAP data. *Bioinformatics, 28*(13), 1800-1801.

Rogakou, E. P., Pilch, D. R., Orr, A. H., Ivanova, V. S., & Bonner, W. M. (1998). DNA double-stranded breaks induce histone H2AX phosphorylation on serine 139. *J Biol Chem, 273*(10), 5858-5868.

Rothbauer, U., Zolghadr, K., Muyldermans, S., Schepers, A., Cardoso, M. C., & Leonhardt, H. (2008). A versatile nanotrap for biochemical and functional studies with fluorescent fusion proteins. *Molecular & Cellular Proteomics, 7*(2), 282-289.

Rothbauer, U., Zolghadr, K., Tillib, S., Nowak, D., Schermelleh, L., Gahl, A., Backmann, N., Conrath, K., Muyldermans, S., Cardoso, M. C., & Leonhardt, H. (2006). Targeting and tracing antigens in live cells with fluorescent nanobodies. *Nat Methods, 3*(11), 887-889.

Salema, V., & Fernandez, L. A. (2013). High yield purification of nanobodies from the periplasm of E. coli as fusions with the maltose binding protein. *Protein Expr Purif, 91*(1), 42-48.

Savic, V., Yin, B., Maas, N. L., Bredemeyer, A. L., Carpenter, A. C., Helmink, B. A., Yang-Iott, K. S., Sleckman, B. P., & Bassing, C. H. (2009). Formation of dynamic gamma-H2AX domains along broken DNA strands is distinctly regulated by ATM and MDC1 and dependent upon H2AX densities in chromatin. *Mol Cell, 34*(3), 298-310.

Schmidthals, K. (2013). Generation and characterization of heavy chain antibodies derived from Camelids. . *LMU München: Faculty of Biology*.

Sharma, A., Singh, K., & Almasan, A. (2012). Histone H2AX phosphorylation: a marker for DNA damage. *Methods Mol Biol, 920*, 613-626.

Stewart, G. S., Wang, B., Bignell, C. R., Taylor, A. M. R., & Elledge, S. J. (2003). MDC1 is a mediator of the mammalian DNA damage checkpoint. *Nature, 421*(6926), 961-966.

Stucki, M., Clapperton, J. A., Mohammad, D., Yaffe, M. B., Smerdon, S. J., & Jackson, S. P. (2005). MDC1 directly binds phosphorylated histone H2AX to regulate cellular responses to DNA double-strand breaks. *Cell, 123*(7), 1213-1226.

Tang, J. C. Y., Szikra, T., Kozorovitskiy, Y., Teixiera, M., Sabatini, B. L., Roska, B., & Cepko, C. L. (2013). A Nanobody-Based System Using Fluorescent Proteins as Scaffolds for Cell-Specific Gene Manipulation. *Cell, 154*(4), 928-939.

van der Linden, R. H., Frenken, L. G., de Geus, B., Harmsen, M. M., Ruuls, R. C., Stok, W., de Ron, L., Wilson, S., Davis, P., & Verrips, C. T. (1999). Comparison of physical chemical properties of llama VHH antibody fragments and mouse monoclonal antibodies. *Biochim Biophys Acta, 1431*(1), 37-46.

Xu, X., & Stern, D. F. (2003). NFBD1/MDC1 regulates ionizing radiation-induced focus formation by DNA checkpoint signaling and repair factors. *FASEB J, 17*(13), 1842-1848.

Zolghadr, K., Gregor, J., Leonhardt, H., & Rothbauer, U. (2012). Case study on live cell apoptosis-assay using lamin-chromobody cell-lines for high-content analysis. *Methods Mol Biol, 911*, 569-575.

Supplementary information

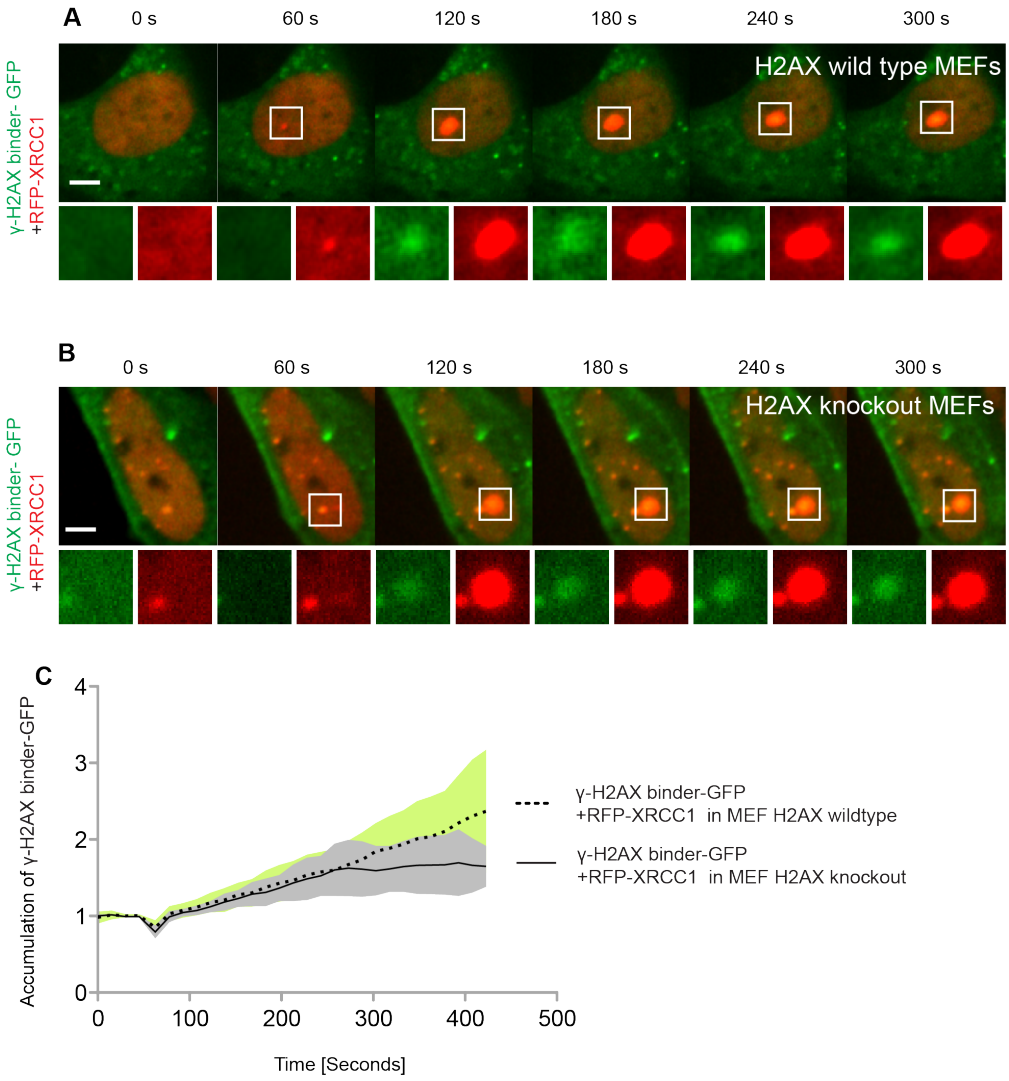

Figure S1. Validation of alternative epitope recognition (A) H2AX wild type cells co-transfected with γ -H2AX binder and XRCC1 were microirradiated with 405 nm laser and the recruited is shown (B) H2AX knockout cell lines showed similar recruitment patterns. (C) Maximum accumulation kinetics of the chromobody in knockout cells in the presence of XRCC1 is shown. Mean values were plotted and the error bar(shades) represents the standard deviation. Scale bar represents 5 µm.

A

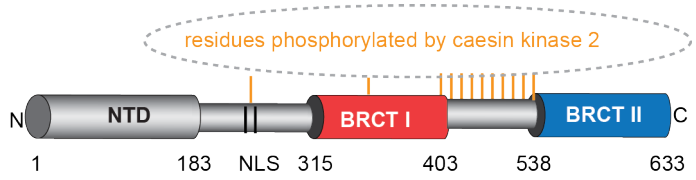


```
  1 MPEIRLRHVV SCSSQDSTHC AENLLKADTY RKWRAAKAGE KTISVVLQLE KEEQIHSVDI 60
 61 GNDGSAFVEV LVGSSAGGAG EQDYEVLLVT SSFMSPSESR SGSNPNRVRM FGPDKLVRAA 120
121 AEKRWDRVKI VCSQPYSKDS PFGLSFVRFH SPPDKDEAEA PSQKVTVTKL GQFRVKEEDE 180
181 SANSLRPGAL FFSRINKTSP VTASDPAGPS YAAATLQASS AASSASPVSR AIGSTSKPQE 240
241 SPKGKRKLDL NQEEKKTPSK PPAQLSPSVP KRPKLPAPTR TPATAPVPAR AQGAVTGKPR 300
301 GEGTEPRRPR AGPEELGKIL QGVVVVLSGF QNPFRSELRD KALELGAKYR PDWTRDSTHL 360
361 ICAFANTPKY SQVLGLGGRI VRKEWVLDCH RMRRRLPSRR YLMAGPGSSS EEDEASHSGG 420
421 SGDEAPKLPQ KQPQTKTKPT QAAGPSSPQK PPTPEETKAA SPVLQEDIDI EGVQSEGQDN 480
481 GAEDSGDTED ELRRVAEQKE HRLPPGQEEN GEDPYAGSTD ENTDSEEHQE PPDLPVPELP 540
541 DFFQGKHFFL YGEFPGDERR KLIRYVTAFN GELEDYMSDR VQFVITAQEW DPSFEEALMD 600
601 NPSLAFVRPR WIYSCNEKQK LLPHQLYGVV PQA
```

B

Unique phospho sites of XRCC1 and H2AX

```
H2AC       MSG--RGKQGGKARAKAKSRSSRAGLQFPVGRVHRLLR--(84)--PKKTESH-KAKSK---------- 129
H2A.J      MSG--RGKQGGKVRAKAKSRSSRAGLQFPVGRVHRLLR--(84)--PKKTESQ-KTKSK---------- 129
H2AD       MSG--RGKQGGKARAKAKTRSSRAGLQFPVGRVHRLLR--(84)--PKKTESHHKAKGK---------- 130
H2AE       MSG--RGKQGGKARAKAKTRSSRAGLQFPVGRVHRLLR--(84)--PKKTESHHKAKGK---------- 130
H2Al       MSG--RGKQGGKARAKAKTRSSRAGLQFPVGRVHRLLR--(84)--PKKTESHHKAKGK---------- 130
H2AG       MSG--RGKQGGKARAKAKTRSSRAGLQFPVGRVHRLLR--(84)--PKKTESHHKAKGK---------- 130
H2am       MSG--RGKQGGKARAKAKTRSSRAGLQFPVGRVHRLLR--(84)--PKKTESHHKAKGK---------- 130
H2AI       MSG--RGKQGGKARAKAKTRSSRAGLQFPVGRVHRLLR--(84)--PKKTESHHKAKGK---------- 130
H2A.2-A    MSG--RGKQGGKARAKAKSRSSRAGLQFPVGRVHRLLR--(84)--PKKTESHHKAKGK---------- 130
H2A.X      MSG--RGKTGGKARAKAKSRSSRAGLQFPVGRVHRLLR--(84)--PKKTSATVGPKAPSGGKKATQASQEY 143
H2A.Z      MAGGKAGKDSGKAKTKAVSRSQRAGLQFPVGRIHRHLK--(87)-- GKKGQQKTV----------------128
```

Figure S2. Mapping of phospho sites. (A) Phosphorylated sites of XRCC1 mapped was using phosphosite mapper in N-terminal, BRCT I, BRCTI, II domain (http://www.phosphosite.org/homeAction.do). (B) SQ motif in KATQASQEY sequence highlighted uniqueness of histone H2AX than other H2A variants found by aligning H2A variants using CLUSTAL 2.1 multiple sequence alignment various.

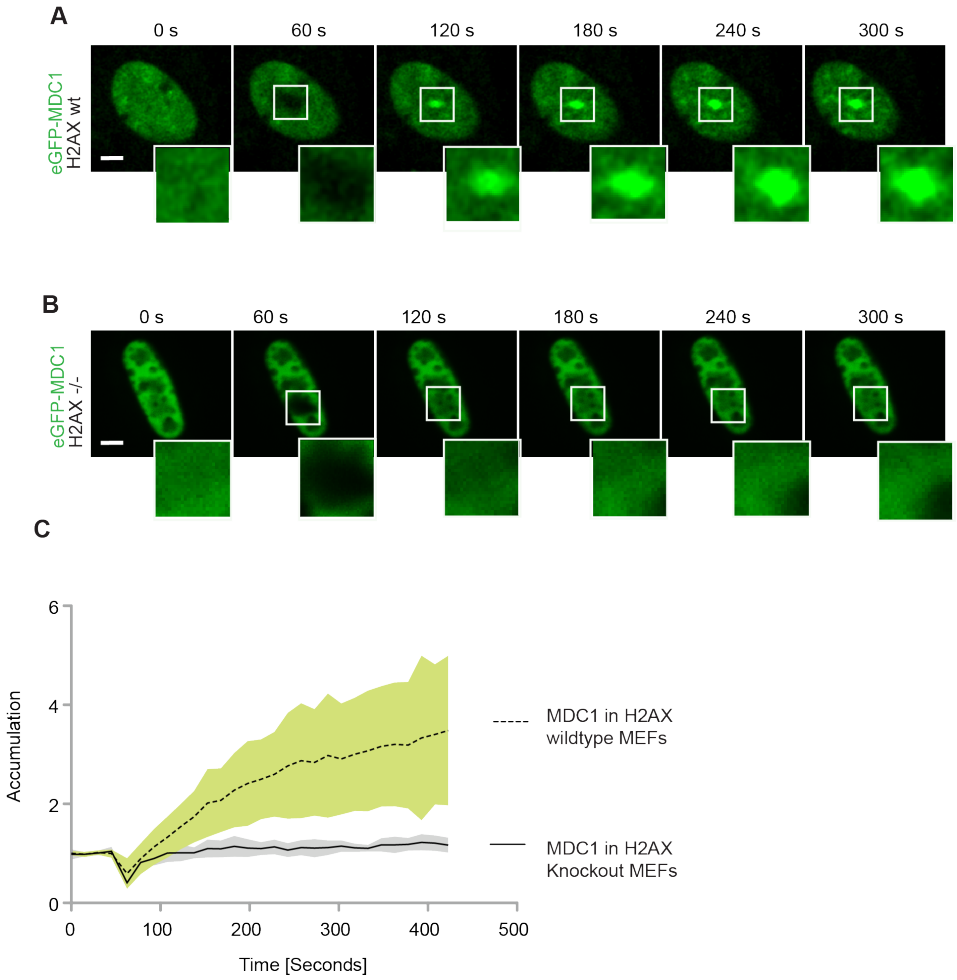

Figure S3. MDC1 binding to DNA double strand breaks depends on H2AX. (A) H2AX wild type MEF cells transfected with MDC1-GFP were microirradiated and showed recruitment. (B) H2AX knock out cells transfected with MDC1-GFP were microirradiated and showed no recruitment. (C) Mean values were plotted and the error bar (shaded) represents the standard deviation. Scale bar represents 5 µm.

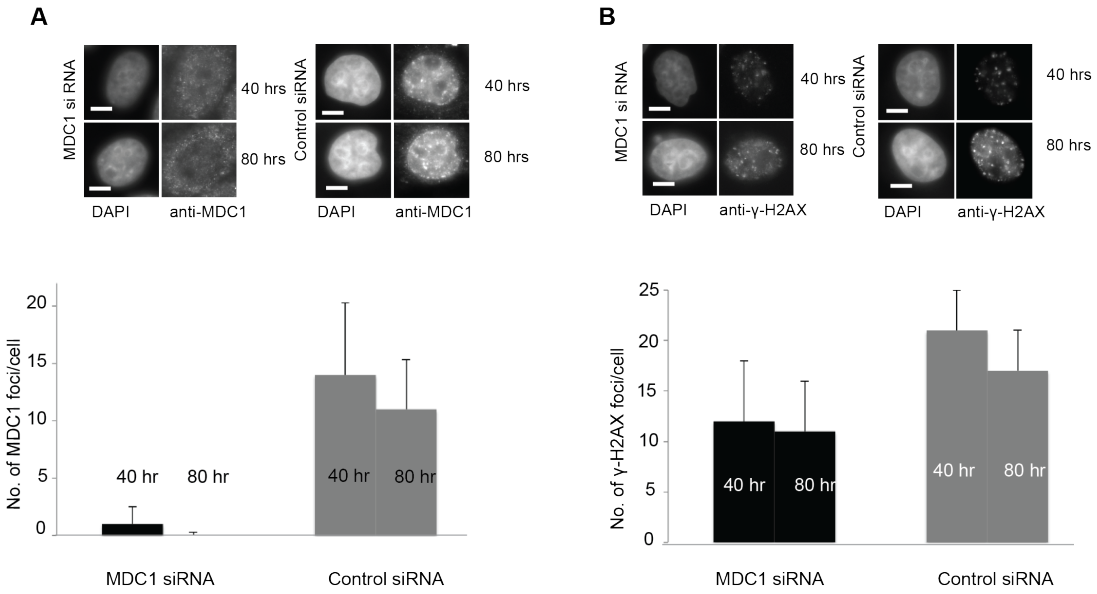

Figure S4. Confirmation of MDC1 knockdown behaviour. (A) MDC1 knockdown was validated by immunostaining for MDC1 and the corresponding MDC1 foci were counted in MDC1 siRNA knockdown cells and the control siRNA cells. They were measured at different time points after irradiating them with 2 Gy X-Rays. (B) γ -H2AX foci were counted corresponding to the MDC1/control knockdown. Scale bar 5 µm.

3.2. A novel cell permeable DNA replication and repair marker

This chapter has the following major contributors

Henry D. Herce[1*], Malini Rajan[1*], Gisela Lättig-Tünnemann[2], Marion Fillies[2], and M. Cristina Cardoso[1]

1- Department of Biology, Technische Universität Darmstadt, Germany

2- Charité-Universitätsmedizin, Berlin, Germany

*- Equaly contributing first authors

The content in this chapter was published in Nucleus 2014

Herce HD*, **Rajan M***, Lattig-Tunnemann G, Fillies M, Cardoso MC.,
"A novel cell permeable DNA replication and repair marker." Nucleus 2014; 5. [Epub ahead of print] *equally contributing authors.

Abstract

Proliferating **C**ell **N**uclear **A**ntigen (PCNA) is a key protein in DNA replication and repair. The dynamics of replication and repair in live cells is usually studied introducing translational fusions of PCNA. To obviate the need for transfection and bypass the problem of difficult to transfect and/or short lived cells, we have now developed a cell permeable replication/repair marker. The design of this marker has three essential molecular components: (a) an optimized artificial PCNA binding peptide; (b) a cell-penetrating peptide, derived from the HIV-1 Trans Activator of Transcription (TAT); (c) an *in vivo* cleavable linker, linking the two peptides. The resulting construct was taken up by human, hamster and mouse cells within minutes of addition to the media. Inside the cells, the cargo separated from the vector peptide and bound PCNA effectively. Both replication and repair sites could be directly labeled in live cells making it the first *in vivo* cell permeable peptide marker for these two fundamental cellular processes. Concurrently, we also introduced a quick peptide based PCNA staining method as an alternative to PCNA antibodies for immunofluorescence applications. In summary, we present here a versatile tool to instantaneously label repair and replication processes in fixed and live cells.

Highlights

- PL peptide can quickly mark the PCNA in fixed cells thus alleviating the need for antibodies.
- TAT-S-S-PL-R can directly label PCNA in living cells.
- Introduction of disulphide bridge inbetween the carrier (TAT) and the binder (PL) facilitated the binding of the PL to PCNA.
- This PCNA biomarker is successfully tried in multiple species.

Introduction

DNA replication and repair are the most fundamental biological processes in any known organism. Several factors have been evolved to control the fidelity and efficiency of these processes. Deregulation of any these processes can lead to several fatal diseases such as cancer.

Proliferating cell nuclear antigen (PCNA) is a central molecule at the crossroads of DNA replication and DNA repair. Its functions include also other vital epigenetic cellular processes, such as chromatin remodeling, sister-chromatid cohesion and cell cycle control (Gorisch et al., 2008; Maga & Hubscher, 2003). It has been even suggested that PCNA could be the main protein that executes ‘‘decisions’’ made by p53 (Paunesku et al., 2001). Its importance is strongly highlighted by its structural and sequence homology between distantly evolved organisms such as plants and animals.

Structurally, PCNA forms a homotrimer that encircles DNA forming a sliding clamp (Figure 1A) that functions as a loading platform directly interacting in this way with several proteins involved in DNA replication and repair (Fan et al., 2004). This platform slides along DNA increasing the processivity of DNA polymerase delta during DNA synthesis (Bravo et al., 1987). One important PCNA interaction partner is the tumor suppressor protein $p21^{WAF1}$ (p21). This protein controls tumor progression by inhibiting cyclin dependent kinases (CDKs) and directly binding to PCNA (Trimis et al., 2008). The C terminus of p21, responsible for its direct binding to PCNA, is well conserved among several PCNA binding partners. However, it is believed that p21 inhibits or disrupts cell cycle progression by having a higher PCNA binding affinity and competitively inhibiting the binding of other PCNA-interacting partners required for DNA replication. This hypothesis has led to the development of several PCNA binding peptides inspired in the C terminus of p21. It has been shown that synthetic peptides derived from p21 can arrest cell-cycle progression and even kill cancer cells (Ball et al., 1997; Gartel & Tyner, 2002; Tunnemann et al., 2006; Warbrick et al., 1995).

During S phase and DNA damage repair, PCNA is co-localized with sites of active DNA synthesis. During DNA damage repair, the excised DNA is resynthesized with the help of PCNA (Cardoso et al., 1993). The development of cell proliferation biomarkers in recent years has provided a much deeper understanding of these processes and has led to new clinical tools. Currently, there are two microscopy based approaches commonly used to visualize the PCNA in replication/repair: (a) immunofluorescence in fixed cells and (b) transfecting fluorescent fusions of PCNA in living cells.

Tumor growth correlates with an increase of PCNA levels. Immunostaining is commonly used to quantify the expression of PCNA in tissue as a diagnostic tool. A potential pitfall in quantifying the levels of PCNA to diagnose tumor growth is that these levels also increase

during DNA repair. Therefore, the results of these tests can be easily altered by everyday natural factors such as sun exposure, which leads to UV induced DNA damage and other skin lesions.

Immunostaining methods cannot be performed directly in live cells as it requires cellular fixation and permeabilization. Live cell studies, on the other hand, currently require the transfection of cells with fluorescent fusions of PCNA thereby visualizing the replication foci (Cardoso et al., 1997). These replication foci form patterns that undergo changes in individual cells throughout S-phase characterizing different stages of DNA synthesis as shown in Figure 1B. If DNA is damaged using laser microirradiation, the repair sites can also be detected by looking at the accumulation of recruited PCNA to the damaged sites as shown in Figure 1C. Successful markers for cell cycle analysis have already made use of these DNA constructs expressing PCNA fluorescent fusion tags (Easwaran et al., 2005). A critical limitation of this approach is that cells need to be expressing the fluorescently labeled PCNA fusion protein. This causes a time delay and is not possible or efficient in primary cells or otherwise difficult to transfect cells.

Here we present the design of an instantaneous live cell replication and repair marker. This design is based on three key components: (a) a high affinity PCNA interacting peptide (PIP), (b) a cell-penetrating peptide (CPP) to transport the PIP into the cells, and (c) an intracellular cleavable linker between the two peptides, so that the PIP can get uncoupled from the CPP after reaching the interior of the cells. We first present the rationale of the peptide design. Then we show its uptake in live mammalian cells instantaneously labeling repair and replication sites.

Material and methods

Peptides

Peptides used for this study (Table 3.1) were synthesized by Biosyntan GmbH (Berlin, Germany). TAMRA-5-tetramethylrhodamine and FITC-fluorescein-isothiocyanate were the fluorophores used for labeling the peptides. Peptide stock solutions were prepared by dissolving the lyophilized peptides in deionized autoclaved water.

Table 3.1. Summary of Peptides

Name	Sequence
F-p21	**FITC**-Ahx-KRR**Q**TSM**TD**FY**H**S**K**RRLIFS
F-p21-08	**FITC**-Ahx-KRR**Q**TSI**TD**FF**H**S**K**RRL
F-PL	**FITC**-Ahx-SAVL**Q**KKI**TD**YF**H**P**K**K
F-TAT-p21-08	**FITC**-GRKKRRQRRRAAAKRR**Q**TSI**TD**FF**H**S**K**RRL
TAT(-SS-)p21-08-F	GRKKRRQRRR-C C-KRR**Q**TSI**TD**FF**H**S**K**RRL-K(**FITC**)
R-TAT(-SS-)p21-08-F	**TAMRA**-GRKKRRQRRR-C C-KRR**Q**TSI**TD**FF**H**S**K**RRL-K(**FITC**)
TAT(-SS-)PL-R	RRRQRRKKRG-C C-SAVL**Q**KKI**TD**YF**H**P**K**KG-EDA-**TAMRA**

The fluorophores 5,6-carboxytetramethylrhodamine (TAMRA) and fluorescein-isothiocyanate (FITC) were used for labeling the peptides. PIP refers to PCNA interacting peptides. FITC is coupled to N terminus through aminohexanoic acid (Ahx). (-SS-) refers to disulfide bridge.

Plasmids

Mammalian expression constructs encoding translational fusions of GFP-PCNA, RFP-PCNA were described in (Leonhardt et al., 2000) and (Sporbert et al., 2005). pFRT-B-OPCNA was generated from pEF5/FRT/V5 Topo (Invitrogen) by replacing hygromycin with blasticidin and inserting Orange-PCNA after the EF1 alpha promoter.

Cells, culture, transfection and microinjection

Human cell line HeLa was cultured in Dulbecco's modified eagle medium (DMEM) and HaCaT with Roswell Park Memorial Institute (RPMI) 1640 medium, both supplemented with 10% fetal calf serum, 50 µg/ml gentamicin and 2 mM glutamine. Mouse myoblasts C2C12 (Yaffe & Saxel, 1977) cells were cultured in DMEM supplemented with 20% fetal calf serum, 50 µg /ml gentamicin and 2 mM glutamine. Mouse 3T3 fibroblasts stably expressing Orange tagged PCNA were generated by Flp recombinase mediated site specific integration of pFRT-B-OPCNA in Flp-In-3T3^{TM} cells (Invitrogen) according to the manufacturer's instructions. Stable clones were selected with blasticidin 2.5 µg/ml in 10% fetal calf serum, 50 µg/ml gentamicin and 2mM glutamine. Baby hamster kidney cell line was grown in Glasgow minimal essential medium supplemented with 10% fetal calf serum, 50 µg/ml gentamicin, 2 mM glutamine and 150 µg/ml hygromycin B as previously described (Tsukamoto et al., 2000).

All cell culture media was purchased from Sigma-Aldrich (Steinheim, Germany). All the cell lines were grown at 37° C in a humidified atmosphere with 5% CO_2. For transfecting the cells polyethylenimine was used as previously described. (Casas-Delucchi et al., 2012).

Microinjection of the peptides was performed using an Eppendorf microinjection and micromanipulation system mounted on a Zeiss LSM510Meta confocal microscope. All the peptides were diluted to 100 µM in PBS and injected into the cells. The parameters for

cytoplasmic microinjection are two seconds injection with 50 fPa injection pressure and a constant back pressure of 20 fPa, i.e. 30 fPa final injection pressure.

Fluorescent labeling with PIP

Cells were fixed with 3.7% formaldehyde for seven minutes at room temperature. They were permeabilized with 0.5% Triton X-100 for 15 minutes and washed with PBS. Fluorescently labeled PL peptide was diluted to 13 µM final concentration with PBS, added to the fixed cells, incubated for 30 minutes at room temperature and washed with ice cold PBS gently. Hence replication and repair sites can be directly visualized in fixed cells without the need of PCNA antibodies. In case of staining for multiple epitopes, normal immunostaining procedure was followed with other antibodies and then the peptide PIP was added followed by 5 minutes post-fixation with 3.5% formaldehyde. The 4',6-diamidino-2-phenylindole (DAPI) was used to stain the DNA content. The coverslips can be mounted in Mowiol 4-88 (Sigma-Aldrich Chemie). PIP binding is not stable to extensive washes when used in combination with other antibody stainings. It should be added at the end avoiding further washes.

Molecular dynamics simulations

Molecular dynamics simulations were performed using the GROMACS package, version 4.5.6 (Pronk et al., 2013), and the Amber ff99SB (Lindorff-Larsen et al., 2010) force field. The temperature of the system was kept constant, coupling independently each group of molecules at 300 K with a v-rescale thermostat. The pressure was coupled to a Berendsen barostat at 1 atm isotropically. The temperature and pressure time constants of the coupling were 0.2 and 2 ps, respectively. The integration of the equations of motion was performed by using a leap frog algorithm with a time step of 2 fs. Periodic boundary conditions were implemented in all systems. A cutoff of 1 nm was implemented for the Lennard–Jones interactions and the direct space part of the Ewald sum for Coulombic interactions. The Fourier space part of the Ewald splitting was computed by using the particle-mesh Ewald method, with a grid length of 0.11 nm and using a cubic spline interpolation. The systems were composed of a PCNA monomer, one peptide, 15000 water molecules and potassium ions to neutralize the total electric charge of each system. The PCNA crystal structure conformation 1VYM (Lindorff-Larsen et al., 2010) from the protein data bank was used as the initial conformation of the PCNA monomer. The PCNA monomer was placed at the center of a cubic periodically replicated simulation box and the peptides were placed in a stretched conformation at a corner of each box. The total simulation time for each system expanded 2 µs. (Simulation protocol written and performed by Henry David Herce)

Live cell peptide uptake, microscopy and microirradiation

Peptides were further diluted in DMEM medium (SIGMA-Aldrich, Steinem, Germany) to a final concentration of 15 µM and directly added to the cells. To visualize the DNA replication,

cells expressing fluorescently tagged PCNA or not were directly imaged. Whereas for visualizing the DNA repair sites, damage was induced by selecting specific spots in the nucleus of the cells and microirradiating with a 405 nm laser as previously described (Mortusewicz & Leonhardt, 2007). After the laser induced DNA damage, peptides at a concentration of 15 μM were added to the cells and the recruitment of the peptide at the repair site was monitored. Imaging for longer time points (> 10 minutes) requires removal of the peptides followed by the addition of growth media to prevent excess uptake by the cells which is preferentially adopted for repair experiments. Confocal microscopic images were collected using an Ultra VIEW VoX spinning disc system (Perkin Elmer) or on a Nikon Ti microscope equipped with an oil immersion Plan-Apochromat ×60/1.45 NA objective lens (pixel size in XY = 111 nm, Z-step = 0.3–1 μm) with laser lines at 405 nm, 488 nm, 561 nm. During this time cells were kept in closed chamber designed to fit the microscopy stage at 37° C in a humidified atmosphere with 5% CO_2 using the ACU control system from Olympus. Microirradiation experiments were carried out with 405 nm diode laser set to maximum power at 100% transmission available in Nikon Ti spinning disc microscope. Preselected spots of 1 μm in diameter within the nucleus were microirradiated for 1.2 s. Prebleach and post bleach images were recorded based on the individual peptide recruitment kinetics.

Results

Live cell assay for the visualization of DNA replication and repair

All replication and repair factors seem to bind to a common region in PCNA, more specifically the p21 protein binds at the PCNA inter-domain connecting loop located within the area encircled with dotted lines in Figure 3.6A. The dual role of PCNA in replication/repair was visualized in living cells by transfecting fluorescent fusions of PCNA. In Figure 3.6B are shown different stages of S phase progression that form distinctive PCNA replication patterns. These characteristic replication patterns might arise as a consequence of higher order chromatin architecture and a timely orchestrated order in which chromatin is replicated. Early replication patterns represent actively transcribed euchromatin, whereas late replication patterns are associated with heterochromatic regions (Chagin et al., 2010). Laser microirradiation produces significant DNA damage leading to high PCNA recruitment at the irradiated sites as shown in Figure 3.6C. Here, we used this live cell assay, for DNA replication and repair using fluorescent tagged PCNA constructs, to directly test the cell permeability and PCNA binding ability of PIPs.

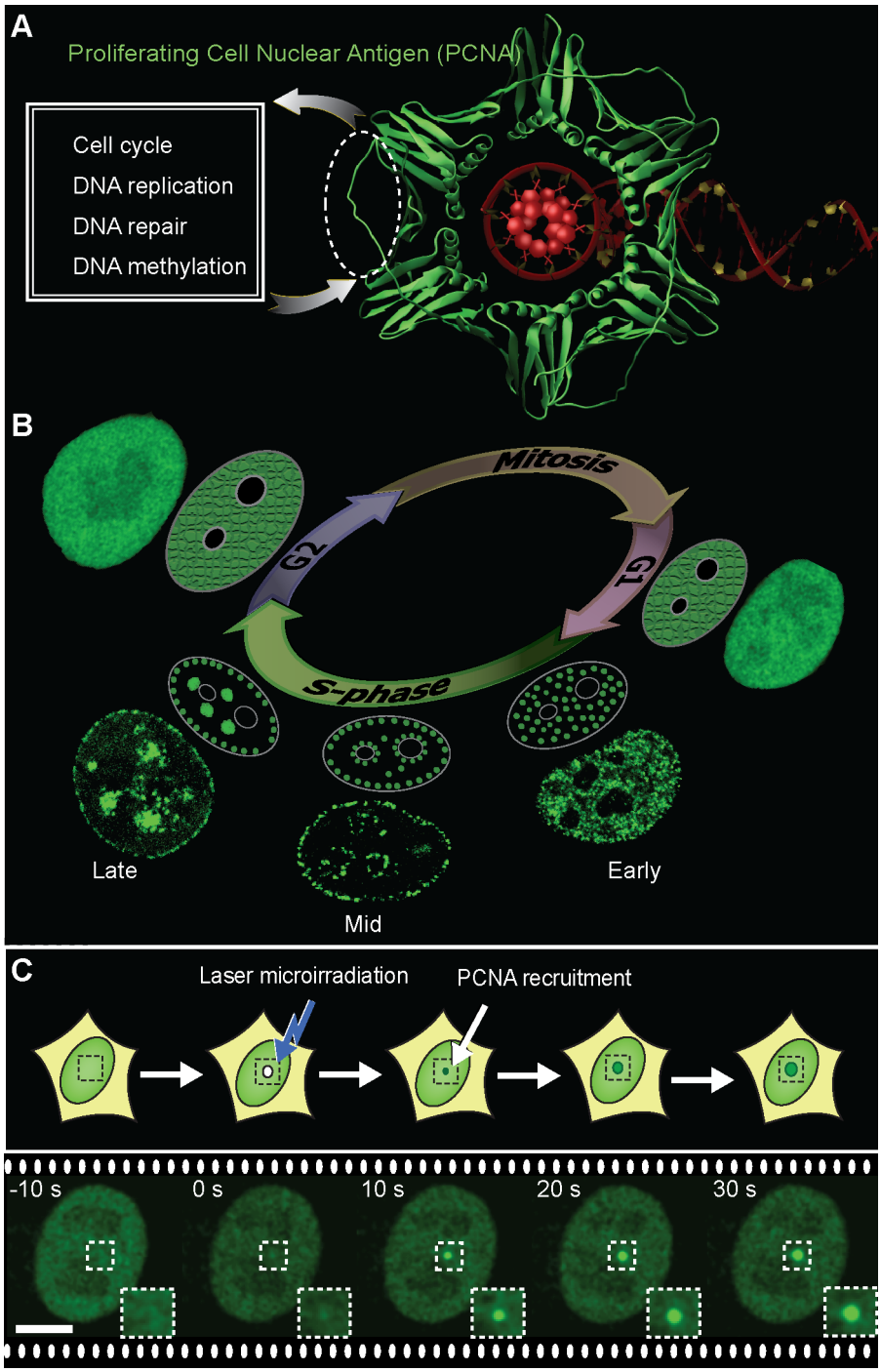

Figure 3.6. PCNA marks DNA replication and repair sites. (A) Crystal structure of PCNA (green) encircling the DNA (red) (PDB 1AXC). PCNA serves as a loading platform for several repair and replication factors that bind to a common PCNA region indicated with a dotted line. (B) During the DNA synthesis phase (S-phase) PCNA is recruited to sub-nuclear sites of DNA replication forming distinctive patterns over time that characterize different S-phase stages (shown schematically and with confocal images of GFP-PCNA expressing cells). (C) PCNA associates with sites of DNA damage induced by laser microirradiation. Scale bar 5 µm.

Strategy behind the design of PCNA interacting peptides

p21 contains a minimal consensus motif critical for its binding to PCNA, also called PIP-box (PCNA interacting protein or peptide), consisting of Q X X (h) X X (a) (a), where Q represents glutamine amino acid, X is any amino acid, (h) a moderately hydrophobic amino acid, and (a) aromatic residues with highly hydrophobic side chains (Warbrick et al., 1998). The $p21_{139-160}$ peptide might be evolutionarily optimized to have higher affinity for PCNA than other replication factors. Therefore, we decided to optimize this peptide by searching for a consensus PIP-box motif as shown in Figure 3.7. We compared the PIP-box of p21, DNA

ligase 1 and Pogo, mutated M147 for I and Y151 for F. The LIFS sequence, $p21_{157-160}$, is also required to bind with CDK-cyclin complexes (Gartel et al., 2002; Kontopidis et al., 2005). Since we were interested in targeting exclusively PCNA, to avoid unspecific binding with CDK-cyclin we removed the IFS sequence ($p21_{158-160}$). The resulting new consensus peptide was named p21-08 (Figure 3.7). Using the same set of sequences, $p21_{141-160}$, DNA ligase I, and Pogo DNA transposase, a peptide called PL (Pogo-Ligase) (Kontopidis et al., 2005; Zheleva et al., 2000) was already reported. PL binds to PCNA with an affinity very similar to that of the $p21_{141-160}$ peptide. The PL peptide was obtained from the sequence of DNA ligase I and Pogo. Therefore, we used those two sequences to optimize instead $p21_{141-157}$ obtaining p21-08 (Figure 3.7). The PL and the newly derived consensus peptide p21-08 are the two PIP sequences we selected for the design of cell-permeable PCNA binding peptides to mark DNA repair and replication sites.

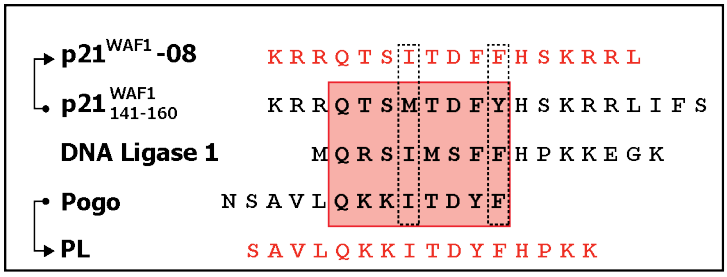

Figure 3.7. **Design of PCNA interacting peptides (PIP).** The red box highlights the residues binding to the PCNA binding pocket. The dotted lines indicate the consensus mutations introduced on the $p21_{141-157}$ peptide to optimize the PIP-box sequence and obtain the p21-08 peptide. The IFS ($p21_{158-160}$) sequence from p21 was removed to reduce the binding between the p21-08 and the CDK-cyclin and make its binding more selective towards PCNA. Additionally a previously described (Kontopidis et al., 2005) synthetic peptide PL derived from Pogo and DNA ligase I was used.

First we asked if these peptides would label replication sites in living cells. In Figure 3.8A are shown the sequences of these PIPs including the wild type $p21_{141-160}$ peptide and the crystal structure of $p21_{139-160}$ bound to PCNA (PDB ID 1AXC) (Gulbis et al., 1996). In Figure 3.8B we show structures of all these peptides interacting with a PCNA monomer obtained from molecular dynamics simulations. In these simulations we found that the wild type $p21_{141-160}$, the p21-08 and the PL all got bound to PCNA. More specifically, all these peptides motifs spontaneously bound at distinctive regions of the inter domain connecting loop, $PCNA_{119–133}$, which is critical for the binding of repair and replication factors. We microinjected these peptides and found that all of them can label PCNA at replication sites in live cells (Figure 3.8C). This confirmed that the *in vitro* derived PL peptide and the new p21-08 peptide can bind to PCNA and labeled replication sites when coupled to a fluorescent tag. Next we asked if any of these labeled peptides would be cell permeable and enter into live cells. We found

that when added to the extracellular media, none of these peptides were able to spontaneously cross the cell membrane, and label PCNA (Figure 3.8D).

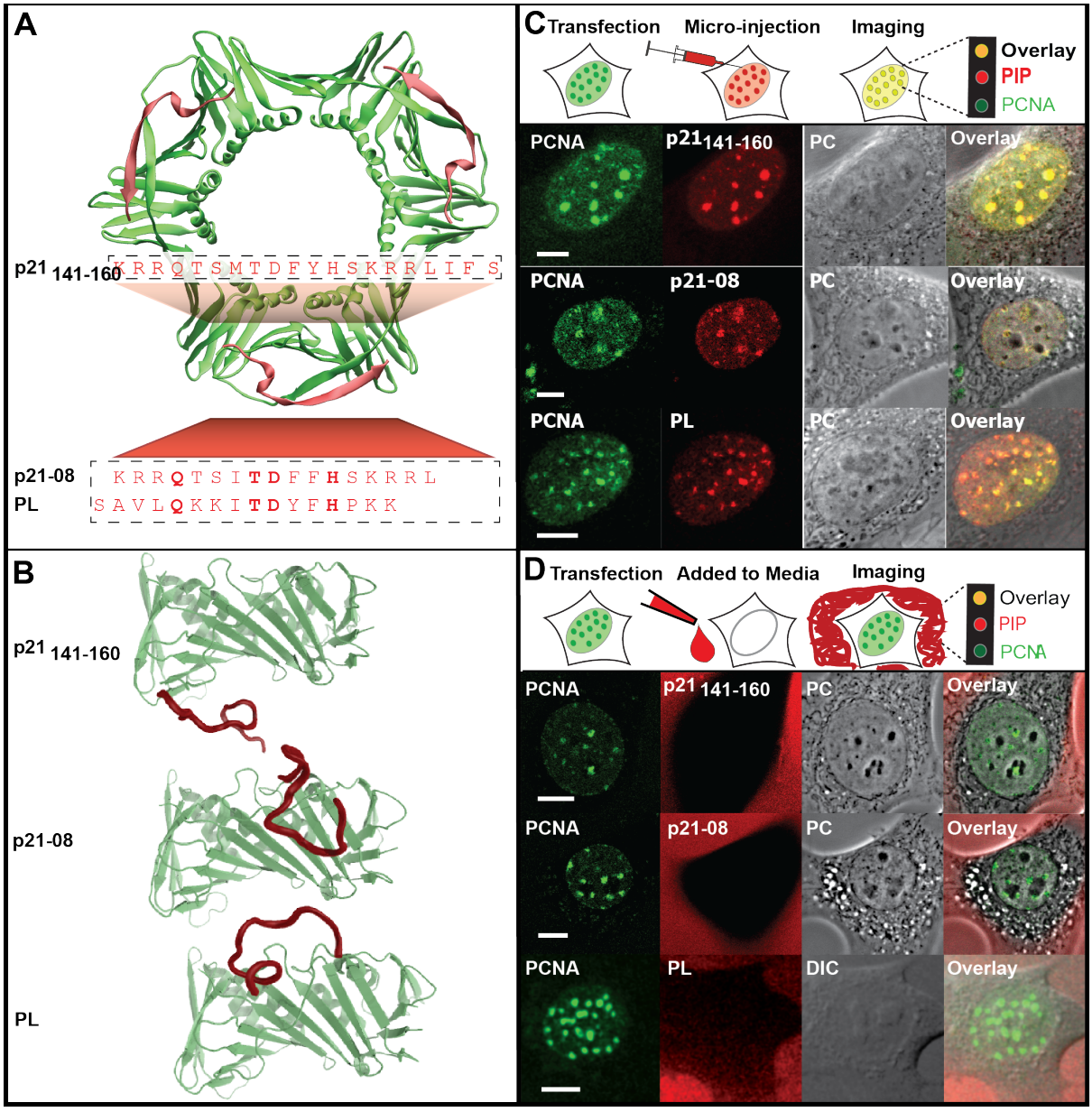

Figure 3.8. PCNA interacting peptides bind to PCNA *in vivo* but are not cell permeable. (A) Crystal structure of the PCNA trimer (green) with the C-terminus region of the p21 protein bound (red) to it (PDB ID 1AXC). The sequences of the p21 peptide and the two highest PCNA binding affinity peptides p21-08 and PL screened are displayed. (B) Structures of the p21 peptides and the two PIPs i.e., p21-08 and PL sequences obtained from molecular dynamics simulations are shown. (C) Images showing that these peptides [[F-p21], [F-p21-08], [F-PL]] after microinjection clearly co-localize with GFP-PCNA at replication sites. **(**D) When the peptides are added to the extracellular media they are not able to enter the cells. The abbreviations PC stands for phase contrast and DIC for differential interference contrast. Scale bar 5 µm. (Simulations from Henry David Herce and Microinjection data from Gisela Laettig Tuennemann)

Development of cell permeable PIPs to label replication/repair sites

These peptides need to efficiently cross the cell membrane in order to label replication and repair sites in living cells when added to the extracellular media. It has been shown that cell-penetrating peptides (CPP) efficiently and spontaneously enter live cells transporting other cargo molecules such as peptides (Tunnemann et al., 2006). Therefore, to make the PIPs membrane permeable we first covalently coupled the p21-08 PIP to a CPP derived from the HIV-1 TAT protein (TAT peptide) able to transduce into live cells and transport other peptides (Frankel & Pabo, 1988; Herce et al., 2013; Herce & Garcia, 2007; Lattig-Tunnemann et al., 2011). The nucleus of a cell expressing fluorescently labeled PCNA was microirradiated recruiting PCNA to the damaged site. Fusion of the PIP with the CPP made the PIP cell permeable. However, the CPP sequence interfered with the PIP binding to PCNA (Figure 3.9A). Coupling the PIP to a CPP can potentially interfere with PCNA binding or mistarget the peptide to the nucleolus, which is a known feature of arginine rich peptides (Lattig-Tunnemann et al., 2011; Martin et al., 2007). This was solved by coupling the PIP to the CPP through a disulfide bridge. This disulfide bridge can be reduced in the reducing environment of the cytosol thereby uncoupling the active peptide (PIP) from the CPP (Figure 3.9B). To test this coupling design we labeled the CPP with TAMRA and the PIP with FITC. If both peptides get uncoupled in the cytosol, the fluorescent label in each peptide should display a different and distinctive intracellular distribution. Importantly, the uncoupled PIP peptide should be recruited by PCNA. To test this idea we delivered the peptide into laser microirradiated cells (Figure 3.9C). It can be seen that the PIP peptide accumulated at microirradiated sites, whereas the CPP distributed mainly in the cytosol and nucleolus. This shows that the TAT peptide was able to transport the PIP peptide into the cells, once inside the cells the PIP peptide was uncoupled from the carrier and freely bound to PCNA. The uncoupling step seemed to be crucial for the PIP binding to PCNA, since only the decoupled PIP was recruited to the microirradiated site (only the PIP fluorescent signal increases at the microirradiated sites). Although this PIP (p21-08) was able to label repair sites we did not detect PCNA labeling at replication sites (Figure S1).

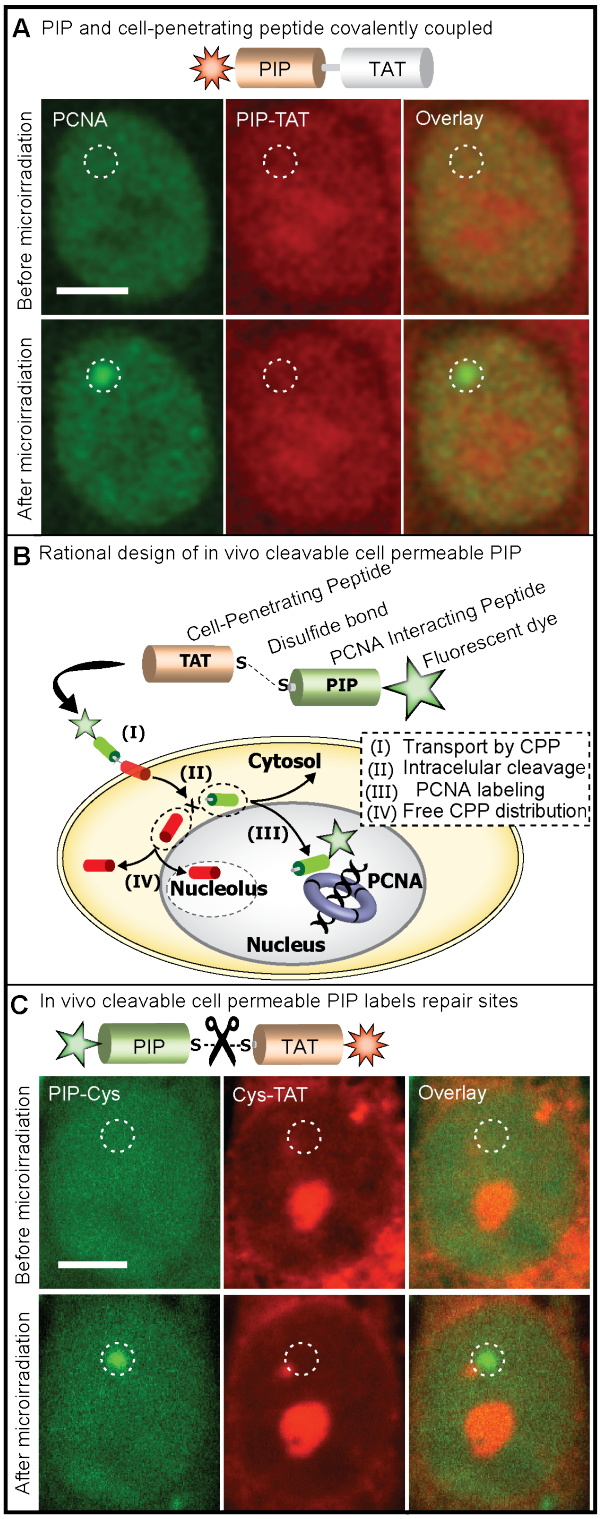

Figure 3.9. Rationale to develop a cell permeable DNA replication and repair marker by targeting PCNA. (A) The nucleus of a cell expressing fluorescently labeled PCNA was microirradiated. PCNA is recruited to damaged DNA sites. Fusion of the PIP with a CPP [F -TAT-p21-08] makes it cell permeable. However, the CPP sequence interferes with the PIP binding to PCNA. (B) Design strategy: the PIP is coupled to a cell-penetrating peptide (in this case the TAT peptide) via a disulfide bridge; after transporting the PIP into the cell the disulfide bridge is reduced; the CPP accumulates mainly in the cytosol and nucleolus, while the PIP is free to reach and bind PCNA. (C) To visualize in live cells the separation of the PIP from CPP, we labeled each sequence with a different fluorescent dye. The TAT peptide labeled with TAMRA is coupled by a disulfide bridge to the PIP peptide labeled with FITC [R-TAT(-SS-)p21-08-F]. It can be seen that the free PIP labels the site of DNA damage, whereas the CPP distributes mainly in the cytosol and nucleolus. Scale bar 5 μm.

PIP labels DNA repair and replication sites in live/fixed cells

Next, we applied the same CPP coupling design for the PL sequence (Figure 3.9B). We coupled the labeled PL peptide through a disulfide bridge to the CPP and added it to the extracellular media of live cells. In Figure 3.10 it can be seen that the PIP fluorescence signal

colocalizes with PCNA at laser microirradiated sites in live cells transfected with GFP tagged PCNA. Therefore, the *in vivo* cleaved PIP marks repair sites.

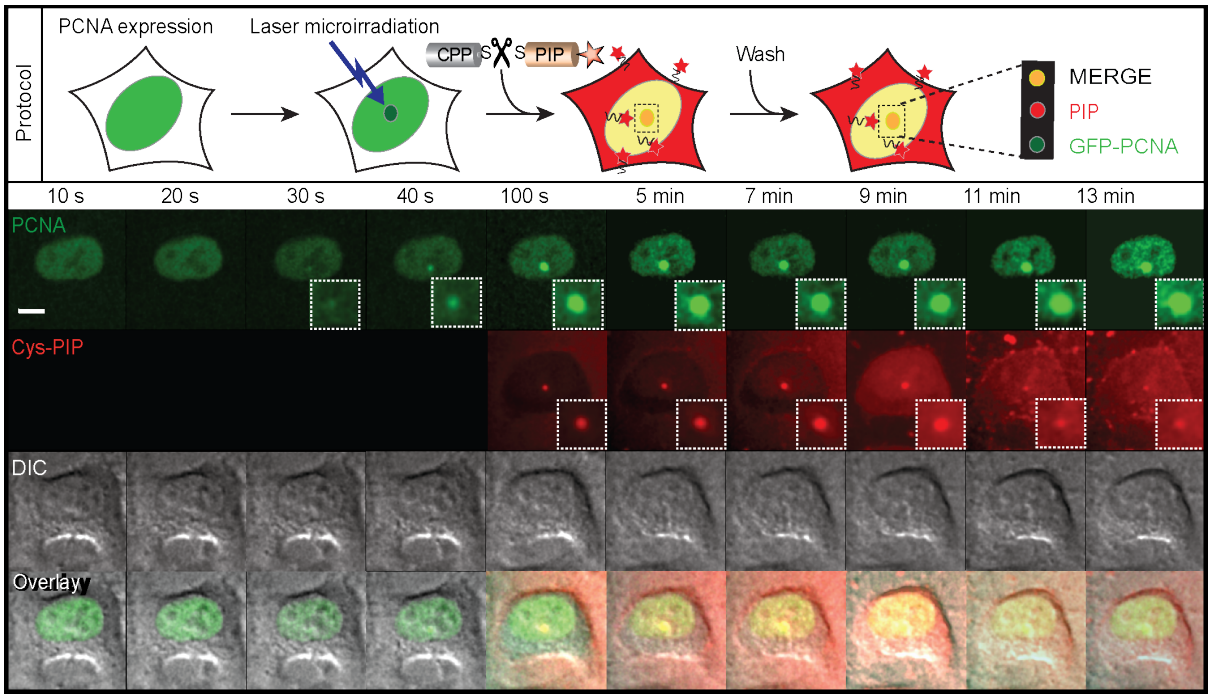

Figure 3.10. ***In vivo*** **immediate labeling of DNA repair sites.** Cartoon representation of the experimental protocol and time-lapse snapshots obtained using confocal microscopy are illustrated. GFP tagged PCNA expressing cells were microirradiated. The PL peptide fluorescently labeled and coupled by a disulfide bridge to the TAT peptide [TAT(-SS-)PL-R] was added to the extracellular media. PIP labels PCNA at repair sites. Scale bar 5 μm.

This peptide was also able to label DNA replication sites. In Figure 3.11 it is shown the nucleus of cells expressing GFP tagged PCNA along different stages of the cell cycle. The PIP added to the extracellular media was able to reach the interior of living cells, co-localize with PCNA at replication sites and distinctively label replicating cells at different stages of the DNA synthesis phase (S-phase). Therefore, this particular *in vivo* cleaved PIP marks both repair and replication sites. At higher concentrations though, the peptide inhibited DNA synthesis as measured by detecting nucleotide incorporation (Figure S2).

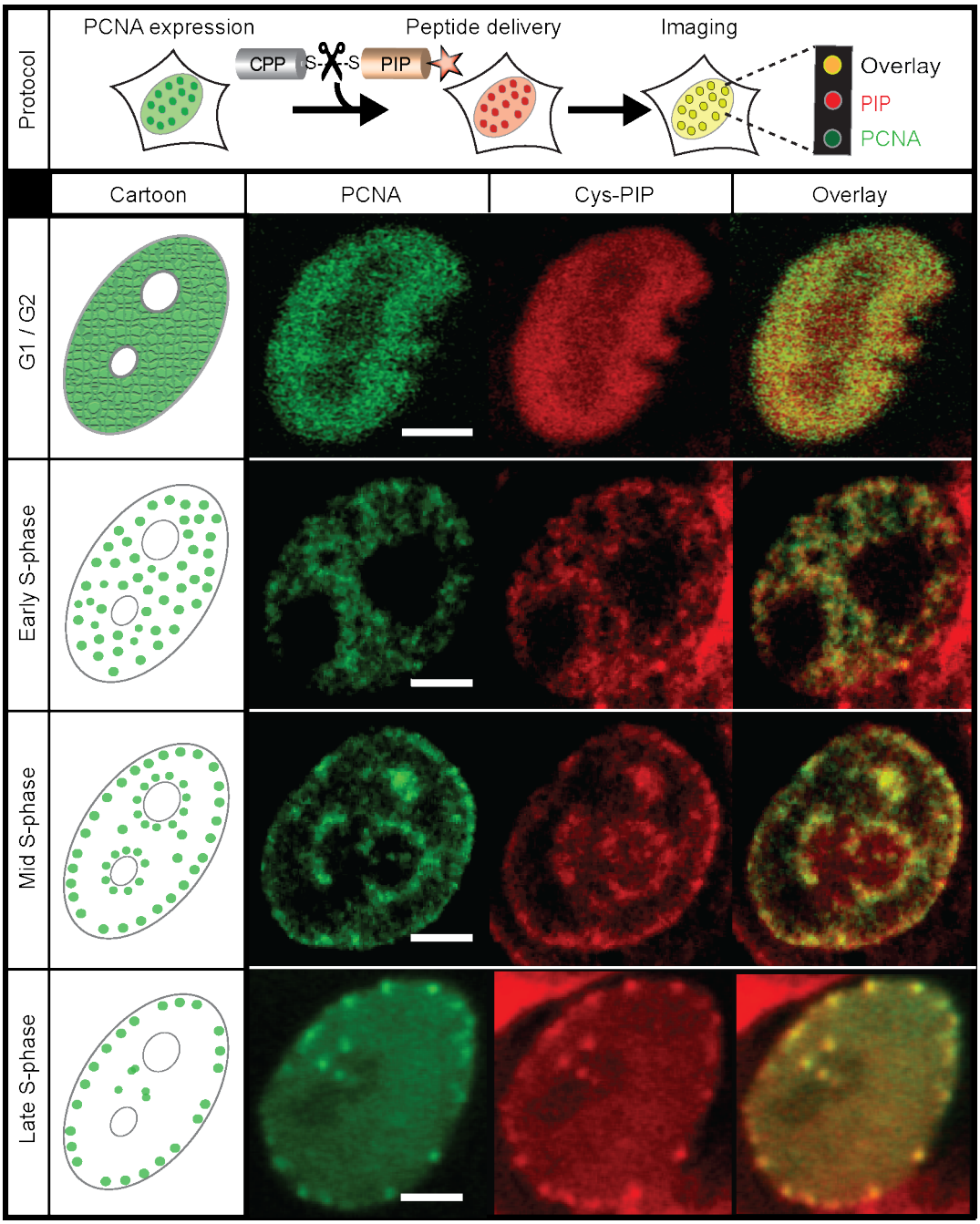

Figure 3.11. *In vivo* immediate labeling of DNA replication sites in S-phase. Cartoon representation of the experimental protocol and time-lapse snapshots obtained using confocal microscopy are illustrated. GFP tagged PCNA expressing cells at different cell cycle stages recognizable by the PCNA sub-nuclear patterns were identified and the same peptide, PL coupled to TAT peptide via disulfide bridge [TAT(-SS-)PL-R], when added to the extracellular media labeled the sites of active DNA replication. Scale bar 5 µm.

These results also suggest that these peptides could potentially be used in the place of antibodies in fixed cells, which can be particularly useful for common immunostaining applications. In Figure 3.12 it is shown that the PL alone can be used in fixed and membrane permeabilized cells to label ectopically expressed (Figure 3.12A) and endogenous PCNA (Figure 3.12B).

The cell-permeable PIP (Figure S3), on the other hand, after fixation would still label repair but not replication sites. After fixation the peptide still marks repair sites but in the case of replication it got redistributed. This indicates that live cells labeled with the cell permeable PIP can be fixed for further postmortem analysis only for DNA repair without disrupting the PCNA labeling.

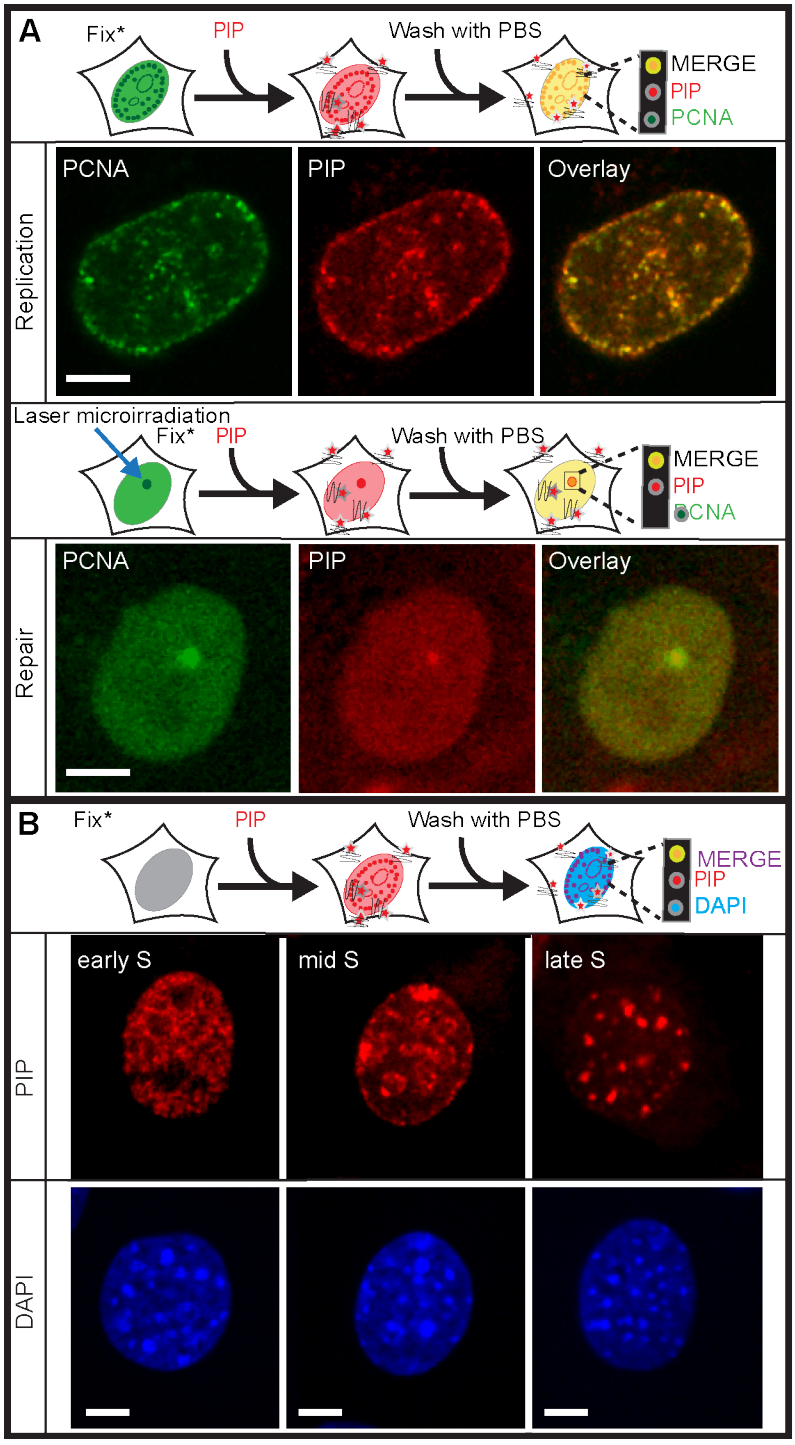

Figure 3.12. PCNA interacting peptide (PIP) labels replication and repair in fixed cells. (A) Here replication and repair sites can be directly visualized in fixed cells without the need of antibodies by PL peptide [F-PL] in the presence of ectopically expressed PCNA. (B) The same PL peptide clearly marks the endogenous PCNA. Scale bar 5 µm.

In Figure 3.13 it is shown that the cell permeable PIP, obtained by coupling the TAT and the PL peptide through the intracellular cleavable disulfide bridge, also labeled DNA replication and repair sites in live cells from different species.

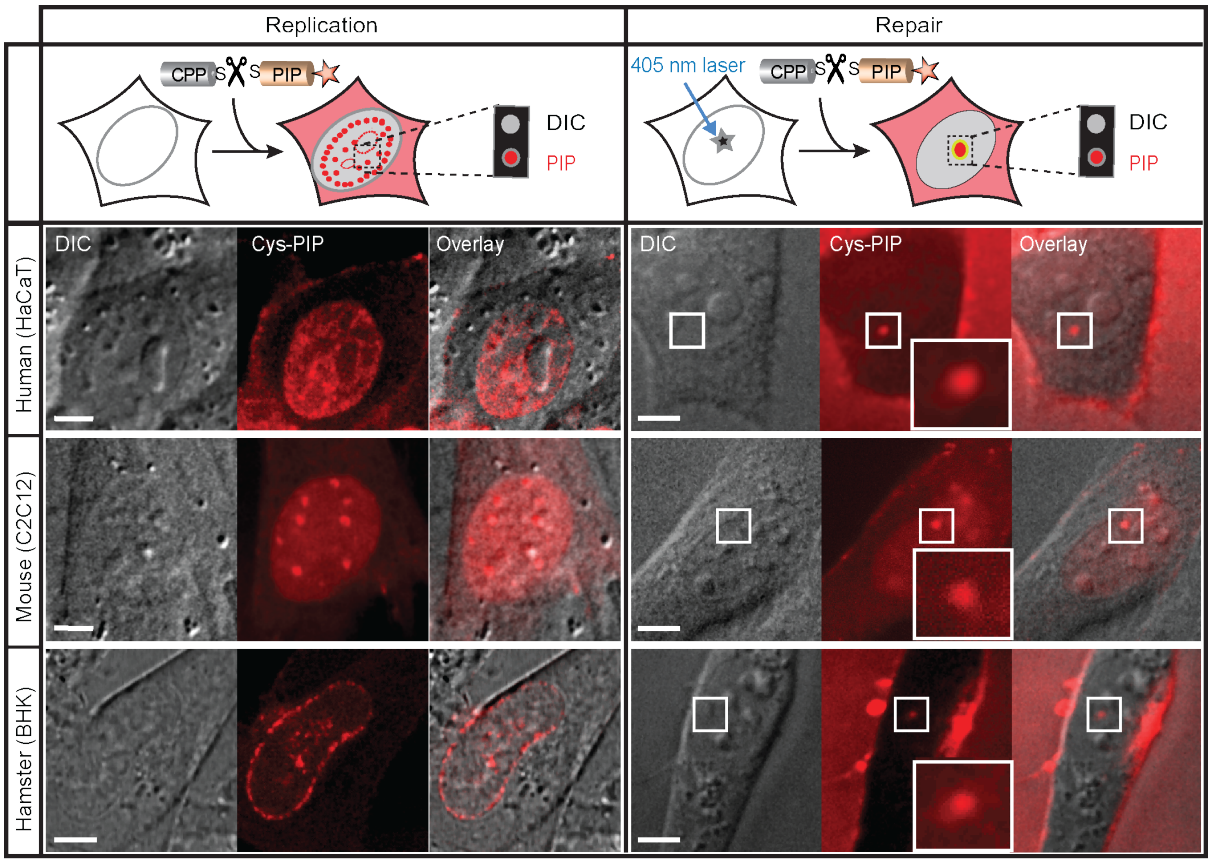

Figure 3.13. The cell permeable and intracellular cleavable PIP directly labels DNA replication and repair in different cell types and species. The PL peptide fluorescently labeled and coupled by a disulfide bridge to the TAT peptide was added to the extracellular media on a variety of cells as indicated, with and without laser microirradiation. In the absence of labeled PCNA the PIP allows a clear classification of S-phase replication stages and damaged DNA sites. Scale bar 5 µm.

Discussion

In this study, we designed a cell permeable peptide able to label DNA replication and repair sites in live cells. The strategy was essentially based on coupling a fluorescent labeled high affinity PCNA binder peptide (PIP) to a cell-penetrating peptide.

When the PIPs were microinjected into the cells these peptides were able to label PCNA. However, none of them were able to spontaneously cross into the cells when added to the extracellular media. To overcome this limitation the PIPs were coupled to a cell-penetrating peptide. When the PIP and the cell-penetrating peptide were covalently coupled we observed that the peptides were able to cross the plasma membrane but the binding and labeling of PCNA was inhibited. At least partially, the reason for this could be that the TAT peptide sequence miss-localized the PIPs. The TAT peptide localizes mainly in the cytosol and

nucleolus while the PIPs need to get distributed in the nucleoplasm to reach and bind to PCNA effectively (Martin et al., 2007).

To this end we coupled the TAT and the PIPs via a disulfide bridge that displayed intracellular cleavage. This partially restored the PCNA binding of the p21-08 PIP. This peptide was able to translocate into the cells and label DNA damaged sites but was unable to label replication sites. It is possible that this is a consequence of the mutation introduced in the p21-08 original sequence by the addition of the cysteine amino acid. The dye linker in this case was also different from the microinjected version of the peptide. All these small changes could have potentially altered the p21-08 PIP's binding affinity to PCNA. Although, the reason why the cell permeable disulfide coupled p21-08 peptide was able to label repair sites and not replicating sites requires further research, this could still be potentially very advantageous to selectively label repair sites.

When the same design strategy was used for the PL peptide, we found that this newly engineered peptide was cell permeable and able to instantaneously label both DNA replication and repair sites in live cells.

We observed that the PCNA labeling is transient, indicating that the PIPs are being actively degraded in live cells. If necessary, there are several strategies that could be further adapted to avoid degradation and extend the intracellular stability of these peptides, such as the introduction of unnatural amino acids or by using PEGylated peptides as previously described (Nischan et al., 2013). However, the best approach is not obvious, since as shown in the case of p21-08 even small modifications in the sequence can significantly alter the PCNA binding of these peptides. All peptides in this study contain also the "PIP degron" motif (Q XX (h) TD (a)(a) XXX K/R). It has been shown that although this motif enhances PCNA binding the last amino acid (K or R) is critical for degradation. This degradation seems to play a regulatory role to avoid proteins bearing this motif from blocking DNA repair (Tsanov et al., 2014). Therefore, mutating this last amino acid offers a simple alternative route to enhance stability of these peptides potentially leading to a simultaneous increase in labeling and blocking DNA repair.

We have shown also that labeled PL, uncoupled to the TAT peptide, can be used on fixed cells following standard fixation protocols. Therefore, this peptide could also be used as a quick PCNA marker replacing primary/secondary antibodies used in immunofluorescence staining methods. Peptides with high PCNA binding affinity derived from consensus motifs, containing the PIP box motif (such as the peptides presented here) or alternatively peptides containing the APIM consensus motif (Gilljam et al., 2009), possess the inherent ability to competitively interfere with the PCNA recruitment of replication and repair factors. Covalently

coupling these peptides to cell-penetrating peptides shows great potential as an effective route to transport these peptides and inhibit proliferative processes (see also Figure S2)

It has been reported that both the PL and p21 peptides interfere with DNA replication. Therefore, they can be used as a versatile tool to potentially target proliferative diseases. Moreover, these cell permeable PCNA binding peptides offer interesting therapeutic venues to selectively mark and distinguish replication and repair.

In summary, here we have designed the first cell permeable PCNA binding peptide that instantaneously labels cells undergoing DNA repair and replication across mammalian species.

References

Ball, K. L., Lain, S., Fahraeus, R., Smythe, C., & Lane, D. P. (1997). Cell-cycle arrest and inhibition of Cdk4 activity by small peptides based on the carboxy-terminal domain of p21WAF1. *Current biology : CB, 7*(1), 71-80.

Bravo, R., Frank, R., Blundell, P. A., & Macdonald-Bravo, H. (1987). Cyclin/PCNA is the auxiliary protein of DNA polymerase-delta. *Nature, 326*(6112), 515-517.

Cardoso, M. C., Joseph, C., Rahn, H. P., Reusch, R., Nadal-Ginard, B., & Leonhardt, H. (1997). Mapping and use of a sequence that targets DNA ligase I to sites of DNA replication in vivo. *The Journal of cell biology, 139*(3), 579-587.

Cardoso, M. C., Leonhardt, H., & Nadal-Ginard, B. (1993). Reversal of terminal differentiation and control of DNA replication: cyclin A and Cdk2 specifically localize at subnuclear sites of DNA replication. *Cell, 74*(6), 979-992.

Casas-Delucchi, C. S., Becker, A., Bolius, J. J., & Cardoso, M. C. (2012). Targeted manipulation of heterochromatin rescues MeCP2 Rett mutants and re-establishes higher order chromatin organization. *Nucleic acids research, 40*(22), e176.

Chagin, V. O., Stear, J. H., & Cardoso, M. C. (2010). Organization of DNA replication. *Cold Spring Harbor perspectives in biology, 2*(4), a000737.

Easwaran, H. P., Leonhardt, H., & Cardoso, M. C. (2005). Cell cycle markers for live cell analyses. *Cell Cycle, 4*(3), 453-455.

Fan, J., Otterlei, M., Wong, H. K., Tomkinson, A. E., & Wilson, D. M., 3rd. (2004). XRCC1 co-localizes and physically interacts with PCNA. *Nucleic acids research, 32*(7), 2193-2201.

Frankel, A. D., & Pabo, C. O. (1988). Cellular uptake of the tat protein from human immunodeficiency virus. *Cell, 55*(6), 1189-1193.

Gartel, A. L., & Tyner, A. L. (2002). The role of the cyclin-dependent kinase inhibitor p21 in apoptosis. *Molecular cancer therapeutics, 1*(8), 639-649.

Gilljam, K. M., Feyzi, E., Aas, P. A., Sousa, M. M., Muller, R., Vagbo, C. B., . . . Otterlei, M. (2009). Identification of a novel, widespread, and functionally important PCNA-binding motif. *J Cell Biol, 186*(5), 645-654.

Gorisch, S. M., Sporbert, A., Stear, J. H., Grunewald, I., Nowak, D., Warbrick, E., Leonhardt, H., and Cardoso, M. C. (2008). Uncoupling the replication machinery: replication fork progression in the absence of processive DNA synthesis. *Cell Cycle, 7*(13), 1983-1990.

Gulbis, J. M., Kelman, Z., Hurwitz, J., O'Donnell, M., & Kuriyan, J. (1996). Structure of the C-terminal region of p21(WAF1/CIP1) complexed with human PCNA. *Cell, 87*(2), 297-306.

Herce, H. D., Deng, W., Helma, J., Leonhardt, H., & Cardoso, M. C. (2013). Visualization and targeted disruption of protein interactions in living cells. *Nat Commun, 4*, 2660.

Herce, H. D., & Garcia, A. E. (2007). Cell penetrating peptides: how do they do it? *Journal of biological physics, 33*(5-6), 345-356.

Kontopidis, G., Wu, S. Y., Zheleva, D. I., Taylor, P., McInnes, C., Lane, D. P., Fischer, P. M., and Walkinshaw, M. D. (2005). Structural and biochemical studies of human proliferating cell nuclear antigen complexes provide a rationale for cyclin association and inhibitor design. *Proceedings of the National Academy of Sciences of the United States of America, 102*(6), 1871-1876.

Lattig-Tunnemann, G., Prinz, M., Hoffmann, D., Behlke, J., Palm-Apergi, C., Morano, I., Herce, H. D., and Cardoso, M. C. (2011). Backbone rigidity and static presentation of guanidinium groups increases cellular uptake of arginine-rich cell-penetrating peptides. *Nat Commun, 2*, 453.

Leonhardt, H., Rahn, H. P., Weinzierl, P., Sporbert, A., Cremer, T., Zink, D., & Cardoso, M. C. (2000). Dynamics of DNA replication factories in living cells. *J Cell Biol, 149*(2), 271-280.

Lindorff-Larsen, K., Piana, S., Palmo, K., Maragakis, P., Klepeis, J. L., Dror, R. O., & Shaw, D. E. (2010). Improved side-chain torsion potentials for the Amber ff99SB protein force field. *Proteins, 78*(8), 1950-1958.

Maga, G., & Hubscher, U. (2003). Proliferating cell nuclear antigen (PCNA): a dancer with many partners. *Journal of cell science, 116*(Pt 15), 3051-3060.

Martin, R. M., Tunnemann, G., Leonhardt, H., & Cardoso, M. C. (2007). Nucleolar marker for living cells. *Histochem Cell Biol, 127*(3), 243-251.

Mortusewicz, O., & Leonhardt, H. (2007). XRCC1 and PCNA are loading platforms with distinct kinetic properties and different capacities to respond to multiple DNA lesions. *BMC molecular biology, 8*, 81.

Nischan, N., Chakrabarti, A., Serwa, R. A., Bovee-Geurts, P. H., Brock, R., & Hackenberger, C. P. (2013). Stabilization of peptides for intracellular applications by phosphoramidate-linked polyethylene glycol chains. *Angewandte Chemie, 52*(45), 11920-11924.

Paunesku, T., Mittal, S., Protic, M., Oryhon, J., Korolev, S. V., Joachimiak, A., & Woloschak, G. E. (2001). Proliferating cell nuclear antigen (PCNA): ringmaster of the genome. *International journal of radiation biology, 77*(10), 1007-1021.

Pronk, S., Pall, S., Schulz, R., Larsson, P., Bjelkmar, P., Apostolov, R., Shirts, M. R., Smith, J. C., Kasson, P. M., van der Spoel, D., et al. (2013). GROMACS 4.5: a high-throughput and highly parallel open source molecular simulation toolkit. *Bioinformatics, 29*(7), 845-854.

Sporbert, A., Domaing, P., Leonhardt, H., & Cardoso, M. C. (2005). PCNA acts as a stationary loading platform for transiently interacting Okazaki fragment maturation proteins. *Nucleic Acids Res, 33*(11), 3521-3528.

Trimis, G., Chatzistamou, I., Politi, K., Kiaris, H., & Papavassiliou, A. G. (2008). Expression of p21waf1/Cip1 in stromal fibroblasts of primary breast tumors. *Hum Mol Genet, 17*(22), 3596-3600.

Tsanov, N., Kermi, C., Coulombe, P., Van der Laan, S., Hodroj, D., & Maiorano, D. (2014). PIP degron proteins, substrates of CRL4Cdt2, and not PIP boxes, interfere with DNA polymerase eta and kappa focus formation on UV damage. *Nucleic Acids Res, 42*(6), 3692-3706.

Tsukamoto, T., Hashiguchi, N., Janicki, S. M., Tumbar, T., Belmont, A. S., & Spector, D. L. (2000). Visualization of gene activity in living cells. *Nat Cell Biol, 2*(12), 871-878.

Tunnemann, G., Martin, R. M., Haupt, S., Patsch, C., Edenhofer, F., & Cardoso, M. C. (2006). Cargo-dependent mode of uptake and bioavailability of TAT-containing proteins and peptides in living cells. *FASEB J, 20*(11), 1775-1784.

Warbrick, E., Heatherington, W., Lane, D. P., & Glover, D. M. (1998). PCNA binding proteins in Drosophila melanogaster : the analysis of a conserved PCNA binding domain. *Nucleic Acids Res, 26*(17), 3925-3932.

Warbrick, E., Lane, D. P., Glover, D. M., & Cox, L. S. (1995). A small peptide inhibitor of DNA replication defines the site of interaction between the cyclin-dependent kinase inhibitor p21WAF1 and proliferating cell nuclear antigen. *Current biology : CB, 5*(3), 275-282.

Yaffe, D., & Saxel, O. (1977). Serial passaging and differentiation of myogenic cells isolated from dystrophic mouse muscle. *Nature, 270*(5639), 725-727.

Zheleva, D. I., Zhelev, N. Z., Fischer, P. M., Duff, S. V., Warbrick, E., Blake, D. G., & Lane, D. P. (2000). A quantitative study of the in vitro binding of the C-terminal domain of p21 to PCNA: affinity, stoichiometry, and thermodynamics. *Biochemistry, 39*(25), 7388-7397.

Supplementary Information

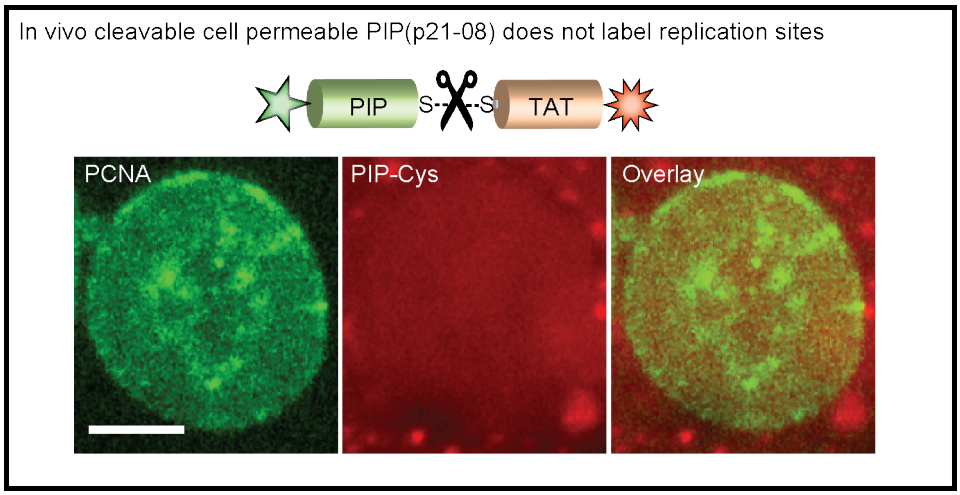

Figure S1. Cell-permeable *in vivo* cleavable p21-08 (PIP) does not label replication sites. The nucleus of a cell expressing fluorescently labeled PCNA undergoing DNA replication. The p21-08 (PIP) is labeled with FITC and coupled by a disulfide bridge to the TAT peptide. The TAT peptide transports the PIP into the cell and both sequences get cleaved in the interior of the cells. However, after cellular uptake and cleaved from the TAT peptide, the PIP still does not mark replication sites labeled by PCNA. Scale bar 5 µm.

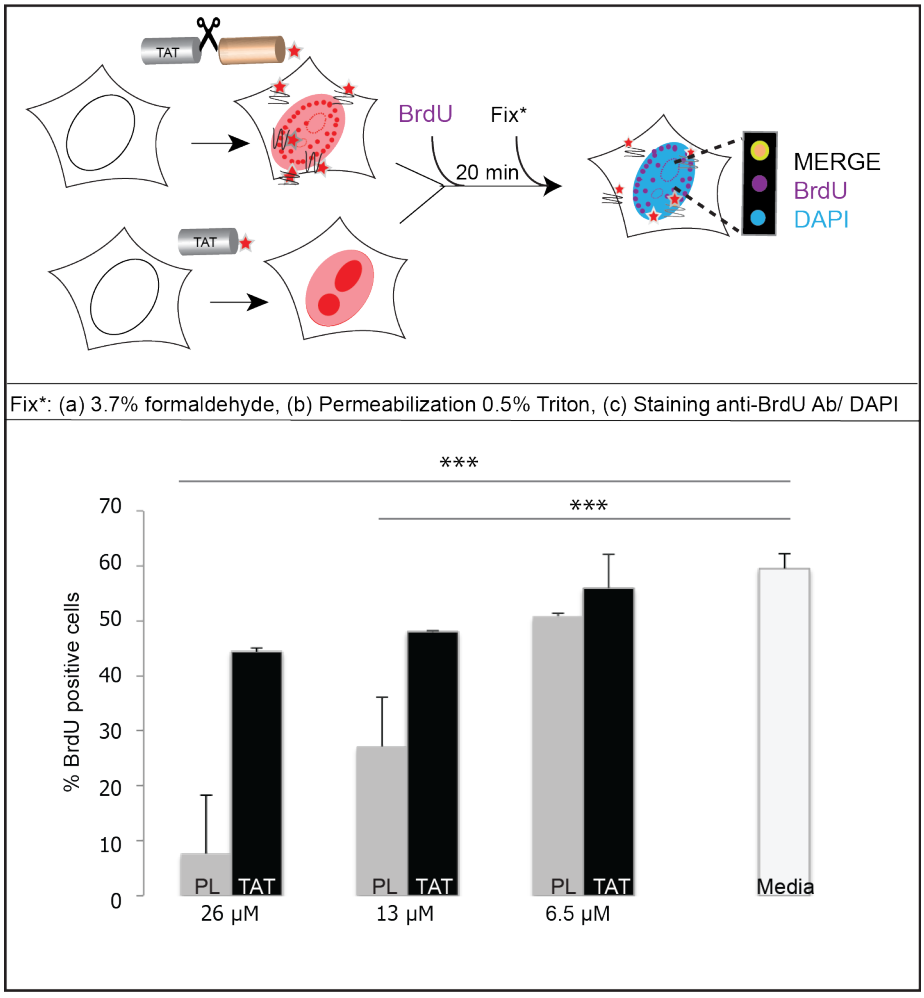

Figure S2. Cell-permeable PCNA marker inhibits DNA synthesis in a dose dependent manner. The [TATS-S-PL] or [TAT] peptides is added to the cells at the concentrations indicated. BrdU thymidine analogue is added at 100 **µ**M final concentration for 20 minutes. Cells are fixed and BrdU incorporationdetected with an anti-BrdU specific antibody and DNA counterstained with DAPI. The percentage of cells positive for BrdU represents Sphase cells and were plotted as mean with the error bars representing the standard deviation. Experiments were repeated two times, with a minimum of 150 cells per condition and per experiment. Student's T test was performed with *** p> 0.001. At the highest concentration of 26 **µ**M, the PL peptide significantly inhibits DNA synthesis, whereas this effect is progressively reduced at lower concentrations with 6.5 **µ**M displaying no significant inhibitory effect.

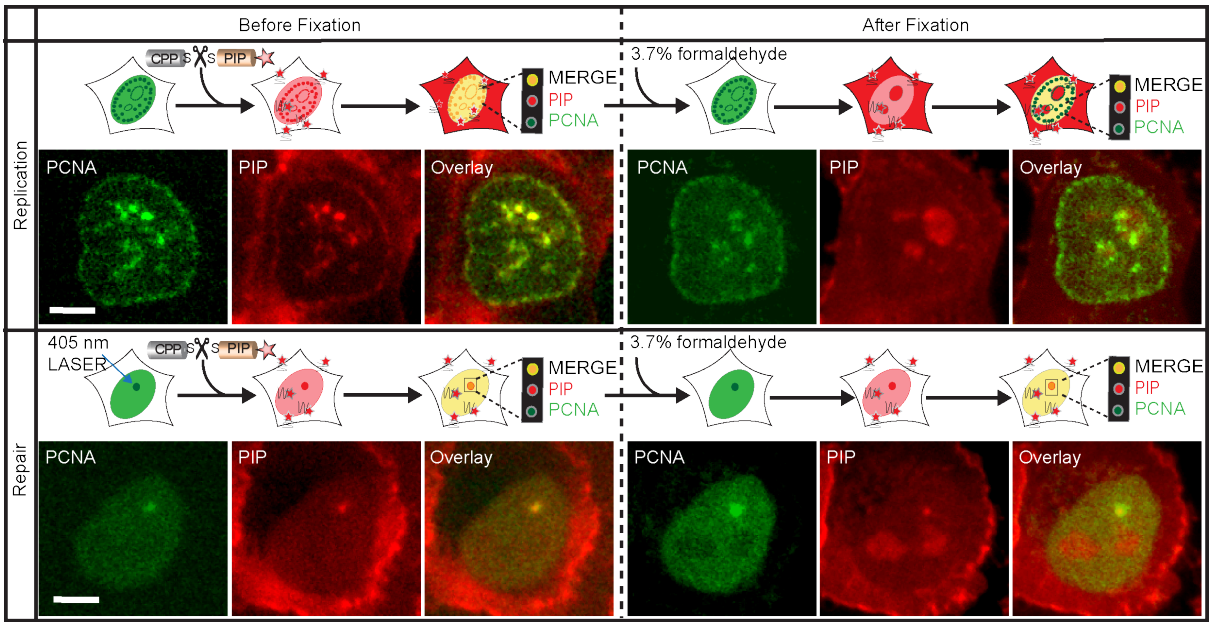

Figure S3. Cell-permeable PCNA marker redistributes upon fixation but it still labels repair sites. The [TAT-S-S-PL] peptide is added to the PCNA expressing cells with the previously described procedure and is found to clearly mark the replication and repair sites. To test whether it can be fixed in place for further analysis we added 3.7% formaldehyde to the cells. We found a redistribution of the peptide from replication sites into the nucleolus. Nonetheless, the peptide at the repair sites was still retained. Scale bars 5 µm.

3.3. Live cell targeting of His-tagged proteins by multivalent N-nitrilotriacetic acid carrier complexes

This chapter has the following major contributors

Malini Rajan[1], Ralph Wieneke[2], M. Cristina Cardoso[1], and Robert Tampé[2]

1. Technische Universität Darmstadt, Germany
2. Goethe-University Frankfurt, Frankfurt am Main, Germany

Some results in this Chapter-3.3 were published in the Journal of the American Chemical Society in 2014.

Wieneke R*, Laboria N*, **Rajan M**, Kollmannsperger A, Natale F, Cardoso MC and Tampe R., "Live-cell targeting of His-tagged proteins by multivalent N-nitrilotriacetic acid carrier complexes" J. Am. Chem. Soc., DOI: 10.1021/ja5063357 • Publication Date (Web): 19 Sep 2014.

Abstract

Cell-penetrating peptide (CPP)-based delivery of molecules and cargoes has been proven to label endogenous proteins like PCNA in live cells as explained in the previous chapter. CPPs can carry a wide variety of cargoes. Our ultimate aim was to label histidine-tagged proteins in live cells using CPP-*tris*NTA (three times of Nitrilotriacetic acid) strategy. His-tag is one of the most widely used tag for recombinant protein expression and purification procedure. It is now established that the high-affinity *tris*NTA enables the formation of stable complexes with hexahistidine containing molecules. In this study, using a peptide tag artificial probe system we have developed a novel three-step approach for labeling His-tagged proteins. (1) An initial coupling step consisted of complexing oligo-histidines tagged to a CPP with fluorescently labeled *tris*NTA. (2) *tris*NTA-hexahistidine-CPP complex was then taken up into the cells via CPP, where *tris*NTA is reversibly uncoupled in the presence of a His-tag competitor ligand (intermediate uncoupling step). (3) In the final labeling step, the uncoupled, *tris*NTA was bound to His-tagged proteins overexpressed in the cells (i.e., the competitor for the hexahistidine of CPP). To understand whether the use of CPP constructs might influence the binding properties of *tris*NTA, we used time-lapse confocal microscopic analysis of living mammalian cells to visualize the uptake of the $(His)_6$-TAT complexed with labeled *tris*NTA, and their subsequent uncoupling and cellular target labeling. The significant selectivity of the *tris*NTA for hexahistidine, as well as its stable yet reversible complex formation provides the basis for our aim to label histidine-tagged proteins. Here we used a His-tagged PCNA construct in order to label replication and repair processes *in vitro*. For proof of concept, we studied the naturally hepta-histidine-bearing protein MeCP2 in live cells. We also introduce a novel *tris*NTA-based staining approach for fixed cells, thus producing an inexpensive replacement for antibodies against histidines.

Highlights

- Labelled *tris*NTA, at safe concentrations, was used successfully in fixed cells to mark the localization of overexpressed His-tagged proteins (e.g., MeCP2, $(His)_6$-GFP-PCNA).
- Labelled *tris*NTA can be used successfully in live cells to label overexpressed His-tag via competitive binding using His-tagged cell-penetrating peptide.
- Labelled *tris*NTA, is a perfect replacement for histidine antibodies in immunostaining applications.

Introduction

Histidine (His) tags are widely used affinity tags. Hochuli first developed purification of His-tag proteins in 1987 (Hochuli et al., 1987). Since its development, numerous proteins or peptides have been purified using His-tags and applied mostly for clinical studies (Mayer et al., 2004). These tags are small and can be incorporated at the termini or in loop regions where they do not perturb the protein's structure and function. In order to visualize the His-tagged proteins in living cells, fluorescent fusions (Tsien, 1998) can be introduced to the respective His-tagged constructs.

Fluorescent proteins (FPs) are the most commonly used fluorescent tags that have enabled us to visualize, track, and quantify molecular events in live cells with space and time resolution. Despite its unquestionable value, the application of FP tags has several problems. The size of the tag can prevent the labeled construct from achieving its natural structure and function and may even sometimes lead to mis-localization (Lisenbee et al., 2003; Tavare et al., 2001). Wild-type versions of common FPs have a tendency to oligomerize. The pH sensitivity of the FPs limits their ability to image acidic regions of the cell. Overexpression of the tagged proteins can itself lead to a whole variety of potential artifacts. Genetic alteration can sometimes overcome these limitations, but this process can be laborious and time consuming.

To alleviate this problem, several small molecular probes and covalent labeling (Keppler et al., 2003) methods are employed to specifically introduce markers for the proteins in live cells. Small molecular probes like NTA can be used to label proteins *in vivo* and can potentially open up new ways of studying proteins in living cells. NTA probes are comprised of a chromophore and a metal-ion-chelating NTA moiety, which binds reversibly and specifically to engineered oligohistidine sequences in the proteins of interest. The labeling of extracellular protein (Goldsmith et al., 2006) and structural investigation of $5HT_3R$ _ENREF_15 (Guignet et al., 2004) ligand-gated ion channel with His-tags in live cells have already been studied using NTA probes. This NTA system has been manipulated in several ways such that it can be used not only for labeling purposes but also for simultaneous His-tagged protein purification via immobilized metal affinity chromatography, surface immobilization for protein assay, interaction studies, and for therapeutic application (Janknecht et al., 1991; Kim et al., 2007). The advantages of the NTA-$(His)_6$ interaction are its unique ability to be reversible and selective. However, this traditional mono-NTA approach for capturing histidine tagged proteins has some disadvantages like weak binding with a dissociation constant of 1 μM (Nieba et al., 1997), which may result in ligand decay and inaccurate kinetic measurements. In order to improve this NTA strategy, conventional mono-NTA was replaced with *tris*NTA conjugated fluorophores. It has been shown that *tris*NTA

stably bound to oligohistidine-tagged proteins results in a complex that has a lifetime of more than an hour (Lata et al., 2006). Nano-molar affinity was achieved when the multivalent NTA was bound to His-tags (Huang et al., 2009).

As these *tris*NTA probes are not cell permeable, we sought a transduction technology like cell penetrating peptide (i.e., trans-activator of transcription (TAT) derived from HIV that can carry *tris*NTA inside the cells). Previous data has already shown that coupling of a TAT-derived peptide (extending from residues 37 to 72) to some proteins can allow their uptake into several cell lines or tissues (Vives et al., 1997). Several cargo varieties, such as drugs, proteins, peptides, and nucleic acids, have been transported across cell membranes using CPPs (Kabouridis, 2003). For our present study, we synthesized TAT peptides with a hexahistidine tag in the N-terminus, which can reversibly be coupled to *tris*NTA moieties conjugated to a fluorophore. The entry of the complex into the cell was facilitated via TAT, and labeling was achieved by reversible uncoupling of *tris*NTA from $(His)_6$-TAT, thereby binding to the histidine tag in the protein of interest.

As described in the previous chapter, PCNA is a protein found to be differentially expressed during the cell cycle (Bravo and Celis, 1980; Bravo et al., 1981; van Diest et al., 1998), and has been employed as a marker for cell proliferation (van Diest et al., 1998). Cancer often correlates with an enhanced level of PCNA, and their levels can be used as a prognostic marker in some cases (Czyzewska et al., 2004; Garrels and Franza, 1989; Morell-Quadreny et al., 1998; Naryzhny, 2008). Histidine-tagged PCNA constructs have been used to biochemically understand the dual role of PCNA in cell replication and repair (Fridman et al., 2010; Kannouche et al., 2004). These His-tagged PCNA constructs were used for our present study, suggesting thereby to alleviating the need for further genetic modification or incorporation of fusion tags into these constructs. In order to broaden the applicability of this system, we also have successfully tested this *tris*NTA system for MeCP2 (Methyl CpG binding protein 2), a chromatin remodeling protein bearing a natural hepta-histidine peptide at its C-terminus. *tris*NTA-based stains of fixed cells have been successfully employed to visualize the protein localization, thus making an inexpensive replacement for histidine antibodies.

Materials and Methods

Synthesis

All reaction steps were performed under microwave-irradiation using the Liberty 1 (CEM). The $(His)_6$-tagged TAT_{49-57} peptide was synthesized using standard coupling protocols for microwave-assisted SPPS. The molar excess of reagents was calculated with regard to resin substitution. In *Fmoc-deprotection*, Fmoc-Rink-Amid MBHA resin was treated with 20%

piperidine in DMF (1x 0.5 min, 1×x 5 min, each 7.0 ml 75 °C, 54 W), followed by washing with DMF (7.0 mL, 4x). During coupling, the resin was treated with Fmoc-aa (5 equiv.), HBTU (5 equiv.), and DiPEA (10 equiv.) in DMF (5.0 mL) for 30 min at RT and 15 min at 75°C with a microwave power of 28 W, followed by washing with DMF (7.0 mL, 4×x). To increase the yield, the coupling steps were repeated twice throughout the synthesis. In cleavage and deprotection steps, the resin was stirred with a freshly prepared cleavage cocktail (95% TFA with phenol, TIPS, Milli-Q water, and EDT, 1.25% each) for 4 h at RT. The TAT_{49-57} peptide was precipitated in ice-cold Et_2O (40 mL) and stored at least 15 min at -20°C. After centrifugation at 3000 rpm for 10 min and decantation, the pellet was washed and centrifuged two more times with Et_2O (40 mL). The peptide was finally dissolved in *tert*-BuOH/H2O (4/1, v/v), lyophilized, and purified by RP-HPLC using a gradient starting from water with 0% methanol and increasing the hydrophobicity to 15% methanol (both buffers contained 0.1% TFA) in 40 min at 1 mL/min on a C4 column. Retention time in RP-HPLC (column: PerfectSil C4) was 28.0 min. MALDI-TOF-MS: m/z 2992.3 (calcd. for [M – H]-: 2592.9 C104H173N54O23S). (Synthesis protocol developed and performed by Ralph Wieneke)

Cell culture

The human cell line HeLa was cultured in Dulbecco's modified eagle medium (DMEM) supplemented with 10% fetal calf serum, 50 µg/ml gentamicin and 2 mM glutamine. Mouse myoblasts C2C12 cells (Yaffe and Saxel, 1977) were cultured in DMEM supplemented with 20% fetal calf serum, 50 µg/ml gentamicin and 2 mM glutamine. All cell culture materials were purchased from Sigma-Aldrich (Steinheim, Germany). The cell lines were grown at 37°C in a humidified atmosphere with 5% CO_2.

Plasmids and transfection

A hexahistidine tag was added to GFP-PCNA (Leonhardt et al., 2000), and MeCP2-cDNA from human was cloned into a pEGFP-C1 vector as described by (Agarwal et al., 2011). C2C12 cells were transfected with Amaxa (Lonza, Cologne, Germany) nucleofection (solution V, program B-032).

Fluorescent labeling with *tris*NTA

Cells transfected with MeCP2-GFP and $(His)_6$-GFP-PCNA were used for immunofluorescence experiments and they were grown on glass coverslips. Cells were fixed with 3.7% formaldehyde for 10 minutes and permeabilized with 0.5% Triton for 20 minutes. For washing the cells, phosphate buffer saline (PBS) was used, and 200 nM *tris*NTA-AlexaFluor 647 diluted in PBS was added to the cells and incubated for 1 hour at room temperature. Followed by gentle removal of *tris*NTA, cells were post fixed again with 3.7%

formaldehyde for 5 minutes. The DNA was stained with 4',6-diamidino-2-phenylindole (DAPI), followed by mounting in Mowiol 4-88 (Sigma-Aldrich Chemie).

_tris_NTA complex uptake experiments

C2C12 cells transfected with MeCP2-GFP were used for the live cell experiments. A 1:1 ratio of peptide:*tris*NTA complex was prepared by mixing ~9 μM $(His)_6$ SGGG-TAT_{49-57} peptide with ~9 μM *tris*NTA-AlexaFluor 647 and incubating them for 40–50 minutes at room temperature. The complex was then added to the cells. After 20–25 minutes the solution was removed and the cells were washed once with media. Finally, fresh media was added to the cells.

Microscopy

Confocal microscopic images were collected using an Ultra VIEW VoX spinning disc system (Perkin Elmer) or a Nikon Ti microscope equipped with an oil immersion Plan-Apochromat ×60/1.45 NA objective lens (pixel size in XY = 111 nm) with laser lines at 405 nm, 488 nm, 561 nm, and 625 nm. During live cell experiments, cells were kept in a closed chamber designed to fit the microscopy stage at 30°C in a humidified atmosphere with 5% CO_2 using the ACU control system from Olympus. DNA damage was induced by selecting a spot inside the nucleus that was then microirradiated with a 405 nm solid state diode laser with full laser power.

Results

Metal chelation based labeling strategy

The scheme for metal chelation-based labeling is shown in Figure 3.14. The present method overcomes several restrictions of existing labeling methods by allowing fast, site-specific, reversible labeling of proteins using non-perturbing probes. This method is applicable to both *in vitro* and *in vivo* investigations of molecular interactions, to visualize His-tagged molecules, and to explain even the structure and topology of proteins.

NTA forms a four times chelate with nickel ions, stoichiometrically. After the NTA chelation with the co-ordination sphere of nickel, two sites were still left free (Ni^{2+}) to interact with the electron donor group of the imidazole group present in the histidines (Khan et al., 2006). *tris*NTA can be conjugated with wide range of dyes to increase its applicability.

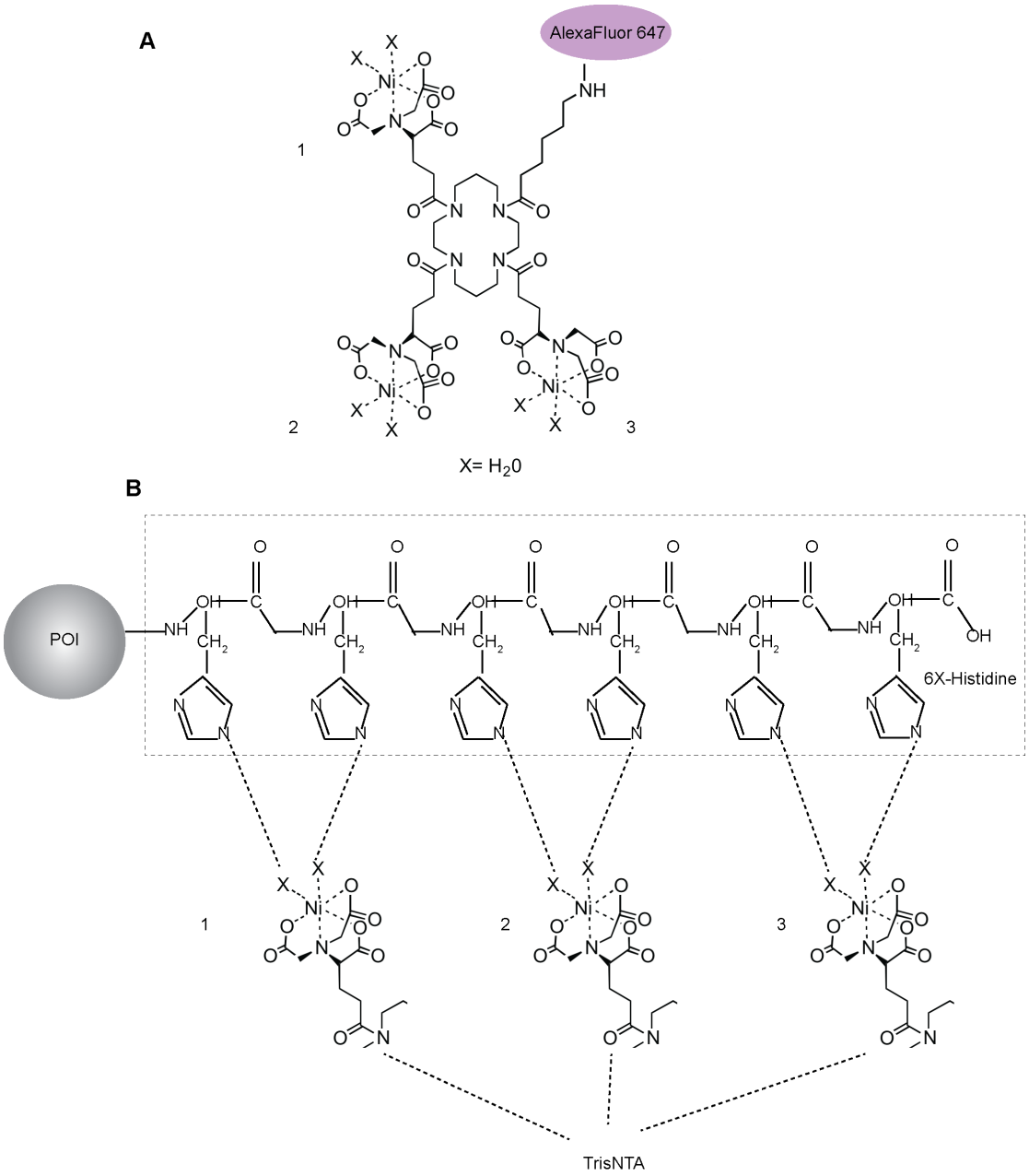

Figure 3.14. **Components for metal chelation-based labeling. (**A) The structure of *tris*NTA conjugated with AlexaFluor 647 is shown. (B) A hexahistidine-tagged protein of interest (POI) is shown. The formation of co-ordination bonds between the Ni^{2+} and nitrogen atoms in the imidazole group of histidine are shown as dotted lines.

In vivo labeling of His-tagged proteins using cell permeable *tris*NTA

As shown in Figure S2, no uptake via endocytosis was observed when *tris*NTA AlexaFluor 647 was added to the cells. Rather, *tris*NTA stayed outside of the cells, showing no toxic effects up to one hour after the treatment. In order to facilitate the uptake of *tris*NTA, $(His)_6$-TAT was used as a carrier. The two moieties (*tris*NTA Alexa488 and $(His)_6$-TAT) were incubated at room temperature to make a stable complex (Figure 3.15). Nitrogen atoms of the imidazole group of histidine are deprotonated to form a co-ordinate bond with the nickel

ion present in each NTA of the *tris*NTA molecule. Thanks to the TAT peptide, the complex penetrated the cell membrane and accumulated into the nucleolar compartment. In the absence of the competitor, *tris*NTA dissociation from the $(His)_6$-tag in the presence of CPP is not favored, thus determining the staining. Also, a minimal amount of *tris*NTA uncoupled from $(His)_6$-TAT is to be expected, due to the reducing environment of the cytoplasm. However, in the presence of a competitor tag in the protein of interest, significant dissociation of the *tris*NTA moiety from the carrier, CPP, and subsequent binding to the protein of interest was observed. Such exchange is likely to be dependent on the number of histidines present in the tag affecting the dissociation constant between the involved moieties (see below).

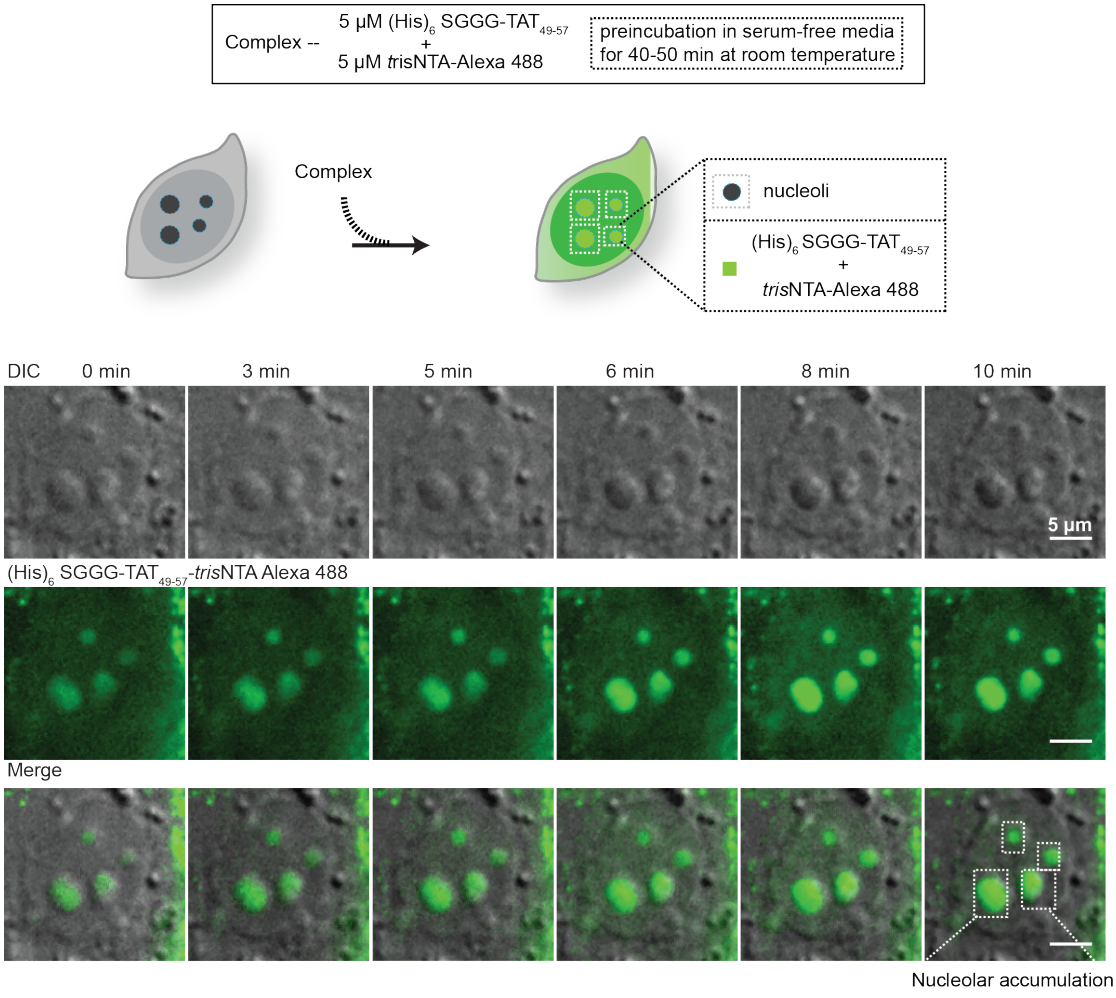

Figure 3.15. **Real time cellular uptake of *tris*NTA Alexa 488 complexed with His-tagged TAT.** Illustrations of the experimental protocol are shown. The $(His)_6$ -tagged TAT was incubated with *tris*NTA-Alexa 488 to form a complex at room temperature. The complex was added to the cells and showed uptake and localization into the nucleoli.

Live cell labeling of overexpressed His_6-GFP-PCNA was visualized in cells undergoing repair, replication, or no replication (Figure 3.16). Repair was studied by microirradiating the

transfected cells with a 405 nm laser to induce a variety of DNA damage at a specific spot. As a result of the DNA damage, PCNA promptly accumulated at the site of irradiation to initiate the repair process. Despite such pronounced accumulation, minimal *tris*NTA exchange was observed between the $(His)_6$ tag present in the CPP and that in PCNA. This resulted in a mild co-localization of *tris*NTA with $(His)_6$-GFP-PCNA at the irradiated spot, and such co-localization only lasted for a few seconds (Fig. 3.16B). In replicating cells (i.e., cells showing a typical PCNA replication pattern), only a minimal amount of *tris*NTA exchange was observed (Fig. 3.16C). In non-replicating cells, a partial exchange was initially observed (Fig. 3.16D). However, at later times, the majority of *tris*NTA bound to $(His)_6$-TAT and was finally taken into the nucleoli (Fig. 3.16E).

It is already well known from the biochemical point of view that in NTA-His tag protein purification systems the His-tagged proteins bound to immobilized NTA can be eluted by the addition of a competitive ligand like imidazole. Similarly, in our case cells over-expressing a competitive ligand with a higher number of histidines than the $(His)_6$-TAT can potentially favor the uncoupling of the *tris*NTA from the $(His)_6$-TAT complex, facilitating the subsequent binding of *tris*NTA with the competitive ligand. Hence, we used MeCP2 bearing a natural heptahistidine peptide in the C-terminus of the coding region. This amino acid sequence is conserved among mouse, rat, and human species (Fig. 3.17A). MeCP2 accumulated in densely methylated pericentric heterochromatin called chromocenters (Agarwal et al., 2011). When the *tris*NTA:$(His)_6$-TAT complex was added to the cells in the presence of the competitor ligand (i.e., MeCP2) with heptahistidines, *tris*NTA was efficiently uncoupled from $(His)_6$-TAT and bound to the MeCP2, thereby showing a clear co-localization (Fig. 3.17B). However, the washing step was critical to avoid the excess uptake of the complex by the cell (Figure S1).

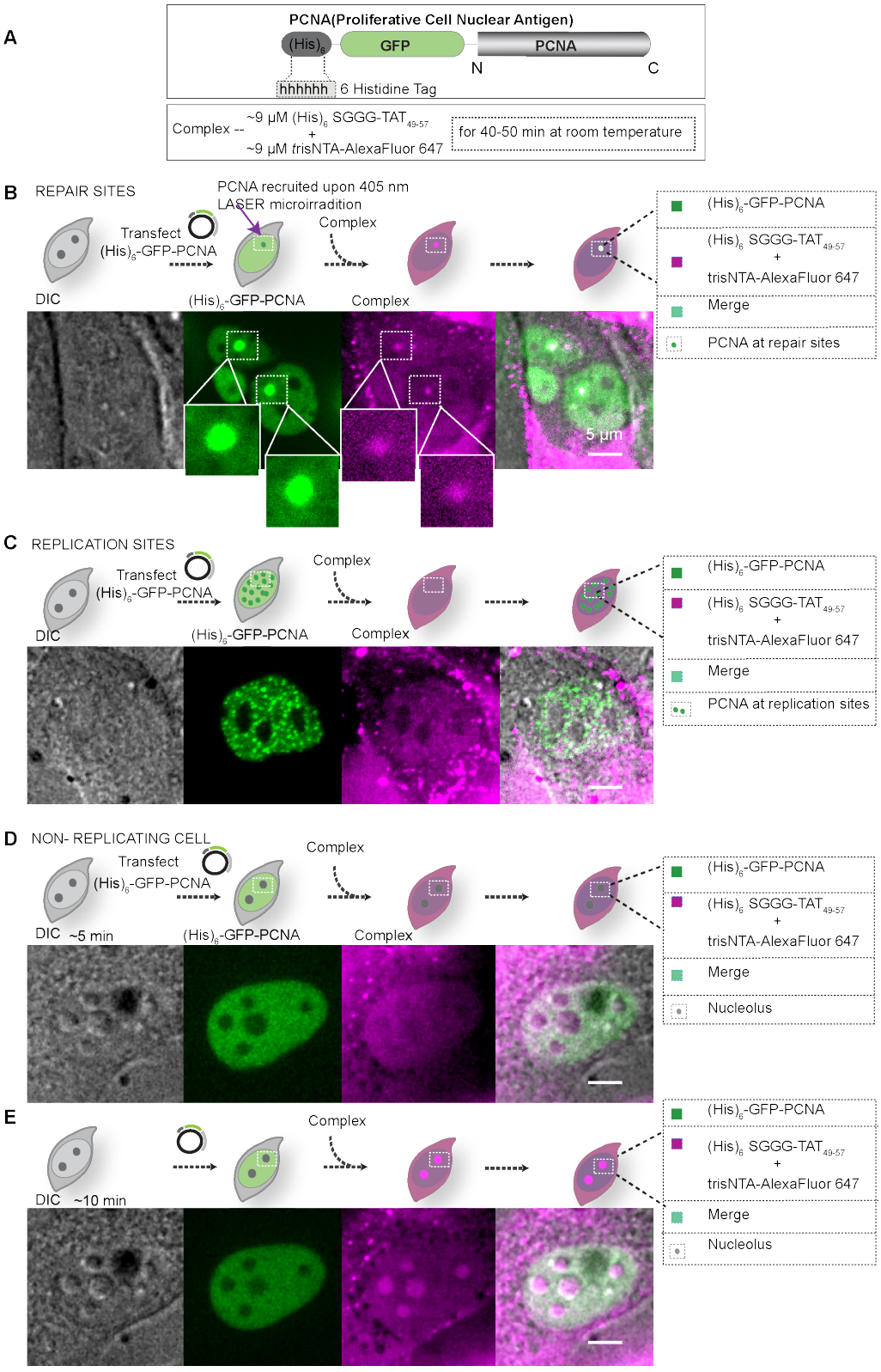

Figure 3.16. *In vivo* labeling of His-tagged PCNA in live cells. (A) The PCNA construct used here is illustrated with its respective $(His)_6$ and GFP tags. (B) PCNA expressing cells in a non-replicating stage chosen for the repair experiments were microirradiated with a 405 nm laser in order to trigger recruitment of $(His)_6$-GFP-PCNA at the irradiated spot. The addition of the pre-incubated complex follows. Slight co-localization of *tris*NTA-AlexaFluor 647 with $(His)_6$-GFP-PCNA was observed at the repair sites. (C) Cells undergoing replication were chosen and the complex was added to them. Little to no co-localization was observed. (D) In the case of non-replicating cells, the

*tris*NTA showed no nucleolar accumulation. (E) However, at later time points nucleolar accumulation was observed.

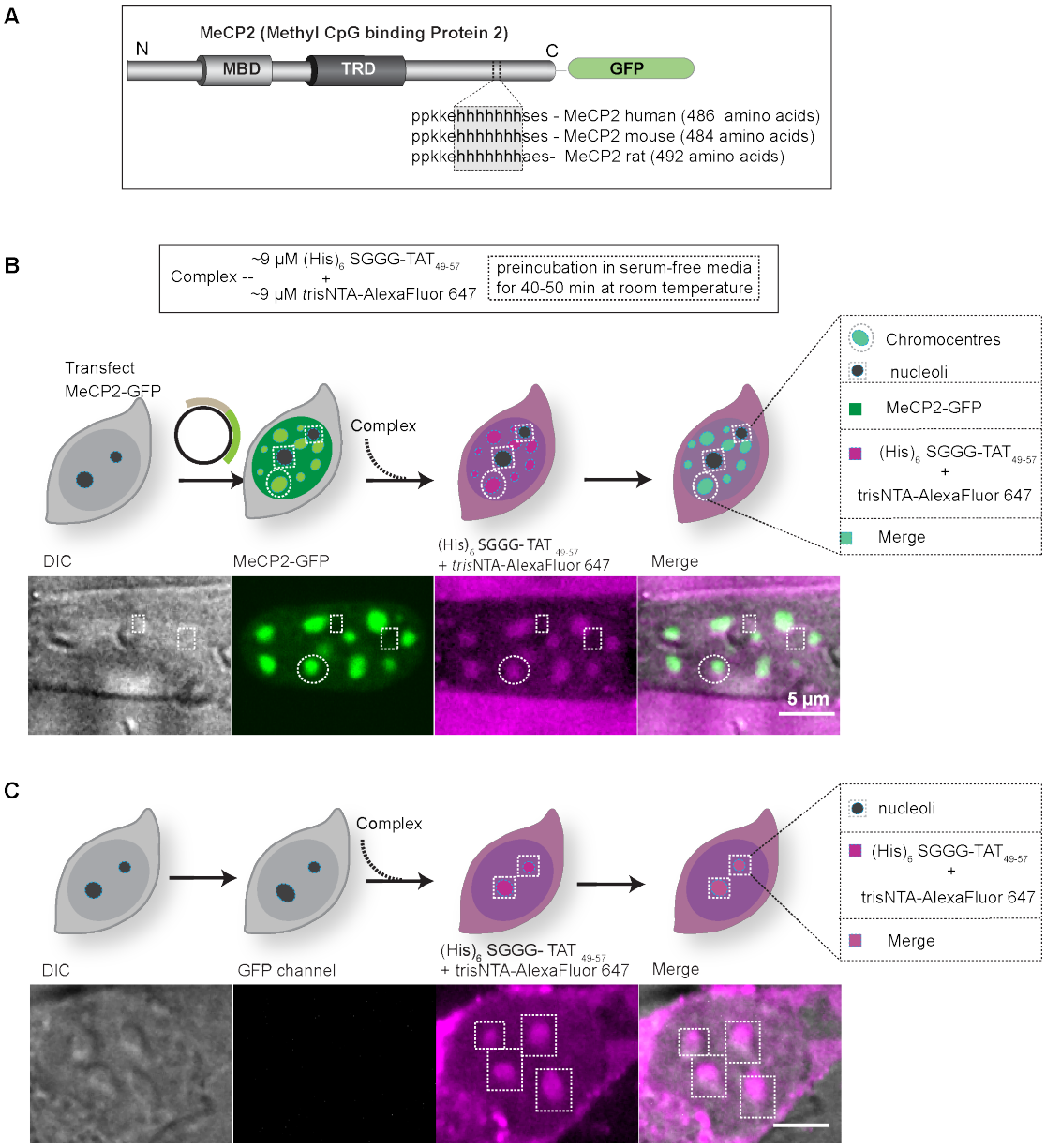

Figure 3.17. *In vivo* labeling of heptahistidine-bearing MeCP2 in live cells. (A) The MeCP2 constructs with conserved histidine residues are shown. (B) Cells transfected with MeCP2-GFP showed accumulation at the chromocenters. 30 minutes post complex addition, *tris*NTA-AlexaFluor 647 dissociated from the complex and bound to the heptahistidine peptide of MeCP2-GFP. (C) In untransfected cells, *tris*NTA-AlexaFluor 647 showed the typical nucleolar accumulation pattern.

As shown in Figure 3.18, *tris*NTA-AlexaFluor 647 alone was used in $(His)_6$-GFP-PCNA or MeCP2-GFP transfected cells to label the sites of replication or chromocenters, respectively, in fixed and permeabilized cells. Early, mid, and late replication patterns of the cells expressing $(His)_6$-GFP-PCNA are shown in figure 3.18A. Chromocenters in MeCP2-GFP

overexpressing cells were clearly labeled with *tris*NTA-AlexaFluor 647 (Figure 3.18B), thereby suggesting six histidines to be sufficient for the *tris*NTA binding.

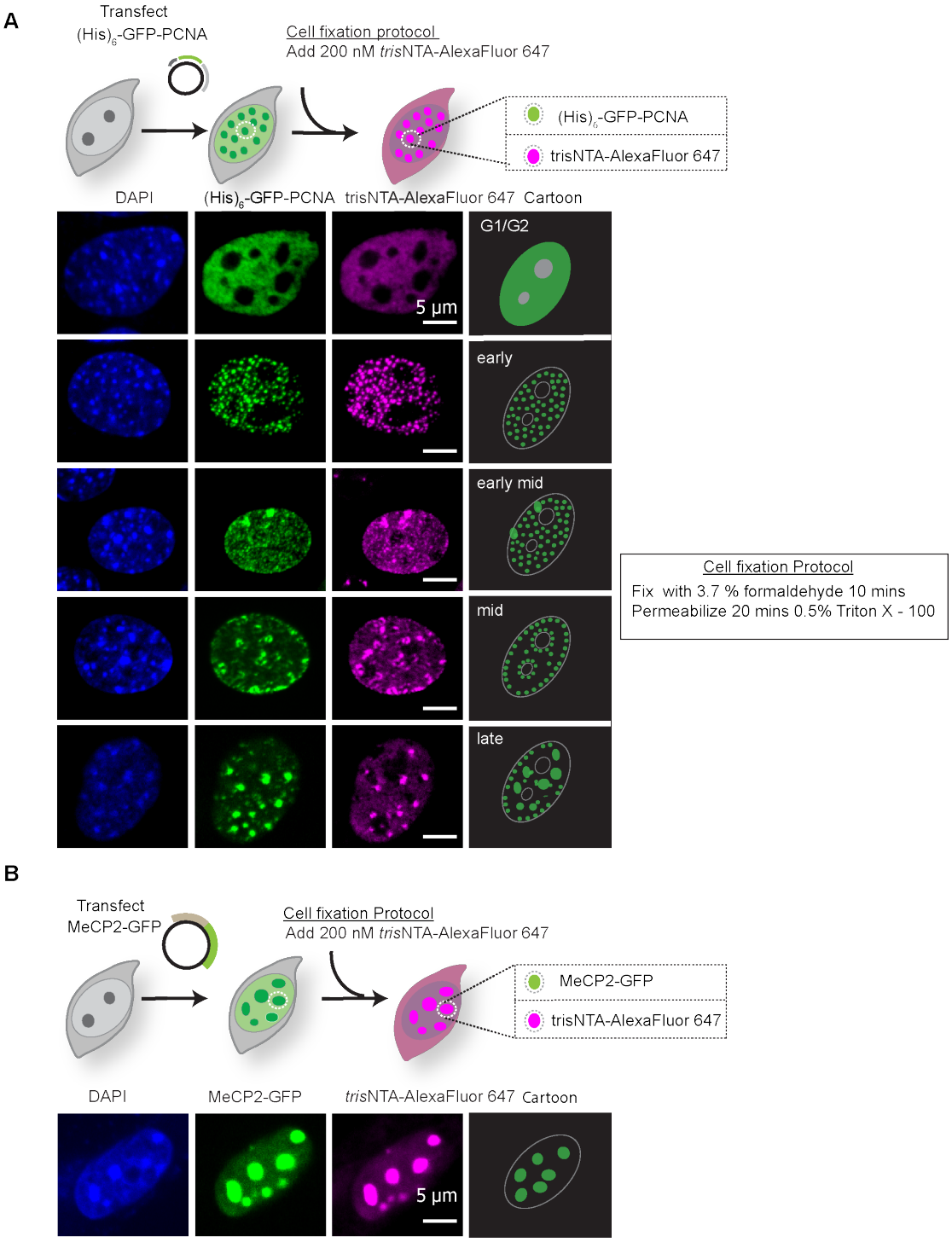

Figure 3.18. Fluorescent labeling of His-tagged proteins with *tris*NTA in fixed cells. (A) *tris*NTA-AlexaFluor 647 labeled $(His)_6$-GFP-PCNA transfected cells using the normal immunostaining procedure. (B) Similar procedures were adopted to label MeCP2-GFP transfected cells.

Discussion

Our results made us envisage that the combinatorial use of *tris*NTA with $(His)_6$-TAT labeling system would be a favorable strategy to explain complex biological events involving His-tagged proteins. We also believe that our present non-covalent labeling method would be useful for bio-imaging studies.

The labeled *tris*NTA did not enter the cell via endocytosis (Figure S2). Efficiently *tris*NTA was taken up by the cells via TAT and accumulated into the nucleoli. This nucleolar accumulation must be due to positive charges of arginine and lysine residues in the TAT moiety (Jarboui et al., 2012; Tunnemann et al., 2006);(Figure 3.15). The *tris*NTA bound to the $(His)_6$-TAT complex underwent uncoupling, leaving some free *tris*NTA. This uncoupling might have occurred in the reducing cellular compartments, thereby protonating the nitrogen atoms in the imidazole group of histidine residues tagged to TAT.

Labeling $(His)_6$-GFP-PCNA with *tris*NTA in living cells in order to visualize the repair events requires DNA damage induction by microirradiation with a 405 nm laser. As explained in Chapter 3.2, the employed laser conditions induced mixed DNA damage and led to massive PCNA recruitment at the irradiated site. Due to its massive recruitment, *tris*NTA that generally is uncoupled from hexahistidine tag of TAT was exchanged to a hexahistidine tag of PCNA at the spot of irradiation (Figure 3.16B). However, this minimal exchange was favored for a short duration. Very low levels of *tris*NTA co-localizing with $(His)_6$-GFP-PCNA at the replication sites (Fig. 3.16C) were due to less PCNA localized at the sites of replication than at the repair sites. The labeling of MeCP2 by *tris*NTA in living cells was enhanced due to the presence of heptahistidine in its coding region, which is one residue longer than its complexing cognate carrier $(His)_6$-TAT (Figure 3.17). The dissociation constant for *tris*NTA binding to a higher number of histidines should be lower than binding to a lower number of histidines. Hence, better uncoupling and labeling was achieved with MeCP2, the latter having a higher number of histidines than PCNA.

However, the fluorescent labeling with *tris*NTA convinced us that in the absence of the complexing partner carrier $(His)_6$-TAT, the expression levels of the $(His)_6$-GFP-PCNA and MeCP2 were sufficient for the *tris*NTA to label them in fixed and permeabilized cells (Fig. 3.18A, 3.18B). The fluorescent labeling with *tris*NTA for His-tagged proteins *in vitro* was a major breakthrough that alleviates the need for using antibodies against histidine. This procedure is a quick and cheap way to examine expression levels and protein localization. However biochemists who extensively use His-tags for protein purification, binding assays can now use this *tris*NTA strategy to label the proteins of interest in live and fixed cells, thereby bypassing the need for cloning fluorescent fusion constructs.

From the experimental observations made so far, there are two major factors that seem to

favor *tris*NTA exchange and subsequent *in vivo* binding in living cells: (a) increasing the number of histidine residues can improve *tris*NTA binding as observed in the case of MeCP2 and (b) despite having same number of histidines, a higher concentration of $(His)_6$-GFP-PCNA at irradiated sites leads to minimal exchange of *tris*NTA from $(His)_6$-TAT and a similarly high concentration of MeCP2 in the chromocenters facilitated the better binding of *tris*NTA. It is shown in Figure S3 that at safe concentrations of trisNTA, it can bind to as low as 0.4 picogram of MeCP2/cell.

Further improvements like altering the number of histidine tags for the protein of interest and multivalent NTA would be of great interest to optimize the efficacy of this system in living cells. The exchange efficiency of *tris*NTA from $(His)_6$-TAT to our protein of interest can be better evaluated by tagging the TAT and *tris*NTA with different fluorophores. This way one could quantify the TAT label in the nucleoli and the *tris*NTA label which is bound to the His-tagged proteins in nuclei or cytoplasm based on their localization. Moreover, *tris*NTA probes are economical, quickly produced, and biocompatible, thus facilitating the quick analysis of various structural and functional elements in the cell.

References

Agarwal, N., Becker, A., Jost, K. L., Haase, S., Thakur, B. K., Brero, A., Hardt, T., Kudo, S., Leonhardt, H., and Cardoso, M. C. (2011). MeCP2 Rett mutations affect large scale chromatin organization. *Hum Mol Genet, 20*(21), 4187-4195.

Bravo, R., and Celis, J. E. (1980). A search for differential polypeptide synthesis throughout the cell cycle of HeLa cells. *J Cell Biol, 84*(3), 795-802.

Bravo, R., Fey, S. J., Bellatin, J., Larsen, P. M., Arevalo, J., and Celis, J. E. (1981). Identification of a nuclear and of a cytoplasmic polypeptide whose relative proportions are sensitive to changes in the rate of cell proliferation. *Exp Cell Res, 136*(2), 311-319.

Czyzewska, J., Guzinska-Ustymowicz, K., Lebelt, A., Zalewski, B., and Kemona, A. (2004). Evaluation of proliferating markers Ki-67, PCNA in gastric cancers. *Rocz Akad Med Bialymst, 49 Suppl 1*, 64-66.

Fridman, Y., Palgi, N., Dovrat, D., Ben-Aroya, S., Hieter, P., and Aharoni, A. (2010). Subtle alterations in PCNA-partner interactions severely impair DNA replication and repair. *PLoS Biol, 8*(10), e1000507.

Garrels, J. I., and Franza, B. R., Jr. (1989). Transformation-sensitive and growth-related changes of protein synthesis in REF52 cells. A two-dimensional gel analysis of SV40-, adenovirus-, and Kirsten murine sarcoma virus-transformed rat cells using the REF52 protein database. *J Biol Chem, 264*(9), 5299-5312.

Goldsmith, C. R., Jaworski, J., Sheng, M., and Lippard, S. J. (2006). Selective labeling of extracellular proteins containing polyhistidine sequences by a fluorescein-nitrilotriacetic acid conjugate. *J Am Chem Soc, 128*(2), 418-419.

Guignet, E. G., Hovius, R., and Vogel, H. (2004). Reversible site-selective labeling of membrane proteins in live cells. *Nat Biotechnol, 22*(4), 440-444.

Hochuli, E., Dobeli, H., and Schacher, A. (1987). New metal chelate adsorbent selective for proteins and peptides containing neighbouring histidine residues. *J Chromatogr, 411*, 177-184.

Huang, Z., Hwang, P., Watson, D. S., Cao, L., and Szoka, F. C., Jr. (2009). Tris-nitrilotriacetic acids of subnanomolar affinity toward hexahistidine tagged molecules. *Bioconjug Chem, 20*(8), 1667-1672.

Janknecht, R., de Martynoff, G., Lou, J., Hipskind, R. A., Nordheim, A., and Stunnenberg, H. G. (1991). Rapid and efficient purification of native histidine-tagged protein expressed by recombinant vaccinia virus. *Proc Natl Acad Sci U S A, 88*(20), 8972-8976.

Jarboui, M. A., Bidoia, C., Woods, E., Roe, B., Wynne, K., Elia, G., Hall, W. W., and Gautier, V. W. (2012). Nucleolar protein trafficking in response to HIV-1 Tat: rewiring the nucleolus. *PLoS One, 7*(11), e48702.

Kabouridis, P. S. (2003). Biological applications of protein transduction technology. *Trends Biotechnol, 21*(11), 498-503.

Kannouche, P. L., Wing, J., and Lehmann, A. R. (2004). Interaction of human DNA polymerase eta with monoubiquitinated PCNA: a possible mechanism for the polymerase switch in response to DNA damage. *Mol Cell, 14*(4), 491-500.

Keppler, A., Gendreizig, S., Gronemeyer, T., Pick, H., Vogel, H., and Johnsson, K. (2003). A general method for the covalent labeling of fusion proteins with small molecules in vivo. *Nat Biotechnol, 21*(1), 86-89.

Khan, F., He, M., and Taussig, M. J. (2006). Double-hexahistidine tag with high-affinity binding for protein immobilization, purification, and detection on ni-nitrilotriacetic acid surfaces. *Anal Chem, 78*(9), 3072-3079.

Kim, S. H., Jeyakumar, M., and Katzenellenbogen, J. A. (2007). Dual-mode fluorophore-doped nickel nitrilotriacetic acid-modified silica nanoparticles combine histidine-tagged protein purification with site-specific fluorophore labeling. *J Am Chem Soc, 129*(43), 13254-13264.

Lata, S., Gavutis, M., Tampe, R., and Piehler, J. (2006). Specific and stable fluorescence labeling of histidine-tagged proteins for dissecting multi-protein complex formation. *J Am Chem Soc, 128*(7), 2365-2372.

Leonhardt, H., Rahn, H. P., Weinzierl, P., Sporbert, A., Cremer, T., Zink, D., and Cardoso, M. C. (2000). Dynamics of DNA replication factories in living cells. *J Cell Biol, 149*(2), 271-280.

Lisenbee, C. S., Karnik, S. K., and Trelease, R. N. (2003). Overexpression and mislocalization of a tail-anchored GFP redefines the identity of peroxisomal ER. *Traffic, 4*(7), 491-501.

Mayer, A., Sharma, S. K., Tolner, B., Minton, N. P., Purdy, D., Amlot, P., Tharakan, G., Begent, R. H., and Chester, K. A. (2004). Modifying an immunogenic epitope on a therapeutic protein: a step towards an improved system for antibody-directed enzyme prodrug therapy (ADEPT). *Br J Cancer, 90*(12), 2402-2410.

Morell-Quadreny, L., Clar-Blanch, F., Fenollosa-Enterna, B., Perez-Bacete, M., Martinez-Lorente, A., and Llombart-Bosch, A. (1998). Proliferating cell nuclear antigen (PCNA) as a prognostic factor in renal cell carcinoma. *Anticancer Res, 18*(1B), 677-682.

Naryzhny, S. N. (2008). Proliferating cell nuclear antigen: a proteomics view. *Cell Mol Life Sci, 65*(23), 3789-3808.

Nieba, L., Nieba-Axmann, S. E., Persson, A., Hamalainen, M., Edebratt, F., Hansson, A., Lidholm, J., Magnusson, K., Karlsson, A. F., and Pluckthun, A. (1997). BIACORE analysis of histidine-tagged proteins using a chelating NTA sensor chip. *Anal Biochem, 252*(2), 217-228.

Tavare, J. M., Fletcher, L. M., and Welsh, G. I. (2001). Using green fluorescent protein to study intracellular signalling. *J Endocrinol, 170*(2), 297-306.

Tsien, R. Y. (1998). The green fluorescent protein. *Annu Rev Biochem, 67*, 509-544.

Tunnemann, G., Martin, R. M., Haupt, S., Patsch, C., Edenhofer, F., and Cardoso, M. C. (2006). Cargo-dependent mode of uptake and bioavailability of TAT-containing proteins and peptides in living cells. *FASEB J, 20*(11), 1775-1784.

van Diest, P. J., Brugal, G., and Baak, J. P. (1998). Proliferation markers in tumours: interpretation and clinical value. *J Clin Pathol, 51*(10), 716-724.

Vives, E., Brodin, P., and Lebleu, B. (1997). A truncated HIV-1 Tat protein basic domain rapidly translocates through the plasma membrane and accumulates in the cell nucleus. *J Biol Chem, 272*(25), 16010-16017.

Yaffe, D., and Saxel, O. (1977). Serial passaging and differentiation of myogenic cells isolated from dystrophic mouse muscle. *Nature, 270*(5639), 725-727.

Supplementary information

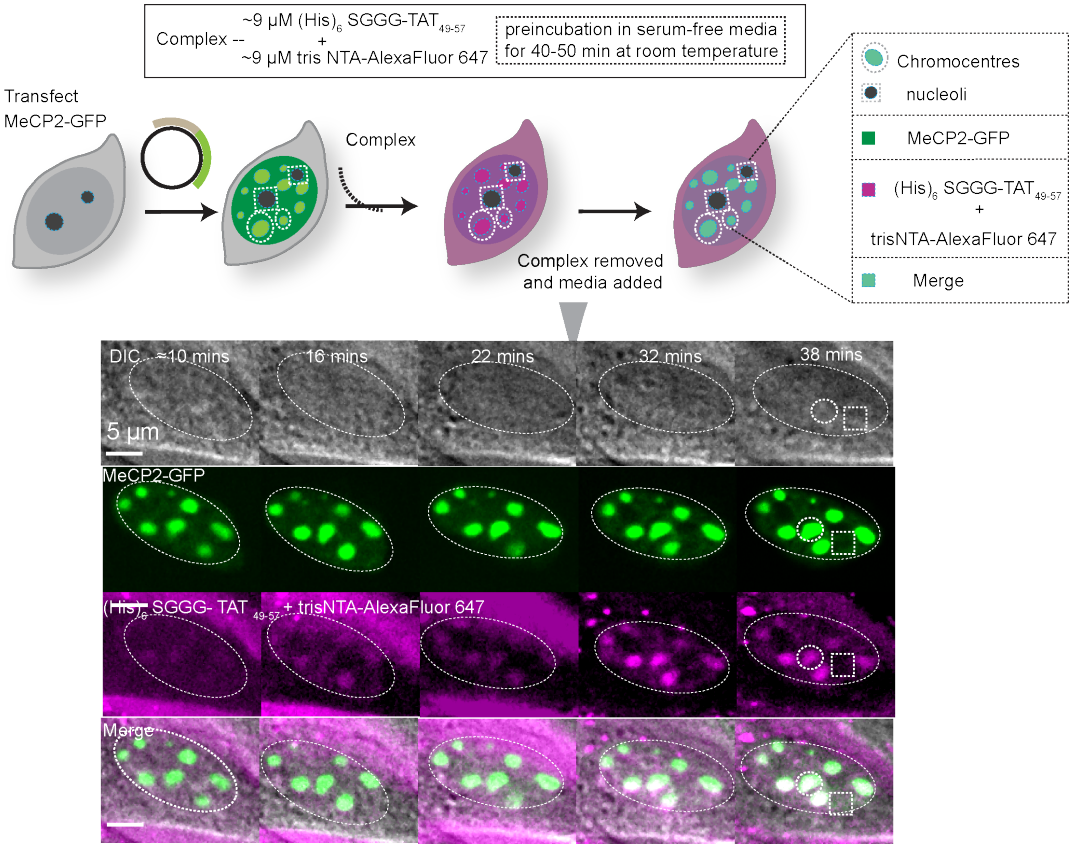

Figure S1. Time lapse of *tris*NTA labeling MeCP2. The preincubated complex was added to the cells transfected with MeCP2-GFP. Washing step was included to reduce the background and the TAT-mediated toxicity to the cells.

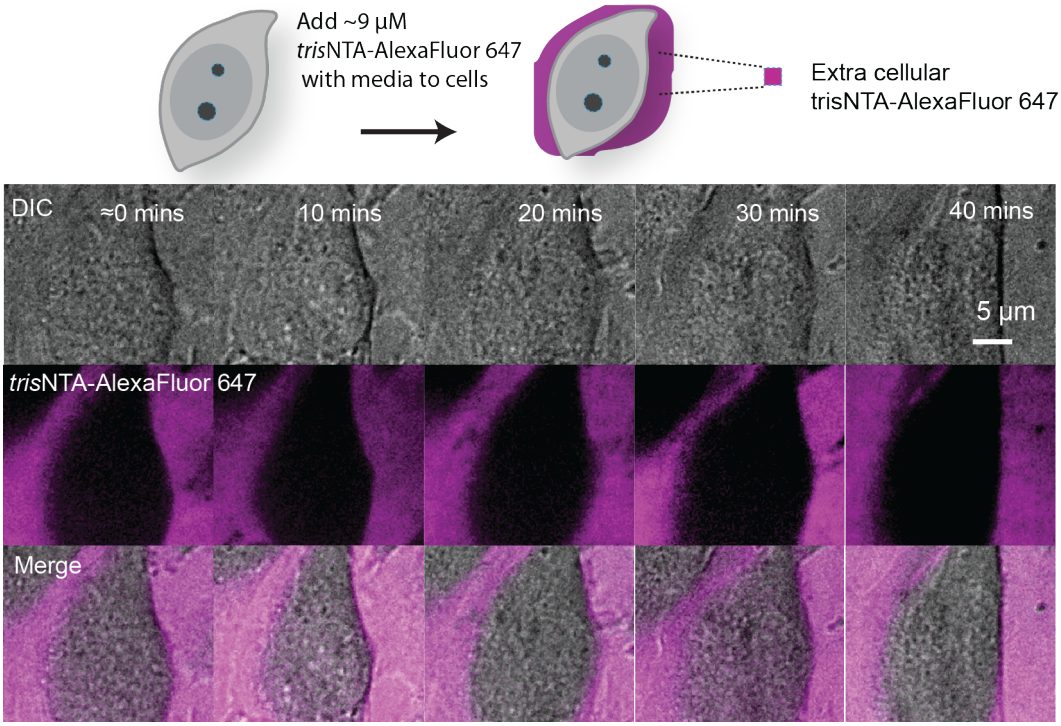

Figure S2. *tris*NTA is not cell permeable. Time lapse images of labeled *tris*NTA show that when it is added to cells, *tris*NTA-AlexaFluor 647 alone is not able to penetrate into cells.

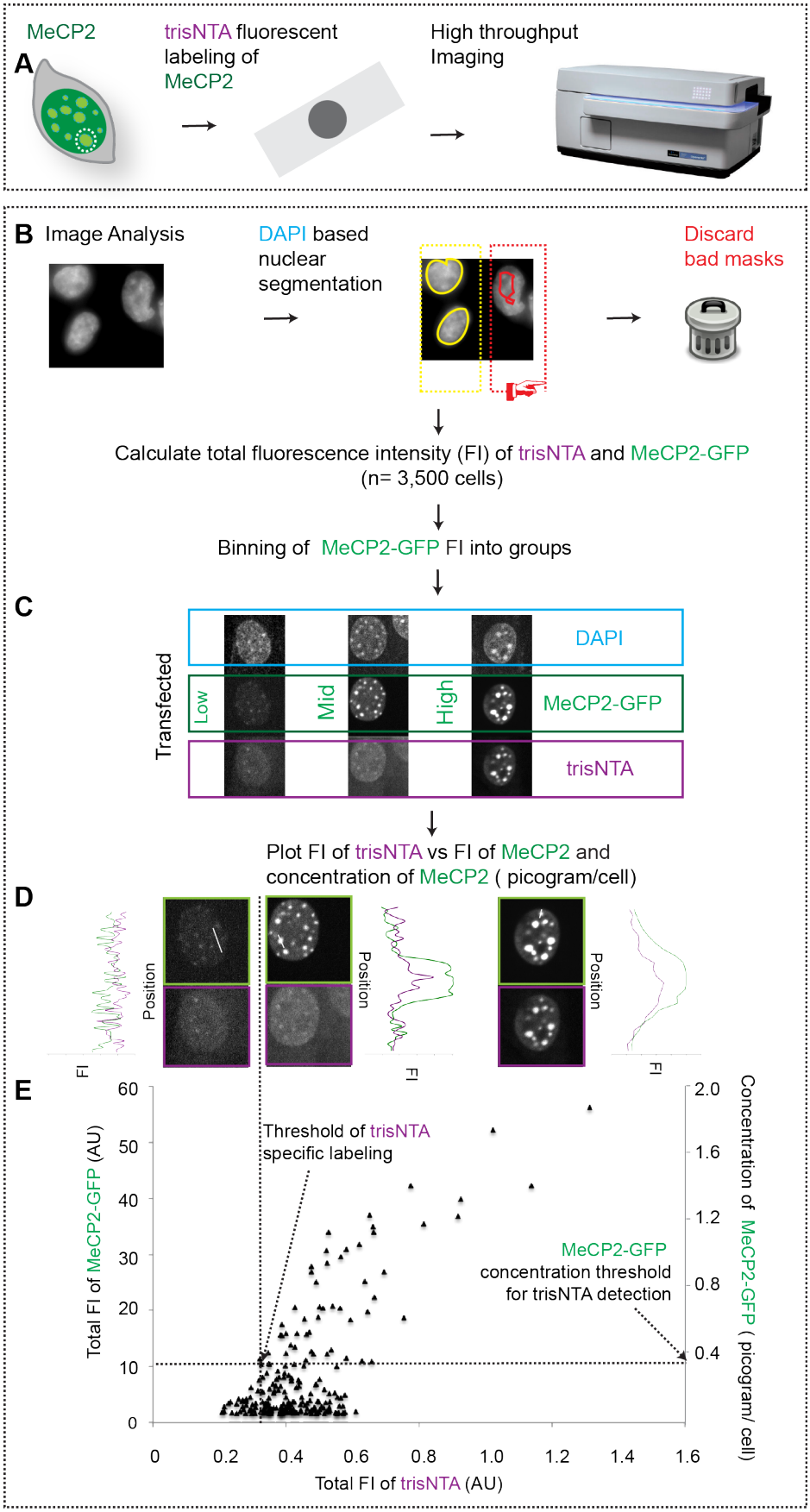

Figure S3. Minimal His-tagged protein concentration was detected using safe amounts of trisNTA. (A) MeCP2 transfected cells were labeled with 200 nM trisNTAAF647 and DNA counterstained with DAPI. Imaging was performed using an Operetta automated imaging system (Perkin Elmer, Buckinghamshire, UK). (B) Image analysis was performed as described in the workflow. (C) Exemplary images with different MeCP2 levels are shown with the corresponding DNA stain and trisNTA labels and magnified (D). Fluorescence intensitiy (FI) profiles were used to score specific trisNTA labels of MeCP2 distribution. (E) A total FI of trisNTA and MeCP2 are plotted based on a purified MeCP2 calibration curve, specifically labeled by trisNTA (as shown in the line profiles in the concentration needed. Scale bar: 5µm.

3.4. Role of H2A variants in DNA damage susceptibility, replication and repair

This chapter has the following major contributors

Malini Rajan[1], Corella S. Casas-Delucchi[1], Viola Sansoni[2], Martin S. Staege[3], Sandra B. Hake[2,4], M. Cristina Cardoso[1], and Axel Imhof[2,4]

1- Technische Universität Darmstadt, Darmstadt, Germany

2- Ludwig Maximilians University, Munich, Germany

3- Martin Luther University, Halle, Germany

4- Adolf-Butenandt Institute, Ludwig Maximilians University, Munich, Germany

Some results from Chapter-3.4 have been published in Nucleic Acids Research in 2014.

Sansoni V, Casas-Delucchi CS, **Rajan M**, Schmidt A, Bonisch C, Thomae AW, Staege MS, Hake SB, Cardoso MC, Imhof A., "The histone variant H2A.Bbd is enriched at sites of DNA synthesis." Nucleic Acids Res. 2014;42(10):6405-20.

Abstract

Chromatin is structured such that it has special histones called variant histones.

Variant histones have evolved to perform functions that are unique from the canonical core histones, including specific histone modifications, chromatin remodeling, transcriptional regulation, protection against DNA damage, and DNA repair. The precise role of histones in these processes remains largely unclear.

Here we focus on H2A.Bbd, a histone H2A variant found in mammals but not in invertebrates. This rapidly evolving histone variant is studied in comparison with its canonical counterpart, H2A. We find H2A.Bbd is localized transiently at the sites of active DNA synthesis during S-phase and DNA repair. Decondensed or relaxed chromatin conformations could be one potential reason for the increased number of fragile sites that have a higher likelihood of being damaged. Taken together, our data suggest that H2A.Bbd is enriched in sites of active DNA replication leading to a shortened S phase duration and more open chromatin conformation, which may result in increased DNA damage susceptibility. H2A.Bbd overexpressing cells have a shorter S-phase duration and increased DNA damage sensitivity; these two phenotypes are observed in Hodgkin's lymphoma cells that aberrantly overexpress this histone.

Highlights

- H2A.Bbd accumulates at sites of DNA replication/repair.
- H2A.Bbd loads faster than H2A at damaged sites.
- H2A.Bbd overexpressing cells are sensitive to UV-C compared to H2A overexpressing cells.
- H2A.Bbd overexpressing cells exhibit shorter S-Phase duration.
- Similarly, Hodgkin's lymphoma cell lines, with high H2A.Bbd mRNA levels, replicate faster.

Introduction

Genomic DNA is packaged and condensed into chromatin in a dynamic manner. Higher order structures of chromatin plays an important role in gene regulation (Bian & Belmont, 2012; Wolffe & Guschin, 2000). The nucleosome is the elementary unit of the chromatin of eukaryotic genomic DNA. Nucleosomes are stable *in vitro* but are dynamically arranged during the transcription, replication, recombination, and repair processes (Groth et al., 2007; Grunstein, 1997; Wolffe, 1997). Nucleosomal compartments contain core canonical histones like H2A, H2B, H3, and H4, which are positively charged and form dimers (Sperling & Bustin, 1976). Two copies of each core histone form an octameric structure, from two dimers of H2A/H2B with the closest central H3/H4 tetramer, which can package about 147 bps of DNA to form the nucleosome core particle (NCP) (Richmond, 1999). Histone variants are non-allelic protein isoforms of canonical histones that differ in their sequence and their expression pattern (Marzluff et al., 2002). Canonical histones are synthesized during the S phase of the cell cycle, whereas the expression of histone variants is replication independent and takes place throughout the cell cycle (Nelson et al., 2002). Core histones are subjected to post-translational modifications, which are largely reversible, like acetylation, methylation, ubiquitination, poly- ADP ribosylation, biotynylation and phosphorylation. These modifications are observed in the N-terminal tails and also in histone fold domains. Chromatin structures that comprise nucleosomal units can undergo morphological and structural changes. Such changes can lead to several fatal diseases, including cancer. Generally, modifications within the N-terminus of the core histone can regulate chromatin compaction. However, when an oncogene is activated, and subsequent deactivation of a tumour suppressor gene may lead to chromatin decondensation (Herrera et al., 1996; Laitinen et al., 1990). Chromatin structural changes that leads to oncogenic transformation can potentially be used as biomarkers for e.g., it was found that EZH2, the component of the polycomb repressive complex 2 (PRC2), was found to be upregulated in prostrate cancer (Varambally et al., 2002). However, past studies showed that the overexpression of some of the histones and their variants are implicated with cancer, for e.g., overexpression of histones like H3.3 was found in carcinoma of esophagus, H2A.1 in hepatocarcinogenesis and phosphorylated histone H3 in gastric adenocarcinoma, (Graber et al., 1996; Khare et al., 2011; Takahashi et al., 2006; Vardabasso et al., 2014).

Hence, the properties of histone variants is important for the better understanding of disease development. One of the variants of histone H2A is H2A.Bbd. H2A.Bbd or H2A Barr body depleted got this name as it is found excluded from the Barr body (Chadwick & Willard, 2001). H2A.Bbd is highly expressed in spermatogenic fractions of mammalian testis (Ishibashi et al., 2010). This histone variant lacks the acidic patch in the C-terminus found in

canonical histones. Accordingly, it has the tendency to relax or destabilize the nucleosome core particle. H2A.Bbd containing nucleosomes protect only 120-130 bps of DNA, whereas 147 bps are protected by canonical nucleosomes that contains histones like H2A (Bao et al., 2004; Chodaparambil et al., 2007; Doyen et al., 2006; Kamakaka & Biggins, 2005). Nucleosomes containing H2A.Bbd form specific chromatin structures that are characterized by smaller DNA protection and nucleosome spacing and are mostly found within actively transcribed genes (Tolstorukov et al., 2012). Moreover, since H2A.Bbd does not have any lysine residue at its C-terminus, it cannot be ubiquitinated. Canonical H2A, on the other hand, is ubiquitinated at the K119 site, which is a transcription repression mark (Cao et al., 2005). Due to the absence of this transcription repression mark at the K119 site, H2A.Bbd positively regulates transcription. Increased expression of different histone variants has been found in multiple types of cancer. As H2A.Bbd plays a role in regulating the key cellular and developmental processes, the deregulation of histone variant expression has been linked to tumor initiation and progression. H2A.Bbd transcripts are found in high levels in Hodgkin Lymphoma cell lines as described in (Winkler et al., 2012), pointing to its potential relevance to cancer. While the biophysical characteristics of this histone variant are well-characterized *in vitro*, deep understanding of its cellular processes, such as DNA damage, replication, repair and its localization, is still lacking. Previous studies already have shown that H2A.Bbd is overexpressed in male spermiogenic fractions as described in (Ishibashi et al., 2010). Still, several potential roles of H2A.Bbd remains unclear. In this study, we focused on understanding the histone variant H2A.Bbd, and their relevance in disease, particularly cancer. To this end, we overexpressed H2A.Bbd in mouse embryonic fibroblasts (MEFs) and elucidated their radiation sensitivity, proliferation behaviour, S-phase duration, and their relevance towards pathophysiological phenotypes (i.e., Hodgkin's lymphoma).

Materials and Methods

Cell culture, transfection and live cell imaging

Female MEF cells were grown in Dulbecco's Modified Eagle Medium (DMEM) supplemented with 10% fetal calf serum (Sigma) and 50 µg/ml gentamicin and 2 mM glutamine. Human Hodgkin's lymphoma (HL) cell lines L-428 (Drexler et al., 1986), L1236 (Wolf et al., 1996), KM-H2 (Kamesaki et al., 1986), HDLM-2 (Drexler et al., 1986), L-540 (Diehl et al., 1981) were obtained from Deutsche Sammlung für Mikroorganismen und Zellkulturen (Braunschweig, Germany). Epstein-Barr virus-immortalized cell lines (LCL) and Peripheral blood mononuclear cells (PBMCs) from healthy donors and patients with HL were isolated as described in (Foell et al., 2008) and were cultured in RPMI 1640 (Sigma) supplemented with 10% fetal calf serum (Sigma), 50 µg/ml gentamicin, and 4 mM glutamine. For stable cell

lines, MEF cells were transfected with GFP-H2A.Bbd and GFP-H2A expression plasmids using FuGENE® HD transfection reagent (Roche) according to the manufacturer's instructions. Stable cell lines were selected using G418 (PAA) at a concentration of 600 µg/ml. For live cell imaging mouse embryonic fibroblast (MEFs) cells stably expressing GFP-H2A.Bbd were transfected with mRFP-PCNA (Ref: Sporbert et al. 2005) using Amaxa nucleofection protocol, was used as described in (Casas-Delucchi et al. (2012).

Nucleofected cells were plated on a p35 glass bottomed dish and grown under standard conditions. 3D stacks were acquired at 20-minute intervals overnight. Time lapse imaging was carried out on a UltraVIEW VoX spinning disc confocal system (PerkinElmer, UK) in a closed live-cell microscopy chamber (ACU control, Olympus, Japan) heated to 37°C, with 5% CO_2, and 60% humidity, mounted on a Nikon Ti microscope (Nikon, Japan), using a 60x/1.45 NA Plan apochromat oil immersion objective lens. Images were obtained with a cooled 14-bit EMCCD camera (C9100-50, CamLink). Maximum intensity Z-projections were assembled into videos and annotated using ImageJ (http://rsb.info.nih.gov/ij/).

Microirradiation experiments

A Nikon Ti spinning disc microscope was used for creating laser-induced DNA damage. A 405 nm diode laser set to 100% transmission was used for creating DNA double strand breaks. Spots of 1 µm in diameter were selected inside the nucleus and were microirradiated with 1 mJ energy. Images were acquired pre- and post-microirradiation. For PCNA independent repair induction, with 561 nm laser DNA damage were induced at 66 mJ energy as described (Muster, 2014).

UV-C irradiation experiments

To assess the sensitivity of H2A.Bbd overexpressing cells to UV-C light, cells were irradiated with a UV-C (254 nm) source containing short wave lamps (Amersham Biosciences) at a power of 5.8 watt. To induce damage, media was removed from the cells and irradiation was performed globally for 10 seconds with a total dosage of 1 mJ/cm^2. Control cells were not irradiated.

Immunofluorescence

Cells were grown on glass coverslips and fixed with 3.7% formaldehyde for 10 minutes at room temperature followed by a combined permeablization and DNA denaturation step with ice cold 0.7% Triton X-100/ 0.4 N HCL/ PBS for 10 minutes. To block unspecific antibody signal, the cells were incubated with 4% BSA for 30 minutes at room temperature. Immunostaining of CPD was performed by incubating the cells with monoclonal anti-CPD antibody (Kamiya Biomedical Company, Cat no: MC-062) at a dilution of 1:200 in BSA for 1 hour at room temperature. For detection, cells were incubated with polyclonal antibody anti-mouse IgG coupled to Cy3 (Jackson Laboratories, Cat no: 715-165-151) at a dilution of

1:330 for 1 hour at room temperature. The DNA content was stained with 4',6-diamidino-2-phenylindole (DAPI) and finally mounted in Mowiol 4-88 (Sigma-Aldrich Chemie).

In situ replication labeling

To visualize newly synthesized DNA, cells grown on coverslips were pulse labeled with 100 µM 5-bromo-2′-deoxyuridine (BrdU, Sigma-Aldrich) and either fixed immediately or chased for the indicated time in pre-warmed medium supplemented with 200 µM thymidine. Cells were fixed with 3.7 % formaldehyde for 10 minutes and permeabilized with 0.5 % Triton X-100 for 20 minutes. BrdU detection was performed with rat-anti-BrdU (Gentaur, Cat no: OBT0030CX, dilution 1:100) in the presence of DNaseI for 1 hour at 37°C.

Chromatin manipulation assay

Cells were grown in DMEM medium supplemented with 10% fetal calf serum, 2 mM L-glutamine, 5 g/ml gentamycin. Hypercondensation medium was composed of a dilution of 10X PBS (1.4 M NaCl, 26.8 mM KCl, 101.4 mM $Na_2HPO_4.2H_2O$, 14.6 mM KH_2PO_4) that were diluted within growth medium to yield dilutions of 4X, 2X, and 1X PBS separately. Cells were treated with the different hypercondensation media for 15 minutes to achieve chromatin condensation as described in (Martin & Cardoso, 2010). Following this, cells with hypercondensed chromatin were irradiated with UV-C irradiation, as described above.

Western blot analysis

MEFs transfected with GFP-histone variant and Hodgkin's lymphoma (HL) cell lines were incubated with 0.1% Triton in PBS supplemented with proteinase inhibitor for 10 min at 4°°C. After centrifugation at 3000 rpm, the nuclear pellet was resuspended in 1X PBS supplemented with proteinase inhibitors, and the DNA was digested with Benzonase (VWR) for 15 min at 37°C. 2X Laemmli buffer was added to the suspension of nuclei and heated for 15 min at 95°C. For the western blot antibodies like anti-GFP antibody, which was a mixture of two mouse anti-GFP monoclonal antibodies (Roche), was used at a dilution of 1:1000, the anti-H3 antibody (Abcam ab1719) was used at a concentration of 1:5000, and the H2A.Bbd antibody (Millipore polyclonal) was used at a dilution of 1:1000. HRP coupled secondary antibodies were used at a dilution of 1:5000, and detection was performed using ECL chemiluminescent reagents (GE Healthcare Life Sciences). Protocol from Ms. Viola Sansoni.

Quantitative reverse transcription-polymerase chain reaction

RNA from HL cell lines and peripheral blood mononuclear cells (PBMCs) was isolated using Trizol reagent (Invitrogen, Karlsruhe, Germany) following the manufacturer's protocol. After reverse transcription of 2 µg of RNA, quantitative reverse transcription-polymerase chain reaction (qRT-PCR) was performed as described in (Neumann et al., 2010). The following primer combinations were used: for actin beta (ACTB), 5′-ggc atc gtg atg gac tcc g-3′ and 5′ -gct gga agg tgg aca gcg a-3′ and; for H2A.Bbd,: 5′ -tcg ttt tca gtg agc cag gt-3′ and 5′-cag aat

taa tga agg ccc aag-3′. Quantification of gene expression was performed using the $2^{-\Delta\Delta Ct}$ method [H], and for comparative analysis the median Dct value from PBMC (21 independent donors) was set as one. Protocol from Mr. Martin Staege.

CPD quantification

The levels of DNA damage were calculated from confocal 3D images of CPD stainings and DNA was counterstained with DAPI using the image analysis platform Priithon (http://code.google.com/p/priithon/). The DAPI images were used to create 3D nuclear masks by applying a median filter (sigma = 5 px) and segmenting the filtered images using automatic thresholding (Otsu, 1979). The integrated CPD signal within the nuclear mask was divided by the mask volume to obtain the mean CPD intensity in each nucleus.

Microirradiation data analysis

For evaluation kinetics of the accumulation of histones from microirradiation data, a minimum of 8–-10 cells was analyzed. The easyFRAP software package (Rapsomaniki et al., 2012) whose function include, data visualization, normalization of the raw recovery curves, and curve fitting. This software allows low quality data to be excluded and quantitative information to be extracted and saved. Raw intensities of bleached area (ROI1), the whole cell (ROI2), and a background area (ROI3) and the corresponding time-points were calculated using a custom made ImageJ macro. Results were saved in .csv, .txt, and .xls file formats. The easyFRAP software package computes the recovery curves, according to the formula of double normalization, and maximal accumulation represents the highest ratio from each experiment.

Results

H2A.Bbd localizes at the sites of DNA synthesis

To understand the composition and function of H2A.Bbd containing chromatin, female MEFs stably expressing GFP-H2A.Bbd and GFP-H2A were generated. These cell lines expressing relevant histones at similar levels were confirmed by fluorescence activated cell sorting. In order to characterize the nuclear distribution of GFP-H2A.Bbd, we used light microscopy to visualize the specific GFP-H2A.Bbd localization pattern. We were able to show that GFP-H2A.Bbd is associated with the replication machinery by co-localizing and following mRFP-PCNA during replication and repair as shown in Figure 3.19B. Co-localization of H2A.Bbd with the endogenous PCNA was confirmed with the addition of PCNA biomarker, as shown in Figures 3.19C and 3.19D with the corresponding line profiles. To check if H2A.Bbd accumulation at the microirradiated sites is PCNA dependent, H2A.Bbd-overexpressing MEFs were microirradiated with 405 nm and 561 nm lasers. The DSBs generated by laser microirradiation are more similar to endogenous DSBs. DNA damage induction by irradiation at a 561 nm wavelength does not lead to accumulation of PCNA. No recruitment of H2A.Bbd

was observed with a 561 nm laser, that does not recruit PCNA. The processive DNA synthesis-related factor PCNA only accumulates at sites of 405 nm laser induced DNA damage. Accordingly, PCNA was recruited at the sites of repair with the 405 nm laser but not with 561 nm laser as described (Muster, 2014). The maximum accumulation of the H2A.Bbd is shown in Figure 3.19E when the DNA damage was induced by these different types of laser.

To check the mobility of H2A.Bbd with respect to H2A at the repair sites, the corresponding cell lines were microirradiated with a 405 nm laser. In comparison to the canonical histone H2A, H2A.Bbd was highly mobile at the repair sites caused by 405 nm laser. The time lapse images and the recruitment kinetics clearly demonstrate the high mobility of H2A.Bbd in Figure 3.20A and B. In contrast, the canonical GFP-H2A remained relatively immobile under the same conditions.

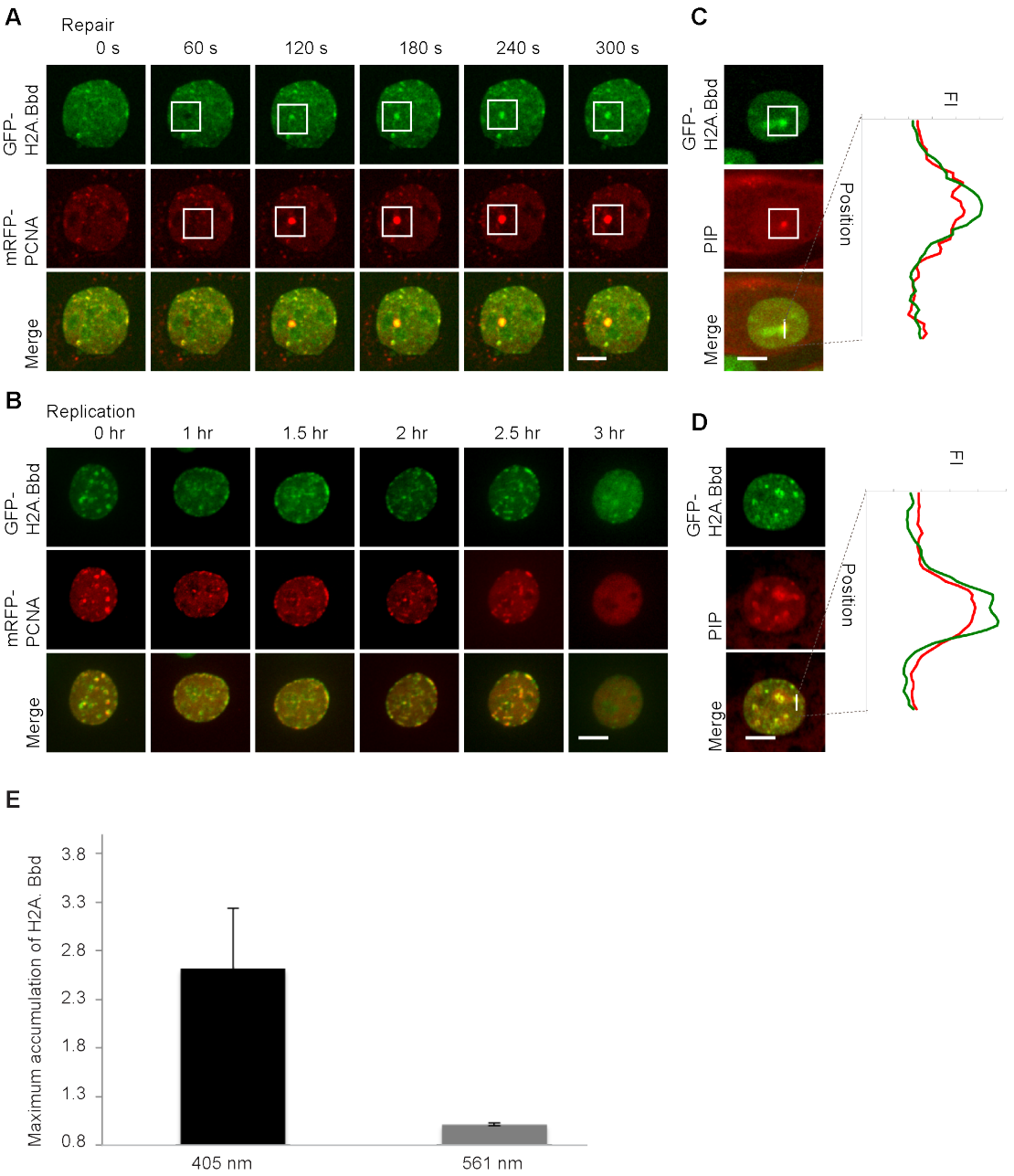

Figure 3.19. **H2A.Bbd is localized at the sites of DNA synthesis and repair**. (A) Cells overexpressing H2A.Bbd were co-transfected with mRFP-PCNA and microirradiated with a 405 nm laser. At the sites of repair it was found that H2A. Bbd localizes and follows PCNA. (B) Time Lapse images of H2A.Bbd following mRFP-PCNA during S-phase are shown. (C) H2A.Bbd overexpressing MEFs alone were microirradiated with 405 nm laser and found to co-localize with endogenous PCNA, which is confirmed by our PCNA biomarker (i.e., TAT-S-S-PL-R or PCNA interacting Peptide [PIP], as described in Chapter-3.3). (D) H2A.Bbd was found to co-localize with the endogenous PCNA at the replication sites. The line intensity plots of H2A.Bbd (green) and PIP (red) show a positive correlation. (E) Maximum accumulation of H2A.Bbd upon DNA double strand breaks induced with 405 nm and 561 nm laser is shown. Error bar represents standard deviation. (Scale bar: 5 μm)

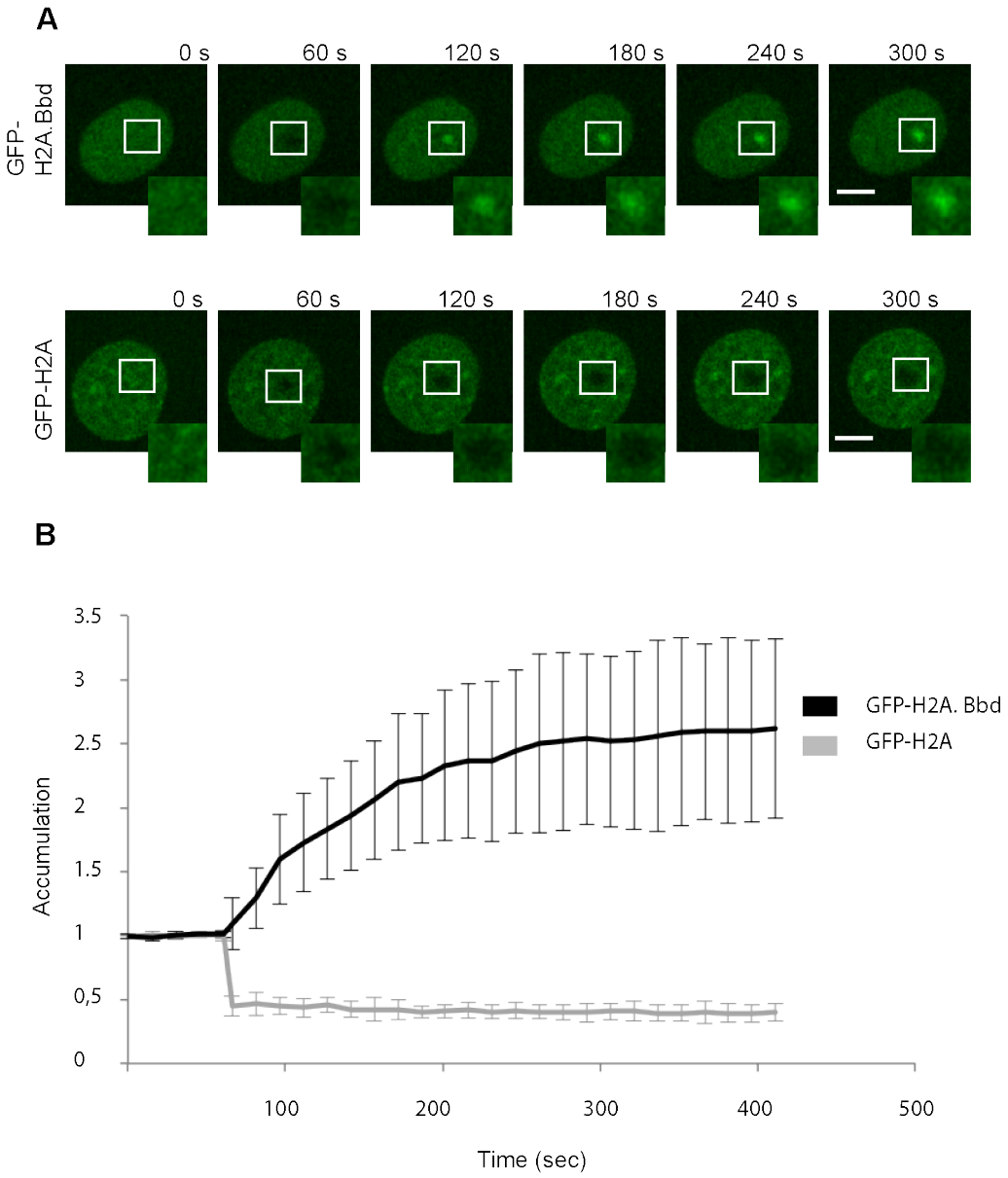

Figure 3.20. Mobility of H2A.Bbd at the microirradiated sites. (A) Cells expressing GFP-H2A or GFP-H2A.Bbd were imaged and compared before and after microirradiation with 405 nm laser. (B) Quantification of the microirradiation data computed by easyFRAP is shown. Values represent mean and error bars represent standard deviation.

H2A.Bbd overexpressing cells are sensitive to non-ionizing radiation

In order to check the sensitivity of H2A.Bbd overexpressing cells in comparison with H2A overexpressing cells to non-ionizing radiation, the cells were exposed to UV-C and subsequently tested for the CPD generation through immunostaining. It was found that H2A.Bbd overexpressing cells showed increased sensitivity to UV-C than H2A overexpressing ones. The amount of CPD was analyzed via custom Priithon code (Figure 3.21).

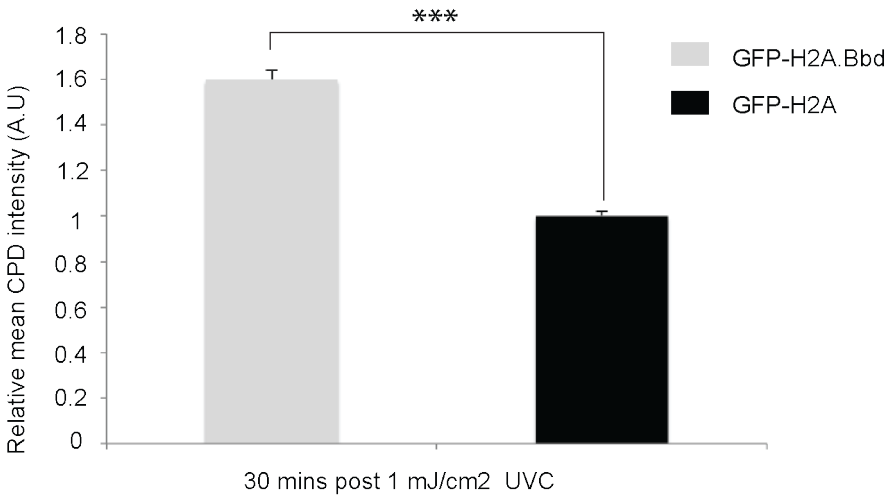

Figure 3.21. Radiation sensitivity of H2A.Bbd overexpressing cell lines. MEFs overexpressing H2A.Bbd and H2A were subjected to UV-C irradiation of 1 mJ/cm^2. Quantification of the whole cell nuclear intensity was double normalized to the H2A counterpart and the unirradiated cells. Error bars represent 95% confidence intervals. (***: $p < 0.001$, calculated using two-tailed *t*-tests)

Different levels of chromatin condensation influence DNA damage sensitivity in H2A variants

To elucidate the increased DNA damage sensitivity in H2A.Bbd over-expressing cells and to test whether changes in higher-order chromatin structure caused by H2A.Bbd over-expression have an influence in the induction of CPDs, we developed a system for chromatin manipulation that uses a hypertonic treatment as described in (Martin et al., 2010;) Figure 3.22. Using this assay, the chromatin condensation levels of H2A.Bbd over-expressing cells were reversed to similar levels of H2A control cells. We found that H2A.Bbd overexpressing cells with condensed chromatin were mildly resistant to DNA damage.

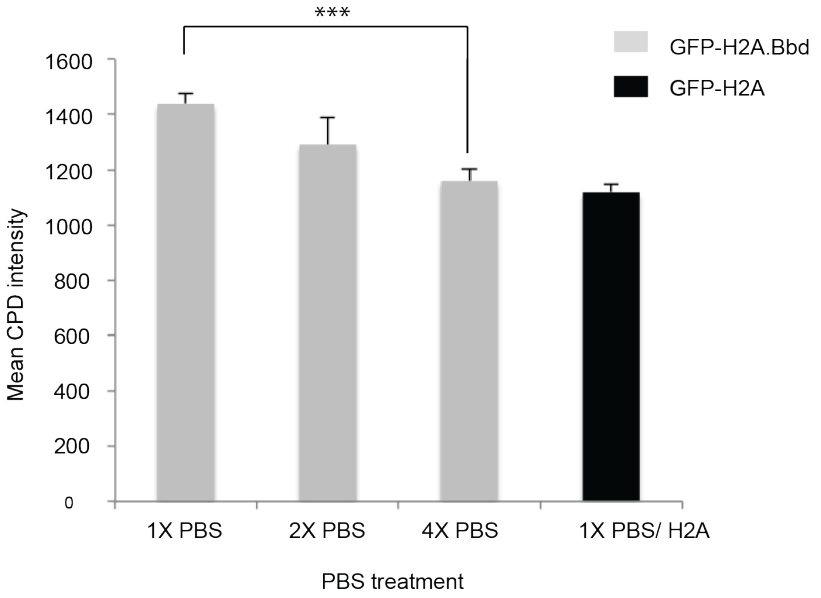

Figure 3.22. Radiation sensitivity at different condensation levels of the histone variants. Chromatin of the MEFs containing H2A.Bbd were treated with different concentration of 1X, 2X, 3X, or 4X PBS, and then they were subjected to UV-C irradiation with the same dose. Then the relative CPD intensity was measured. Error bars represent 95% confidence intervals. (***: $p < 0.001$, calculated using two-tailed *t*-tests)

H2A.Bbd is over-expressed in Hodgkin's lymphoma cancer cells.

As H2A.Bbd actively localizes at the sites of DNA replication, we wanted to know if the expression of H2A.Bbd had any influence on the replication timing. For that we used BrdU pulse for the H2A.Bbd and H2A overexpressing cells, and then from BrdU positive cells, we calculated the percentage of S-phase cells. Doubling time was measured in both the cell lines. S-phase duration was calculated by multiplying doubling time with the percentage of S-phase cells. Here we found a 20% shorter S-phase duration in the GFP-H2A.Bbd-expressing MEFs compared to the GFP-H2A expressing cells as shown in Figure 3.23A.

A shorter S-phase duration and its increased DNA damage susceptibility are important features of cancer cells. In previous studies the analysis of Gene Expression Omnibus microarray data sets from Hodgkin's lymphoma cell line samples showed increased levels of H2A.Bbd RNA in comparison with normal tissue (Winkler et al., 2012). Consistent with this finding, chromatin isolated from HL cells contains much higher levels of H2A.Bbd than control cells, where H2A.Bbd is not detectable. Interestingly, the total levels of H2A.Bbd vary substantially in different HL lines with the lines containing highly expressed H2A.Bbd having a shorter doubling time than the ones with lower expression levels. This suggests that H2A.Bbd overexpression might have a similar effect in MEFs and tumor cells (Figure 3.23).

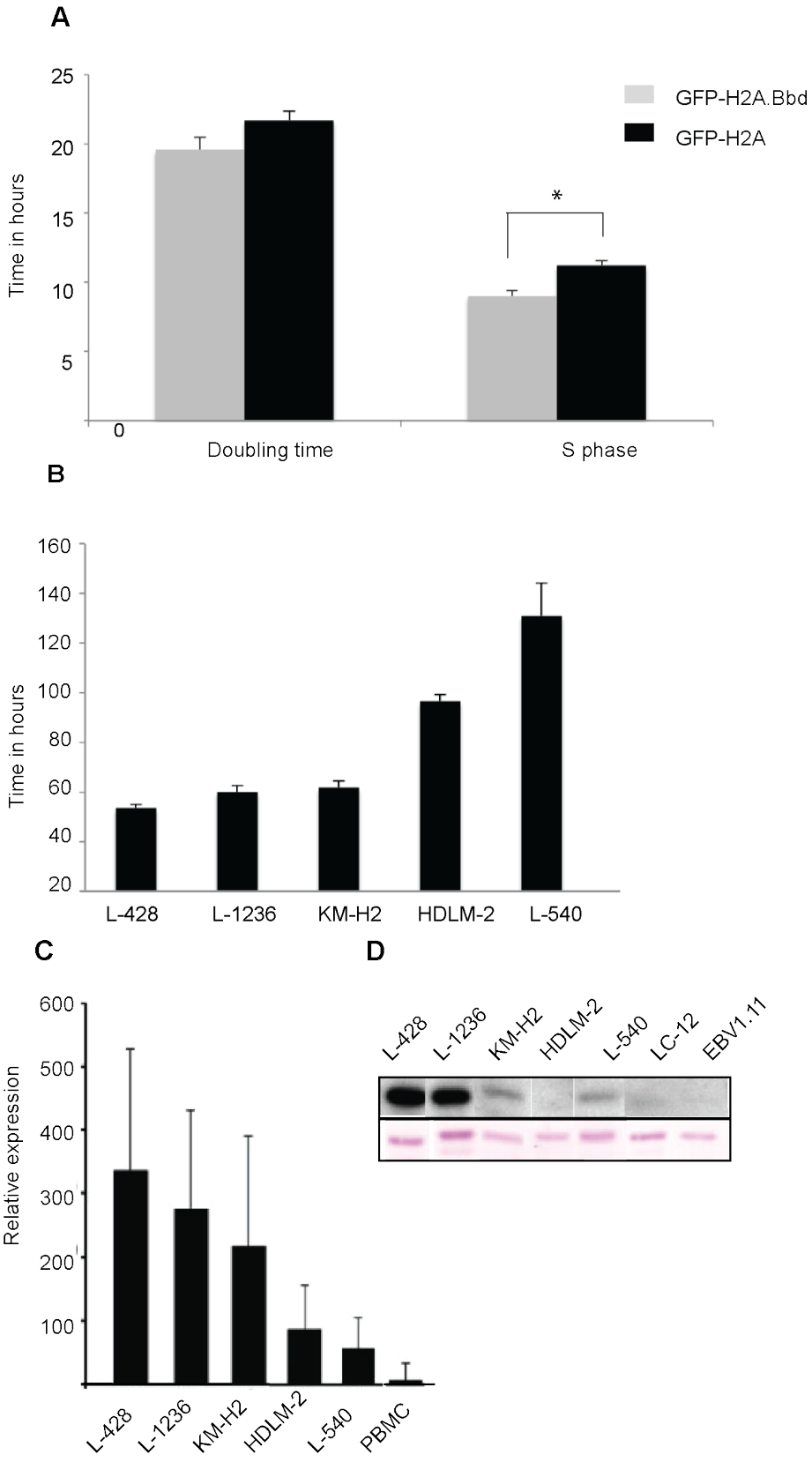

Figure 3.23. Proliferation behavior of H2A.Bbd-overexpressing cells lines. (A) Doubling time and S-phase progression was compared between the MEFs overexpressing GFP-H2A.Bbd and GFP-H2A. Error bars represent 95% confidence intervals. (*: $p < 0.05$, calculated using two-tailed *t*-tests)

(B) Hodgkin's lymphoma cells expressing different levels of H2A.Bbd have different. Error bars represent standard deviation. (C) Expression analysis of H2A.Bbd in HL cells and control cells using qRT-PCR is summarized. For this experiment cDNA from HL cell lines and normal PBMC were used as templates for quantitative PCR. For calculation of relative expression values, actin beta was used as housekeeping control and the median expression in normal PBMC was set as 1 (Data from Viola Sansoni). (D) Western blots of Hodgkin's lymphoma cells (HL) and control cell lines were tested for H2A.Bbd using western blot analysis. Histone H3 was used as a control for Ponceau staining (Data from Martin Staege).

Discussion

Time-lapse microscopy data revealed that GFP-H2A.Bbd is incorporated into chromatin just after DNA replication and repair, and is shortly thereafter replaced by the canonical H2A. This observation is consistent with the reduced stability of nucleosomal H2A.Bbd in live cells as described in (Gautier et al., 2004) using FRAP (Fluorescent recovery after photobleaching). Here the TAT-S-S-PL described in Chapter-3.3 was used to mark the sites where the endogenous PCNA is localized. This biomarker allowed us to recognize the localization of H2A.Bbd along with endogenous and ectopically expressed levels of PCNA. Clearly, the live cell data shows that H2A.Bbd interacts with PCNA at repair sites, thus validating real time biochemical data from mass spec as described (Sansoni et al. 2014).

H2A.Bbd nucleosomes, which have a more relaxed structure, are proposed to be less stable and undergo transcription more quickly than conventional nucleosomes, and they are resistant to remodeling by SWI/SNF (SWItch/Sucrose NonFermentable) complexes (Doyen et al., 2006; Menoni et al., 2007). Also the repair of conventional, but not H2A.Bbd, nucleosomes was greatly facilitated by the chromatin remodeler SWI/SNF. As H2A.Bbd is highly expressed in spermatogenic cells, H2A.Bbd at sites of DNA replication could physiologically contribute to the maturation of sperm and the replacement of the canonical histone with protamines. Thus, H2A.Bbd is a unique histone variant that may play a key role in the histone-to-protamine packing.

Furthermore, some structural and biochemical analyses studies have shown that H2A.Bbd possibly forms a transitional nucleosome with shorter DNA fragments during DNA replication, repair, and transcription (Arimura et al., 2013). Our data also show that the decondensed and relaxed levels of the chromatin plays a major role in exposing the DNA to damage from UV-C. It follows from our results that lower susceptibility of DNA to damage by non-ionizing radiation is due to hypercondensation as well as the presence of a higher amount of proteins in comparison to genetically active and decondensed chromatin. Increased sensitivity and shorter S-phase duration are characteristics of cancer cells. Hence Hodgkin's lymphoma cells tested for the expression levels of H2A.Bbd were found to proliferate faster and proportionally to their H2A.Bbd expression levels. The high sensitivity of HL to radiotherapy and its treatment strategies are deeply reviewed (Winkler et al. 2012 ; Yeoh & Mikhaeel 2011). H2A.Bbd is specifically overexpressed in HL cell lines and the present radio-sensitivity data can open up new avenues for its treatment.

References

Arimura, Y., Kimura, H., Oda, T., Sato, K., Osakabe, A., Tachiwana, H., Sato, Y., Kinugasa, Y., Ikura, T., Sugiyama, M., Sato, M., & Kurumizaka, H. (2013). Structural basis of a nucleosome containing histone H2A.B/H2A.Bbd that transiently associates with reorganized chromatin. *Scientific Reports, 3*.

Bao, Y., Konesky, K., Park, Y. J., Rosu, S., Dyer, P. N., Rangasamy, D., Tremethick, D. J., Laybourn, P. J., & Luger, K. (2004). Nucleosomes containing the histone variant H2A.Bbd organize only 118 base pairs of DNA. *EMBO J, 23*(16), 3314-3324.

Bian, Q., & Belmont, A. S. (2012). Revisiting higher-order and large-scale chromatin organization. *Curr Opin Cell Biol, 24*(3), 359-366.

Cao, R., Tsukada, Y., & Zhang, Y. (2005). Role of Bmi-1 and Ring1A in H2A ubiquitylation and Hox gene silencing. *Mol Cell, 20*(6), 845-854.

Casas-Delucchi, C. S., Becker, A., Bolius, J. J., & Cardoso, M. C. (2012). Targeted manipulation of heterochromatin rescues MeCP2 Rett mutants and re-establishes higher order chromatin organization. *Nucleic Acids Res, 40*(22), e176.

Chadwick, B. P., & Willard, H. F. (2001). A novel chromatin protein, distantly related to histone H2A, is largely excluded from the inactive X chromosome. *Journal of Cell Biology, 152*(2), 375-384.

Chodaparambil, J. V., Barbera, A. J., Lu, X., Kaye, K. M., Hansen, J. C., & Luger, K. (2007). A charged and contoured surface on the nucleosome regulates chromatin compaction. *Nat Struct Mol Biol, 14*(11), 1105-1107.

Diehl, V., Kirchner, H. H., Schaadt, M., Fonatsch, C., Stein, H., Gerdes, J., & Boie, C. (1981). Hodgkin's disease: establishment and characterization of four in vitro cell lies. *J Cancer Res Clin Oncol, 101*(1), 111-124.

Doyen, C. M., Montel, F., Gautier, T., Menoni, H., Claudet, C., Delacour-Larose, M., Angelov, D., Hamiche, A., Bednar, J., Faivre-Moskalenko, C., Bouvet, P., & Dimitrov, S. (2006). Dissection of the unusual structural and functional properties of the variant H2A.Bbd nucleosome. *EMBO J, 25*(18), 4234-4244.

Drexler, H. G., Gaedicke, G., Lok, M. S., Diehl, V., & Minowada, J. (1986). Hodgkin's disease derived cell lines HDLM-2 and L-428: comparison of morphology, immunological and isoenzyme profiles. *Leuk Res, 10*(5), 487-500.

Foell, J. L., Volkmer, I., Giersberg, C., Kornhuber, M., Horneff, G., & Staege, M. S. (2008). Loss of detectability of Charcot-Leyden crystal protein transcripts in blood cells after treatment with dimethyl sulfoxide. *J Immunol Methods, 339*(1), 99-103.

Gautier, T., Abbott, D. W., Molla, A., Verdel, A., Ausio, J., & Dimitrov, S. (2004). Histone variant H2ABbd confers lower stability to the nucleosome. *EMBO Rep, 5*(7), 715-720.

Graber, M. W., Schweinfest, C. W., Reed, C. E., Papas, T. S., & Baron, P. L. (1996). Isolation of differentially expressed genes in carcinoma of the esophagus. *Ann Surg Oncol, 3*(2), 192-197.

Groth, A., Rocha, W., Verreault, A., & Almouzni, G. (2007). Chromatin challenges during DNA replication and repair. *Cell, 128*(4), 721-733.

Grunstein, M. (1997). Histone acetylation in chromatin structure and transcription. *Nature, 389*(6649), 349-352.

Herrera, R. E., Chen, F., & Weinberg, R. A. (1996). Increased histone H1 phosphorylation and relaxed chromatin structure in Rb-deficient fibroblasts. *Proc Natl Acad Sci U S A, 93*(21), 11510-11515.

Ishibashi, T., Li, A., Eirin-Lopez, J. M., Zhao, M., Missiaen, K., Abbott, D. W., Meistrich, M., Hendzel, M. J., & Ausio, J. (2010). H2A.Bbd: an X-chromosome-encoded histone involved in mammalian spermiogenesis. *Nucleic Acids Res, 38*(6), 1780-1789.

Kamakaka, R. T., & Biggins, S. (2005). Histone variants: deviants? *Genes Dev, 19*(3), 295-310.

Kamesaki, H., Fukuhara, S., Tatsumi, E., Uchino, H., Yamabe, H., Miwa, H., Shirakawa, S., Hatanaka, M., & Honjo, T. (1986). Cytochemical, immunologic, chromosomal, and

molecular genetic analysis of a novel cell line derived from Hodgkin's disease. *Blood, 68*(1), 285-292.

Khare, S. P., Sharma, A., Deodhar, K. K., & Gupta, S. (2011). Overexpression of histone variant H2A.1 and cellular transformation are related in N-nitrosodiethylamine-induced sequential hepatocarcinogenesis. *Experimental Biology and Medicine, 236*(1), 30-35.

Laitinen, J., Sistonen, L., Alitalo, K., & Holtta, E. (1990). C-Ha-Ras Val-12 Oncogene-Transformed Nih-3t3 Fibroblasts Display More Decondensed Nucleosomal Organization Than Normal Fibroblasts. *Journal of Cell Biology, 111*(1), 9-17.

Martin, R. M., & Cardoso, M. C. (2010). Chromatin condensation modulates access and binding of nuclear proteins. *FASEB J, 24*(4), 1066-1072.

Marzluff, W. F., Gongidi, P., Woods, K. R., Jin, J., & Maltais, L. J. (2002). The human and mouse replication-dependent histone genes. *Genomics, 80*(5), 487-498.

Menoni, H., Gasparutto, D., Hamiche, A., Cadet, J., Dimitrov, S., Bouvet, P., & Angelov, D. (2007). ATP-dependent chromatin remodeling is required for base excision repair in conventional but not in variant H2A.Bbd nucleosomesv. *Mol Cell Biol, 27*(17), 5949-5956.

Muster, B. (2014). DNA repair and chromatin. *[Online-Edition:* http://tuprints.ulb.tu-darmstadt.de/id/eprint/3989*] TU Darmstadt*.

Nelson, D. M., Ye, X., Hall, C., Santos, H., Ma, T., Kao, G. D., Yen, T. J., Harper, J. W., & Adams, P. D. (2002). Coupling of DNA synthesis and histone synthesis in S phase independent of cyclin/cdk2 activity. *Mol Cell Biol, 22*(21), 7459-7472.

Neumann, I., Foell, J. L., Bremer, M., Volkmer, I., Korholz, D., Burdach, S., & Staege, M. S. (2010). Retinoic acid enhances sensitivity of neuroblastoma cells for imatinib mesylate. *Pediatr Blood Cancer, 55*(3), 464-470.

Otsu, N. (1979). A Threshold Selection Method from Gray-Level Histograms. *IEEE Transactions on Systems, Man, and Cybernetics, 9*(1), 62-66.

Rapsomaniki, M. A., Kotsantis, P., Symeonidou, I. E., Giakoumakis, N. N., Taraviras, S., & Lygerou, Z. (2012). easyFRAP: an interactive, easy-to-use tool for qualitative and quantitative analysis of FRAP data. *Bioinformatics, 28*(13), 1800-1801.

Richmond, T. J. (1999). Hot papers - Crystal structure - Crystal structure of the nucleosome core particle at 2.8 angstrom resolution by K. Luger, A.W. Mader, R.K. Richmond, D.F. Sargent, T.J. Richmond - Comments. *Scientist, 13*(23), 15-15.

Sansoni, V., Casas-Delucchi, C. S., Rajan, M., Schmidt, A., Bonisch, C., Thomae, A. W., Staege, M. S., Hake, S. B., Cardoso, M. C., & Imhof, A. (2014). The histone variant H2A.Bbd is enriched at sites of DNA synthesis. *Nucleic Acids Res, 42*(10), 6405-6420.

Sperling, R., & Bustin, M. (1976). Histone dimers: a fundamental unit in histone assembly. *Nucleic Acids Res, 3*(5), 1263-1275.

Takahashi, H., Murai, Y., Tsuneyama, K., Nomoto, K., Okada, E., Fujita, H., & Takano, Y. (2006). Overexpression of phosphorylated histone H3 is an indicator of poor prognosis in gastric adenocarcinoma patients. *Applied Immunohistochemistry & Molecular Morphology, 14*(3), 296-302.

Tolstorukov, M. Y., Goldman, J. A., Gilbert, C., Ogryzko, V., Kingston, R. E., & Park, P. J. (2012). Histone variant H2A.Bbd is associated with active transcription and mRNA processing in human cells. *Mol Cell, 47*(4), 596-607.

Varambally, S., Dhanasekaran, S. M., Zhou, M., Barrette, T. R., Kumar-Sinha, C., Sanda, M. G., Ghosh, D., Pienta, K. J., Sewalt, R. G., Otte, A. P., Rubin, M. A., & Chinnaiyan, A. M. (2002). The polycomb group protein EZH2 is involved in progression of prostate cancer. *Nature, 419*(6907), 624-629.

Vardabasso, C., Hasson, D., Ratnakumar, K., Chung, C. Y., Duarte, L. F., & Bernstein, E. (2014). Histone variants: emerging players in cancer biology. *Cell Mol Life Sci, 71*(3), 379-404.

Winkler, C., Steingrube, D. S., Altermann, W., Schlaf, G., Max, D., Kewitz, S., Emmer, A., Kornhuber, M., Banning-Eichenseer, U., & Staege, M. S. (2012). Hodgkin's lymphoma RNA-transfected dendritic cells induce cancer/testis antigen-specific immune responses. *Cancer Immunol Immunother, 61*(10), 1769-1779.

Wolf, J., Kapp, U., Bohlen, H., Kornacker, M., Schoch, C., Stahl, B., Mucke, S., von Kalle, C., Fonatsch, C., Schaefer, H. E., Hansmann, M. L., & Diehl, V. (1996). Peripheral blood mononuclear cells of a patient with advanced Hodgkin's lymphoma give rise to permanently growing Hodgkin-Reed Sternberg cells. *Blood, 87*(8), 3418-3428.

Wolffe, A. P. (1997). Histones, nucleosomes and the roles of chromatin structure in transcriptional control. *Biochem Soc Trans, 25*(2), 354-358.

Wolffe, A. P., & Guschin, D. (2000). Review: chromatin structural features and targets that regulate transcription. *J Struct Biol, 129*(2-3), 102-122.

Yeoh, K. W., & Mikhaeel, N. G. (2011). Role of Radiotherapy in Modern Treatment of Hodgkin's Lymphoma. *Adv Hematol, 2011*, 258797.

4. Conclusion and Outlook

Chromobody based γ-H2AX binder - bypassing the challenges

The main objective of the Chapter-3.1 was generation and characterization of γ-H2AX specific VHHs used for biochemical and intracellular applications. The generated VHHs were tested for its usability *in vitro* and *in vivo* and were found to be functional *in vitro*. In addition, the functionality *in vivo* was assessed by the localization of the fluorescently tagged γ-H2AX VHH (chromobody) at the sites of DNA damage. The ability to identify the native proteins is the ultimate test for the application of VHHs in living cells as chromobody. However, during *in vivo* characterization we encountered major problems, alternative epitope recognition and epitope masking. These two major pitfalls are analyzed in this chapter and illustrated in Figure 4.1.

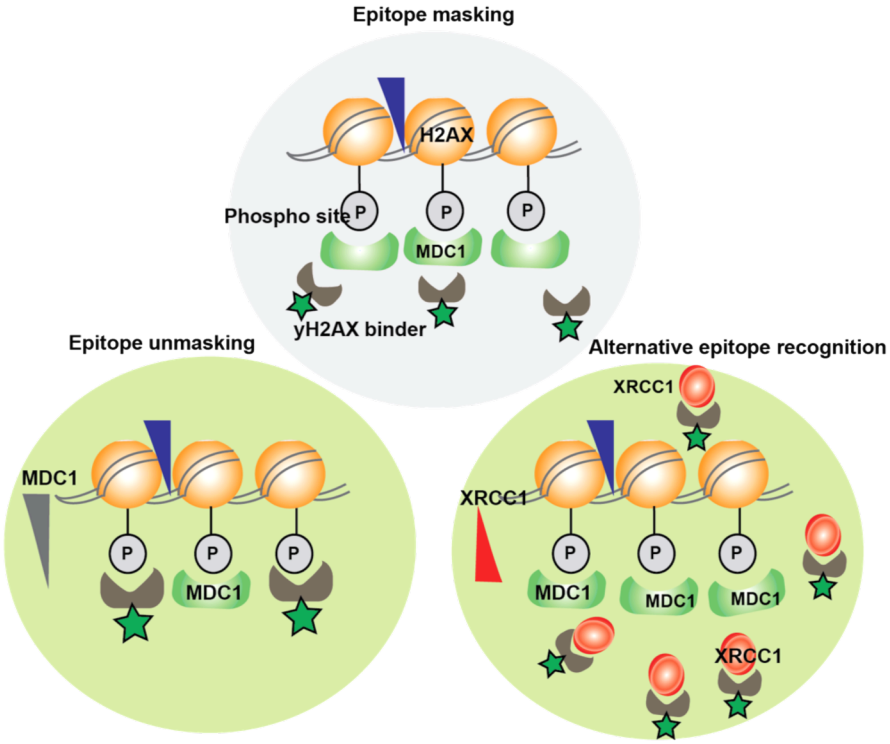

Figure 4.1. **Model for γ-H2AX binder recruitment upon epitope unmasking and alternative epitope recognition.** Here we show that upon XRCC1 overexpression and MDC1 knockdown, the **γ**-H2AX binder was recruited at the sites of DNA damage.

Diverse factors have a role on the efficient usability of VHHs for cellular applications, such as the selection process of VHHs. It is very important to recapitulate the most critical steps in the VHH generation that could have influenced the specificity of the VHHs.

1. The solid phase panning step has numerous drawbacks concerning the way antigens are presented. In order to select VHHs of high specificity, for recognizing epitopes in a native

environment, the presentation of antigens is very crucial. It has been previously shown that filamentous phages have a high inclination to bind unspecifically to diversified structures. In order to overcome this problem, the native panning method (Jespersen et al., 2000), which employs recombinant antigens with native conformations, could have been employed. 2. When generating larger VHH libraries, the evaluation of library diversity is very complex and time consuming. The sequencing method, which is the most preferable way to test libraries, provides additional information that cannot be obtained from restriction analysis (Carmen & Jermutus, 2002). However, sequencing of large libraries is costly and time-consuming. Therefore, for the evaluation of the diversity of the VHHs, very few clones that exhibited diversity were analysed. Hence sequencing analysis of more clones is critical to identify the clones with high specificity. 3. Theoretically, it is important to carefully check sequencing data for the presence of cysteine residues within complementary determining regions (CDRs). Previous studies show that cysteines in VHHs can form a CDR3 intraloop or an cysteine bridge that will stably connect CDR3 with CDR1, which eventually stabilizes the VHH (Davies & Riechmann, 1996). VHH regions can be successfully modeled theoretically (Sircar et al., 2011). Accordingly, one could improve the specificity of the antibody by minimising cross-reactivity, thus rendering increased binding affinity to the epitope.

Though we could not achieve a high specific VHHs for γ-H2AX. It is still feasible to achieve high specific clones by trying the aforementioned steps.

Cell penetrating peptide-based PCNA marker

As nanobody technology is time consuming and laborious, we tried quick cell penetrating peptide technology in Chapter 3.2 for the development of a cell-permeable DNA replication and repair biomarker by targeting PCNA interactions. We initially demonstrated the usability and binding capacity of fluorescently labeled PCNA binding peptides by microinjection. As we successfully noticed the dynamic co-localization of the peptide and PCNA, we used a cell penetrating peptide strategy for simply carrying the PCNA binding peptide inside the cell.

First we covalently coupled the cell penetrating peptide (TAT) with PCNA binding peptide, and we did not see any binding of the peptide to PCNA (Tunnemann et al., 2006). Later, we improved this strategy by introducing a di-sulfide bridge between the carrier and the cargo. We were successful, as we saw the labeling of the PCNA with the peptide (Figure 4.2).

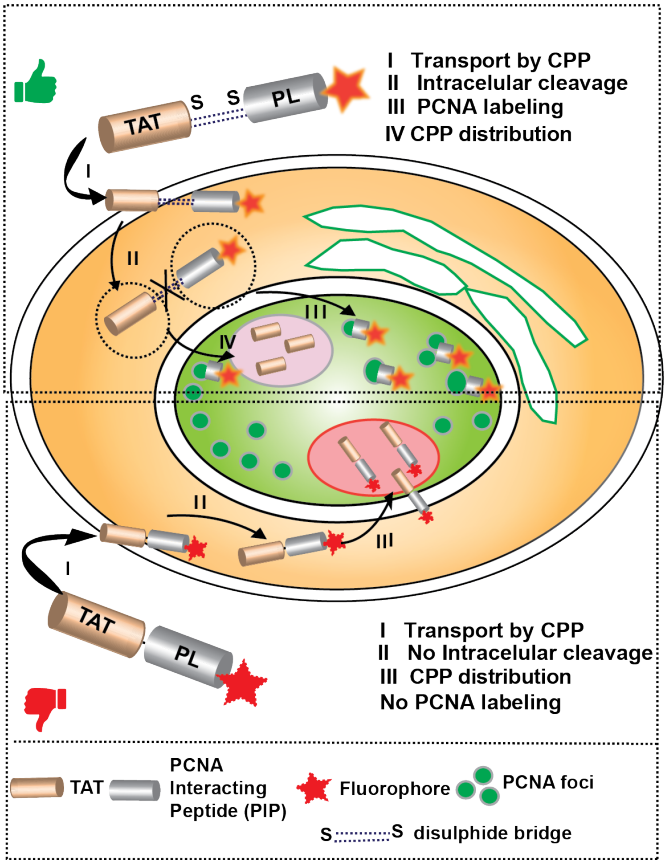

Figure 4.2. Strategies to target PCNA in living cells. Here the steps involved in labeling the PCNA are illustrated. The strategy described above the cell uses a disulfide bridge and the one below does not use a disulfide bridge between the career and the cargo.

Apart from labeling studies, there is interest in developing PCNA inhibitors as they could serve as anti-cancer agents, because PCNA regulates DNA replication and most DNA repair pathways. It would be interesting to understand the therapeutic advantages of these peptides that have high clinical value (Stevenson, 2009). Peptides designed for the cancer-associated PCNA (caPCNA) isoform found mainly in tumor cells, rather than in non-tumor cells, successfully inhibited the growth of neuroblastoma cells (Gu et al., 2014). Studies show that the AlkB homologue 2 PCNA-interacting motif (APIM) peptide was bound with the PCNA thereby inducing apoptosis in multiple myeloma cells (Muller et al., 2013). Hence it would be interesting to compare our PIP and its mutants with multiple cancer cell lines and look for an inhibitory effect in replication and repair to clarify its potential clinical relevance.

Universal cell-penetrating peptide-based histidine-tag marker

In Chapter 3.3 we extended the usability of cell-penetrating peptides for delivering small molecular probes (i.e., trisNTA) in order to label any histidine tagged recombinant proteins. The usage of His-tag in biological applications is extensive (e.g., protein purification, protein–protein interaction assays, protein immobilization etc.). Studies on the applications of mono-

and multivalent NTAs showed no loss of activity or functionality of the protein of interest (Lata et al., 2006). His-tag is used in biotechnological applications like affinity purification.

Mainly to avoid time consuming cloning procedures we used CPP technology to transport trisNTA into the cells and label the His-tagged proteins.

Our approach has three main advantages for live-cell investigations: (i) it can label His-tagged proteins of interest in living cells, (ii) a wide choice of fluorophores for *tris*NTA labeling, and (iii) a minimalistic tag (<2 kDa) minimizes loss of protein function. Organic dyes are flexible in their spectral range and combinatorial spectral possibilities. As they are very photo-stable, they are versatile enough to detect at a single-molecule level. However, our approach demonstrates for the first time the labeling of MeCP2 and recombinant His-tagged PCNA protein in living cells, as shown in Figure 4.3 with complete mechanism and highlights listed below.

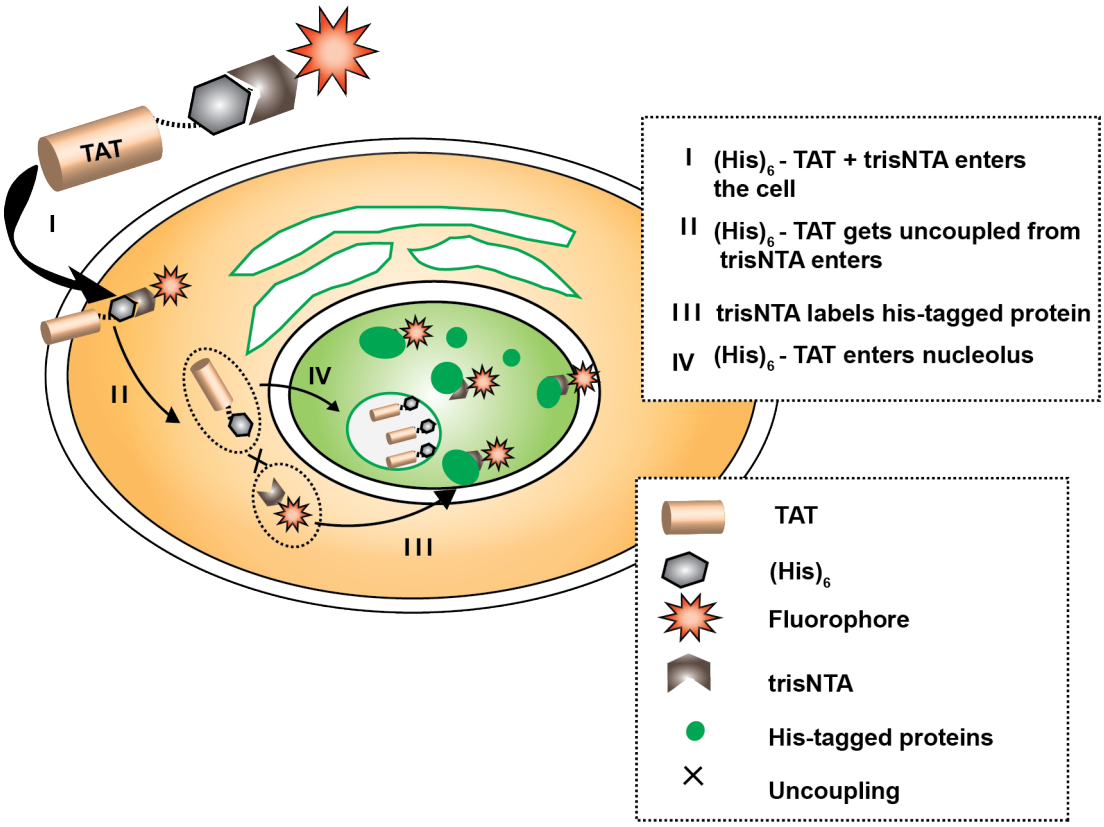

Figure 4.3. Illustration for the mechanism of trisNTA labeling His-tagged protein in living the cells. Here we show the four step mechanism: (A) trisNTA coupling to His-TAT and cell penetration, (B) uncoupling of His-TAT from trisNTA, (C) labeling of His-tagged proteins by trisNTA, and (D) TAT redistributed in the nucleolus.

In our present study we used histidines (n = 6, 7) in the protein of interest. However, it would be interesting to validate a range of histidines and also compare the efficiency of the system with the cyclic TATs (Lattig-Tunnemann et al., 2011) in the place of the linear TAT used in this study. The strategy of the previous chapter (i.e., the disulfide bridge) should be tried for

its versatility and efficiency in comparison with the present coupling and uncoupling method. Finally, the small size, great flexibility (e.g., choice of the fluorophore), quick, and stoichiometric labeling of this method is of great use for *in vivo* super-resolution microscopy and single-molecule tracking analysis.

H2A.Bbd and its potential role in carcinogenesis

In Chapter 3.4, we discussed the newly found histone variant H2A.Bbd and its participation in different cellular processes. Hence, its primary proteomic profile was analyzed using mass spectrometry by Axel Imhof and his co-workers at LMU-Munich. Their results showed that H2A.Bbd interacts with the DNA replication factors. In this thesis, we show that GFP-Bbd overexpressed in MEF cells were found to form dynamic localization at the sites of DNA replication and repair sites and showed high DNA damage sensitivity to non-ionizing radiation like UV-C.

It has been shown that H2A.Bbd is removed from the sites of replication in less than one hour by a pulse chase experiment (Sansoni et al., 2014), whereas the microirradiation experiments showed that it was retained for more time at the sites of repair. There may be different residence times at the sites of repair and replication by H2A.Bbd, which is also characteristic of PCNA (Essers et al., 2005). Here we also show that H2A.Bbd overexpressing cells were more sensitive to UV-C irradiation than were H2A overexpressing cells.

In order to investigate the DNA damage sensitivity we first hypothesized that the relaxed nature of the H2A.Bbd comprising chromatin makes an unprotected environment for radiation induced DNA damage. To validate our hypothesis we reversed the chromatin condensation levels of H2A.Bbd to behave like H2A. Upon increasing the salt levels, the chromatin was more condensed and got less sensitive to UV-C. Our reasoning for this DNA damage sensitivity of H2A.Bbd in the context of chromatin condensation is illustrated in Figure 4.4.

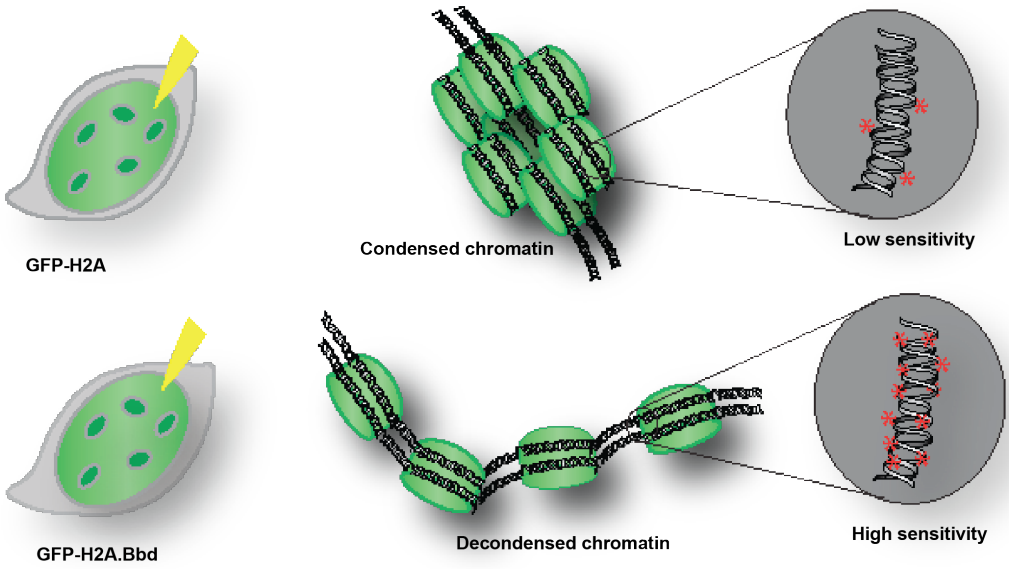

Figure 4.4. Illustration of nucleosome comprising different H2A variants and their sensitivity to UV-C. Here we show that H2A and H2A.Bbd comprising nucleosomes have different levels of chromatin condensation, and this could potentially lead to the formation of fragile or damaged sites in DNA upon UV-C irradiation.

The higher sensitivity of chromatin in H2A.Bbd-overexpressing cells is probably not due to the simple chromatin decondensation but the presence of a decreased amount of proteins protecting the DNA than more condensed chromatin.

It was found from our data that H2A.Bbd-overexpressing cells replicate faster than H2A-overexpressing MEFs. However, contrary results were published that showed that H2A.Bbd leads to cell cycle arrest and apoptosis (Goshima et al., 2014). The difference of phenotypes in the two studies could be attributed to the different cell types used or different levels of H2A.Bbd expression. To make this determination, one should express different levels of H2A.Bbd and see if this changes replication or apoptosis rates. It would be interesting to compare the radiation sensitivity data with the cells overexpressing macro H2A as it is found contrastingly enriched in the Barr body.

Multiple Hodgkin's lymphoma cell lines were found to express H2A.Bbd. It was observed that the cells that express high levels of H2A.Bbd replicate faster, and the literature reveals that HL cells have high radiosensitivity (Yeoh & Mikhaeel, 2011). From the above findings, an unusual presence of H2A.Bbd in somatic cells could contribute to cancer progression and development. On the whole, this investigation of H2A.Bbd has not only have given some interesting data on DNA damage sensitivity, replication, repair, and chromatin condensation levels but also suggests the need for further research regarding H2A.Bbd's unique role in cancer and spermatogenesis.

References

Carmen, S., & Jermutus, L. (2002). Concepts in antibody phage display. *Brief Funct Genomic Proteomic, 1*(2), 189-203.

Davies, J., & Riechmann, L. (1996). Single antibody domains as small recognition units: design and in vitro antigen selection of camelized, human VH domains with improved protein stability. *Protein Eng, 9*(6), 531-537.

Gu, L., Smith, S., Li, C., Hickey, R. J., Stark, J. M., Fields, G. B., Lang, W. H., Sandoval, J. A., & Malkas, L. H. (2014). A PCNA-derived cell permeable peptide selectively inhibits neuroblastoma cell growth. *PLoS One, 9*(4), e94773.

Jespersen, L. K., Kuusinen, A., Orellana, A., Keinanen, K., & Engberg, J. (2000). Use of proteoliposomes to generate phage antibodies against native AMPA receptor. *Eur J Biochem, 267*(5), 1382-1389.

Lata, S., Gavutis, M., Tampe, R., & Piehler, J. (2006). Specific and stable fluorescence labeling of histidine-tagged proteins for dissecting multi-protein complex formation. *J Am Chem Soc, 128*(7), 2365-2372.

Lattig-Tunnemann, G., Prinz, M., Hoffmann, D., Behlke, J., Palm-Apergi, C., Morano, I., Herce, H. D., & Cardoso, M. C. (2011). Backbone rigidity and static presentation of guanidinium groups increases cellular uptake of arginine-rich cell-penetrating peptides. *Nat Commun, 2*, 453.

Muller, R., Misund, K., Holien, T., Bachke, S., Gilljam, K. M., Vatsveen, T. K., Ro, T. B., Bellacchio, E., Sundan, A., & Otterlei, M. (2013). Targeting proliferating cell nuclear antigen and its protein interactions induces apoptosis in multiple myeloma cells. *PLoS One, 8*(7), e70430.

Sansoni, V., Casas-Delucchi, C. S., Rajan, M., Schmidt, A., Bonisch, C., Thomae, A. W., Staege, M. S., Hake, S. B., Cardoso, M. C., & Imhof, A. (2014). The histone variant H2A.Bbd is enriched at sites of DNA synthesis. *Nucleic Acids Res, 42*(10), 6405-6420.

Sircar, A., Sanni, K. A., Shi, J., & Gray, J. J. (2011). Analysis and modeling of the variable region of camelid single-domain antibodies. *J Immunol, 186*(11), 6357-6367.

Stevenson, C. L. (2009). Advances in peptide pharmaceuticals. *Curr Pharm Biotechnol, 10*(1), 122-137.

Tunnemann, G., Martin, R. M., Haupt, S., Patsch, C., Edenhofer, F., & Cardoso, M. C. (2006). Cargo-dependent mode of uptake and bioavailability of TAT-containing proteins and peptides in living cells. *FASEB J, 20*(11), 1775-1784.

Yeoh, K. W., & Mikhaeel, N. G. (2011). Role of Radiotherapy in Modern Treatment of Hodgkin's Lymphoma. *Adv Hematol, 2011*, 258797.

5. Annex

5.1. Abbreviations

Bbd - Barr body depleted

BER- Base excision repair

BrdU - bromodeoxyuridine

BSA - Bovine serum albumin

CDC - cell division cycle

CDK- cyclin dependent kinase

CKM- Caesin kinase 2 mutant

DMEM - Dulbecco's modified Eagle's medium

DSB - Double Strand Break

FRAP - Fluorescence recovery after photobleaching

GFP - Green fluorescent protein

H2AX - Histone H2AX

His - Histidine

HL – Hodgkin's lymphoma

HR - Homologus recombination

HRP-Horse radish peroxidase

IR - Ionizing radiation

MCM - Mini chromosome maintanence

MDC1- Mediator of DNA damage checkpoint-1

MeCP2 - Methyl CPG binding protein

MEFs - Mouse embryonic fibroblast

mRFP - Monomeric red fluorescent protein

NER - Nucleotide excision repair

PARP - Poly (ADP-ribose) polymerase

PBS - Phosphate buffer saline

PCNA - Proliferating cell nuclear antigen

PIP- PCNA interacting peptide

RT - Room temperature

S-Phase - Synthesis phase

ssDNA - Single stranded Deoxyribose nucleic acid

TAT - Trans activator of transcription

trisNTA - Tris-nitrilotriacetic acids

UV - Ultra violet

XRCC1 or 4 - X-ray repair complementing defective repair in Chinese hamster cells 1 or 4

5.2. List of Contributions

Chapter-3.1	
Malini Rajan	Carried out all the experiments and all Figure preparation and writing.
Katrin schmidthals	Performed Dot Blot and Phage ELISA experiment
Ulrich Rothbauer	Immunoprecipitation
Alexander Rapp	Supervised the experimental work writing and, wrote Image J macro.
M. Cristina Cardoso	Designed and supervised the project
Heindrich Leonhardt	Designed the project
Chapter-3.2	
Malini Rajan	Carried out all the experiments and all figure preparation and written jointly with Henry David Herce
Henry David Herce	Carried out simulations in Figure 3 and supervised and corrected figure preparation
Gilla Tuenemann	Carried out microinjections in Figure 3
M. Cristina Cardoso	Designed and supervised the project
Chapter-3.3	
Malini Rajan	Carried out all the experiments, all Figure preparation and writing
Ralph Weineke	Carried out trisNTA and His-TAT peptide synthesis
M. Cristina Cardoso	Designed and supervised the project
Robert Tampe	Designed and supervised the project
Chapter-3.4	
Malini Rajan	Carried out all the experiments, all Figure preparation and writing
Corella Casas Deluchi	Wrote the source code in priithon
Viola Sansoni	Western Blot figure
Martin Staege	Real time PCR analysis figure
M Cristina Cardoso	Designed and supervised the project
Axel Imhof	Designed the project

5.3. Acknowledgements

I would like to thank Prof. M. Cristina Cardoso for providing me an opportunity to work in her laboratory. The extent of time, support, advice, encouragement she showed during the projects, is the sole reason which brought me to this level. A well balanced criticism and encouragement from her helped me a lot to progress ahead in all the projects. The limitless meetings, discussion sessions and preparation for GrK talks have been shown in this piece of work and will no doubt frame my attitude and character for the rest of my career. I especially regarded the efforts in setting me up with interesting projects. I also thank her highly for exhibiting huge tolerance towards many of my shortcomings.

I am thankful to project collaborators Heindrich Leonhardt (LMU), Katrin Schmidthals Chromotek GmbH, Axel Imhof & Viola Sansoni (LMU), Martin Staege, Ralph Wieneke and Robert Tampe (Goethe Universitaet) for the technical knowledge transfer and fruitful discussions.

I would like to thank GRK1657, STIBET-DAAD for providing me scholarship.

I am very much indebted to Alexander Rapp for providing anytime support and suggestions in the middle of his work. His patience and humility have to be appreciated when it comes to explaining concepts and trouble shooting microscopic issues any number of times.
I would like to thank Henry for showing me light towards cell penetrating peptides project. His suggestions and inputs has definitely helped me a lot towards progress of my work and making nice illustrations. He constantly supported and encouraged throughout the other projects. I thank Corella casas delucchi for being such a great supervisor /colleague/ friend and I thank her for helping me with Bbd project, She remained a student role model for many of us. I should thank her for teaching me microscopy, ImageJ, Priithon and methodical way of experimenting. Her timely help and inputs definitely led to the progress of my ongoing projects too.

I thank Lena Allman the first friendly face helping me over every small things when I was totally new to the lab. I thank my senior labmates Annette becker and Laurence Jost for being such a great friends.

I thank Anne Lehmkul & Anne Ludwig, Patrick Weber (ofcourse for Rotweinkuchen recipe), Florian (Dr. Bo) and Kathrin who were more than colleagues and for sharing a pleasant friendship. I specially thank Florian, kathrin (&thomas), Anne(s) during my medical emergency situations who remained true example for “A friend in need is a friend in deed”.

I am very thankful to Bianca, Peng, Wei, Marius, Manu, Sven, Stephan, Annina, Diana, Angela, Stephi, Francesco for being helpful at various stages of my work and sharing a cordial relationship.

I am deeply indebted to Mrs. Waltraud haffmann goody (Max Planck Society), Prof. Wulf Blankenfeldt (MPI-Dortmund), Prof. Marcus Frohme (TH-Wildau), Mr. Ulrich M Tillich (TH-Wildau), with several helps from personal to professional during most critical times, thus making the possibility of my stay in germany a successful one.

I also thank Prof. M. N. Gupta (IIT-Delhi), Prof. Adline Princy (SASTRA University) who helped me during my Master’s studies in India.

A big fat thanks to my mom and dad without their support and blessings nothing would have been possible.

Final thanks to my best buddies avinash and ppd and their family for their support during various stages of my PhD and life.
I am not sure If I can totally repay the support and help my professor, labmates, family, friends showed for me during this PhD journey. But I will definitely have them in my daily prayers for their success and well being.

5.4. Declaration - Ehrenwörtliche Erklärung

Ich erkläre hiermit ehrenwörtlich, dass ich die vorliegende Arbeit entsprechend den Regeln guter wissenschaftlicher Praxis selbstständig und ohne unzulässige Hilfe Dritter angefertigt habe.

Sämtliche aus fremden Quellen direkt oder indirekt übernommenen Gedanken sowie sämtliche von Anderen direkt oder indirekt übernommenen Daten, Techniken und Materialien sind als solche kenntlich gemacht. Die Arbeit wurde bisher bei keiner anderen Hochschule zu Prüfungszwecken eingereicht.

Darmstadt, den . 2014

_____

5.5. Curriculum vitae

Personal details

Name: Malini Rajan
Address: Technische Universität Darmstadt
Schnittspahnstrasse 10
64287 Darmstadt, Germany
Date of birth: 12.12.1985
Place of birth: Madurai Indien

Education

Ph.D. Candidate Technische Universitaet, Darmstadt, Germany
May 2011 - March 2015 FB Biologie

M. Tech SASTRA University, Tanjore, India
Jun 2007 - May 2009 Industrial Biotechnology, CGPA – 9.0/10.0

B. Tech. Anna University, Chennai, India.
Aug 2003 - Apr 2007 Industrial Biotechnology, Percentage: 80%

Experience

Graduate Student
May 2011 – March 2015
Prof. Dr. M. Cristina Cardoso
Department of Biologie, TU-Darmstadt, Germany.
Topic- "Development of biomarkers and their application to the study of chromatin epistate effect on DNA damage and repair".

Research Assistant
Jun 2010 - Feb 2011
Prof. Dr. Sc. Hum. Marcus Frohme
Molecular Biology and Functional Genomics, TH-Wildau, Germany.
Topic -"Golden Gate Shuffling of RuBisCo gene".

Internship
Sep 2009 - Feb 2010
Prof. Dr. Andreas Schmid
TU Dortmund, Germany.
Topic- "Sequential purification and assay optimization of proline hydroxylase".

Master's Thesis
Dec 2008 - May 2009
Prof. Dr. M. N. Gupta
Dept. of Chemistry, IIT Delhi, India.
Topic- "Preparation of novel high performance biocatalyst for improved starch hydrolysis".

Bachelor's Thesis
Dec. 2006 - Apr. 2007
Dr. K. Veluraja
Manonmaniam Sundaranar University, Tirunelveli, India.
Topic- "Proteome database analysis of Mycobacterial species".

Publications

1. Sansoni V, Casas-Delucchi CS, **Rajan M**, Schmidt A, Bonisch C, Thomae AW, Staege MS, Hake SB, Cardoso MC, Imhof A., "The histone variant H2A.Bbd is enriched at sites of DNA synthesis." Nucleic Acids Res. 2014;42(10):6405-20.

2. Herce HD*, **Rajan M***, Lattig-Tunnemann G, Fillies M, Cardoso MC.,
"A novel cell permeable DNA replication and repair marker." Nucleus 2014; 5. [Epub ahead of print] *equally contributing authors.

3. Wieneke R*, Laboria N*, **Rajan M**, Kollmannsperger A, Natale F, Cardoso MC and Tampe R., "Live-cell targeting of His-tagged proteins by multivalent N-nitrilotriacetic acid carrier complexes" J. Am. Chem. Soc., DOI: 10.1021/ja5063357 • Publication Date (Web): 19 Sep 2014.

Manuscripts in preparation (for peer-reviewed journals only!)

1. *In vivo* epitope recognition pitfalls affect γ-H2AX chromobody function in living cells
Rajan M, Mortusewicz O, Rothbauer U, Zolghadr K, Schmidthals K, Rapp A, Leonhardt H, Cardoso M. C.

Conference contributions

1. Gordon Research conferences on DNA damage mutation and cancer, Ventura, USA (Poster presentation, 03/21/14 - 03/25/14).

2. Gesellschaft für Biologische Strahlenforschung meeting, Darmstadt, Germany (Poster presentation, 09/24/13 - 09/25/13).

3. International Joint Meeting of the German Society for Cell Biology (DGZ) and the German Society for Developmental Biology (GfE) – Heidelberg, Germany (Poster presentation, 03/20/2013 – 03/23/2013).